“Dispersive mixing of oil in plasticized starch by extrusion processing to design functional foods”

zur Erlangung des akademischen Grades eines
DOKTORS DER INGENIEURWISSENSCHAFTEN (Dr.-Ing.)

der Fakultät für Chemieingenieurwesen und Verfahrenstechnik des
Karlsruher Institut für Technologie (KIT)

genehmigte
DISSERTATION

von
M.Sc. M. Azad Emin
aus Nikosia / Zypern

Referent: Prof. Dr.-Ing. Heike P. Schuchmann
Korreferent: Prof. Dr. Ir. Remko Boom
Tag der mündlichen Prüfung: 29. April 2013

Contents

1 General Introduction

1.1 Introduction

A large and growing body of literature has indicated that apart from vitamins, there are functional bioactives in foods that have shown desirable health benefits beyond basic nutrition such as preventing cancer, obesity, diabetes or heart disease (Mayne, 1996; Steinmetz and Potter, 1996; Awad and Fink, 2000; Dillard and German, 2000; Krinsky et al., 2004; Kaur and Kapoor, 2008). Yet, the modern world's diet is not well balanced and in many cases it is lack of the foods containing these functional bioactives (Lobstein et al., 2004; Mente et al., 2009; Mozaffarian et al., 2011). The health benefits can simply be acquired from going "back to nature" and consuming more fresh and unprocessed food (Block et al., 1992; WHO and FAO Expert Consultation, 2003). This is probably the most reliable approach, and therefore good for those who can afford it and are ready to give up some specific characteristics of the modern food products, such as appeal and convenience.

This increasing awareness of the impact of diet on human health and well–being has been compelling the food industry to undergo a major concept revolutions, by shifting from traditional foods to benefit based food products (Garti, 2008). With an ambition to "catch up with nature", and thereby to satisfy the consumer demands, the food industry has started to apply a new approach by incorporating into the food the ingredients that were lost during processing, or fortifying the food with components that are less common in modern food products (Garti, 2008).

Often, this cannot be realized by directly adding a bioactive into food, as many of the bioactives are either not bioavailable in their isolated form and/or susceptible to a variety of physical and chemical conditions, which results in their degradation and loss of biological functionality (Augustin and Sanguansri, 2008; Garti, 2008; Zuidam and Shimoni, 2009). Furthermore, the incorporation of bioactives can have an adverse effect on flavour, odour and texture of foods (Augustin and Sanguansri, 2008; Garti, 2008).

Therefore, food research is facing a major challenge in delivering the functional bioactives through the food products using efficient, safe and robust processing methods without sacrificing its appeal and convenience character, and in a manner that they will indeed promote health and well–being of the consumers (i.e. bioavailable).

This chapter firstly focuses on the challenges relating to the delivery of lipophilic bioac-

tives, such as carotenoids, phytosterols and ω–3 fatty acids through foods. Then, the most common approach and techniques used for the manufacture of functional foods are briefly presented. Finally, the potential of extrusion technologies are discussed and the associated challenges together with the aim and outline of this thesis are presented.

1.2 Challenges to delivery of lipophilic bioactives through foods

The range of food components now considered as lipophilic bioactives include carotenoids, phytosterols and fatty acids (Wildman, 2001). The most important types of these bioactives and their potential health benefits are briefly listed in Table 1.1. The molecular structure of lipophilic bioactives varies widely, which leads to differences in their physicochemical and physiological properties, such as solubility and bioavailability, respectively. Consequently, delivery systems or food matrix itself must be designed in such a way that they fulfill the requirements associated with the unique concerns of each specific bioactive. The major challenges related to delivery of lipophilic bioactives through foods are (Augustin and Sanguansri, 2008; Garti, 2008; McClements et al., 2009; Zuidam and Shimoni, 2009):

i. **Stability:** Most lipophilic bioactives (e.g. carotenoids and ω–3 fatty acids) are relatively unstable in food systems, as they are susceptible to light, oxygen, and autooxidation (Kulås et al., 2003; Xianquan et al., 2005). Direct dispersion of these bioactives into food systems can result in their rapid degradation (Heinonen et al., 1997; Ribeiro et al., 2003). To overcome this challenge, the bioactives must be encapsulated into a delivery system, in which their bioactivity within the food product is maintained during its processing, storage and consumption. However, this is not a straightforward task, as it is crucial to characterize the chemical and physical conditions involved during the manufacturing of food product to be able to choose an appropriate delivery system.

ii. **Bioavailability:** At room temperature, most lipophilic bioactives (e.g. carotenoids and phytosterols) are in crystalline form, at which they are mostly not bioavailable in human body (Horn, 1989; Horn and Rieger, 2001; McClements, 2012). To overcome this problem, they must be dissolved in a lipophilic carrier (e.g. triglycerides),

which leads to dramatic increase in their bioavailability (Horn, 1989; Pouton, 2006; Porter et al., 2007). To increase the bioavailability further, the solution of bioactives-in-lipophilic carrier must be dispersed into the delivery system to achieve small droplets. This way, the crystallization can be suppressed, and therefore higher amount of bioactives can be kept in dissolved form (Horn and Rieger, 2001; Engel and Schubert, 2005). Furthermore, smaller droplet sizes of the solution also can improve the the cellular uptake of bioactives in the gastrointestinal tract (Horn, 1989; Grolier et al., 1995; Borel, 2003; Ribeiro et al. 2006; Gonnet et al., 2010).

iii. **Compatibility:** The associated delivery system should mask a possible off-flavor of the bioactive and be easily incorporated into the formulation of final food product without adversely affecting its appearance, texture, stability, or flavor.

iv. **Controlled release:** The delivery system should release the bioactives at desired rate and at the desired site–of–action in human body, e.g. it may have to protect the bioactives from the severe conditions in stomach and be trigerred to release them in small intestine.

Table 1.1: Overview of lipophilic bioactives and their potential health benefits

Group	Type	Potential health benefits	References
carotenoids	β–carotene, lycopene, lutein, and zeaxanthin	cancer, coronary heart disease, macular degeneration, and cataracts	(Giovannucci et al., 1995; Mayne, 1996; Krinsky et al., 2004)
phytosterols	stigmasterol, β–sitosterol, and campesterol	coronary heart disease, cancer, prostatitis	(Awad and Fink, 2000; Jones and Abumweis, 2009)
fatty acids	ω–3, 6, 9 fatty acids, conjugated linoleic acid	coronary heart disease, bone health, immune response disorders, weight gain, stroke prevention, cancer	(Simopoulos, 1991; Kris–Etherton, 2002)

1.3 Multiple step processing: Common approach to the delivery of lipophilic bioactives

Successful delivery of bioactives may be accomplished by firstly dissolving lipophilic bioactives in a lipophilic carrier (e.g. triglycerides), emulsifying this solution into an aqueous phase and microencapsulating the emulsified droplets within a secondary material for delivery into food products (Augustin and Sanguansri, 2008; Zuidam and Shimoni, 2009) . The emulsification step mainly improves bioavailability and allow mixing the lipophilic solution with a secondary material (i.e. delivery system). The microencapsulation step prevents undesirable interactions of the bioactive with other food ingredients or chemical reactions that can result in degradation of the bioactive, with the possible adverse effects on taste and odor. Depending on the microencapsulation method applied, the delivery system can be in a form of matrix or reservoir type. An illustration of delivery systems is given in Figure 1.1. These structured delivery systems can then be incorporated into the formulation of the final food product.

This common approach (i.e. emulsification, microencapsulation and final food processing) as well as the methods available to encapsulate the lipophilic bioactives and deliver them through the food products are shown in Figure 1.2. Most these methods have been adapted from technologies originally developed for the chemical and pharmaceutical industries, at which the microencapsulation technology is well developed and commercialized. Physical processes use conventional equipments (e.g. spray drier) to create the matrix

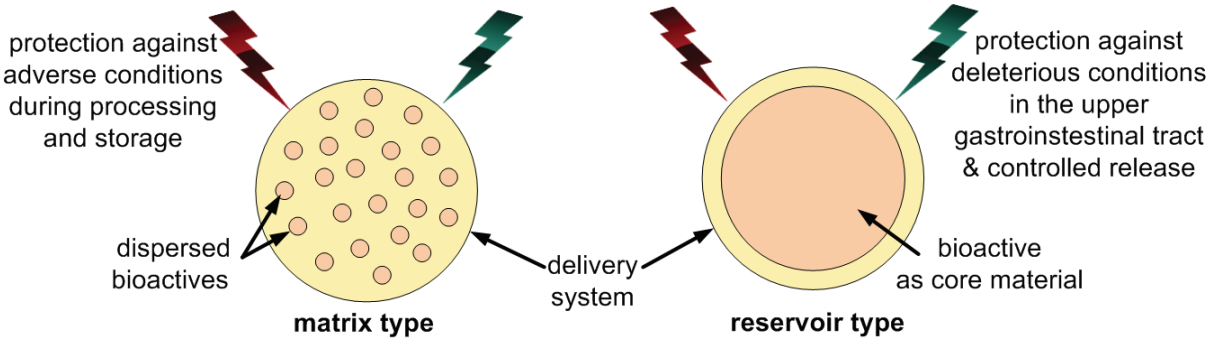

Figure 1.1: Illustration of the matrix type and reservoir type delivery systems used to protect bioactives against the severe conditions during processing and storage, and against the deleterious conditions in the upper gastrointestinal tract.

type delivery systems in solid form. Chemical processes utilize the possible interactions (e.g. electrostatic interactions) that can be promoted by varying the process conditions (e.g. pH, ionic strength) to create the delivery systems, often in liquid or semi–liquid form (Zuidam and Shimoni, 2009).

Spray drying is the most commonly used process in food industry for microencapsulation of lipophilic bioactives into dry powdery matrices (Gouin, 2004; Gharsallaoui et al., 2007). The technology is well established, and uses unit processes and equipments readily available in most food processing plants. Furthermore, it is efficient and rather

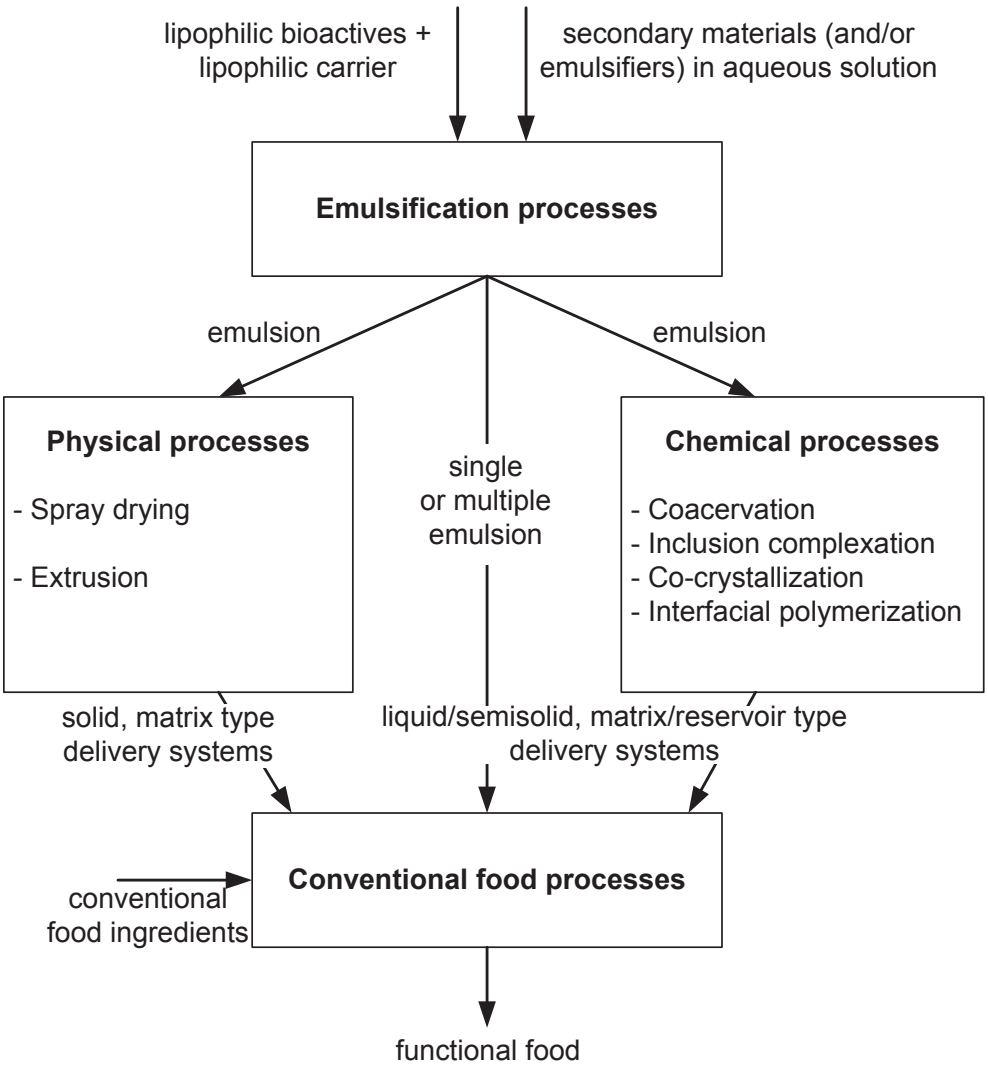

Figure 1.2: Illustration of the common approach and associated methods to encapsulate the lipophilic bioactives and deliver through the food products.

inexpensive. The spray–dried powders have reasonably good compatibility (i.e. good powder characteristics) and good stability (Gouin, 2004). This method typically involves the preparation of an emulsion including the secondary materials of the encapsulant (e.g., protein, carbohydrate) and atomization of the emulsion into the drying chamber. This leads to evaporation of the aqueous phase and the formation of matrix type delivery system (Barbosa–Cánovas et al., 2005; Gharsallaoui et al., 2007). The delivery systems prepared by this method can be incorporated into wide variety of food products such as milk powder, instant desserts and instant beverages (Gouin, 2004).

Extrusion is an alternative technology for encapsulation of lipophilic bioactives in an amorphous carbohydrate based matrix, although it has been almost exclusively used for flavor encapsulation (Madene et al., 2006). This process is often named hot melt extrusion to differentiate it from extrusion cooking which is mostly used to produce texturized and shaped food products, e.g. ready–to–eat breakfast cereals. The potential of hot melt extrusion for delivery of lipophilic bioactives was demonstrated by the study of Yilmaz et al. (2001) and the patent of (Lengerich, 2001) on encapsulation of vegetable oil, as model lipophilic carrier in a starch matrix. Figure 1.3 illustrates a typical hot melt extrusion process for encapsulation applications according to Lakkis (2007). Extruders are thermomechanical mixers that consist of one or more screws in a barrel. Mostly, co–rotating twin screw extruders are preferred for encapsulation, due to their flexibility and self cleaning nature. Typically, carbohydrate is fed into the extruder at the first barrel and melted by a combination of heat and shear in the extruder leading to the transformation of the crystalline structure into an amorphous phase. The emulsion comprising lipophilic bioactives can be incorporated into the plasticized matrix at the desired location of the extruder, e.g. often at the end of extruder to minimize the adverse effects of the thermomechanical treatment. The mixture exits the die below 100 °C to prevent the evaporation of water and thereby expansion (Lakkis, 2007), and shaped by single or multiple die orifices. Then, it is cooled to form a solid glassy material which can be grounded to a desired particle size to form compact microgranules of high bulk density. The main advantage of this process is the reasonably long shelf life of the oxidation–labile bioactives due to strong impermeability of the carbohydrate matrices in the glassy state against oxygen (Gouin, 2004; Lakkis, 2007). However, from economic point of view, the relatively limited load capacity in these systems which is around 10% makes it an unattractive encapsulation process (Gouin, 2004). Furthermore, large size of the granules,

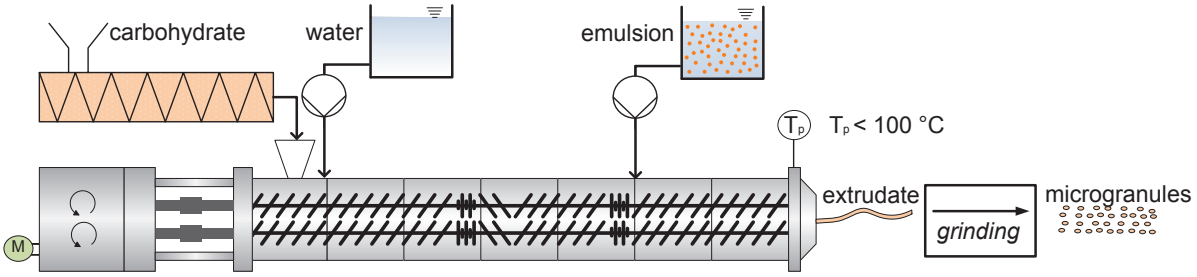

Figure 1.3: Schematic illustration of hot melt extrusion for encapsulation applications.

typically 500 – 1000 µm, formed by extrusion limit their usage in food applications due to its negative effect on mouth–feel (Gouin, 2004; Lakkis, 2007).

Besides being the first processing step in almost all industrial techniques for microencapsulation, emulsification technology may also be used solely to create delivery systems in foods for utilization mainly in aqueous–based food products (McClements et al., 2007; Sagalowicz and Leser, 2010). Oil–in–water emulsions or multiple emulsions are suitable for the delivery of lipophilic bioactives without any need of further chemical of physical processes. Kinetically stable single emulsions are commonly made by homogenizing a mixture of oil, with an aqueous solution containing the surface active encapsulating materials, such as emulsifiers and/or biopolymers which provides a means of isolating and protecting lipophilic cores. Many types of proteins and gums with emulsifying capacity have been used to encapsulate lipophilic bioactives in emulsion based delivery systems (Dickinson, 2009; 2010). Food emulsions possibly undergo several types of stresses during their manufacture, storage, transport and utilization, including pH extremes, high ionic strengths, thermal processing, freeze–thaw cycling, drying and mechanical agitation. Many of the emulsions prepared with the currently available emulsifiers for the food industry are not capable of withstanding these environmental stresses without destabilizing due to droplet flocculation or coalescence (Guzey and McClements, 2006; Garti and Amar, 2008). Nevertheless, a wide variety of emulsion–based delivery systems are currently available for the encapsulation of lipophilic bioactives. Each system has its particular features and characteristics which allow their application to a variety of food products after thorough examinations, especially regarding their stability. Fruit juices, energy drinks and dairy products are potential application areas for the emulsion based

delivery systems (Garti and Amar, 2008; Sagalowicz and Leser, 2010).

Among the various chemical encapsulation processes available, only coacervation found an application area in the food industry (Sanguansri and Augustin, 2010). Coacervates are formed by mixing two oppositely charged biopolymers in an aqueous medium under controlled conditions. This can be achieved by changing pH leading to complex formation of oppositely charged biopolymers, followed by changing the temperature to harden the complex formed around the droplets comprising the bioactive. Chemical methods have a potential for controlled release and delivery of bioactives in foods (Turgeon et al., 2007; Livney, 2010); however most of them are currently batch processes at relatively small scale. Therefore, there is significant effort going into the development of continuous processes.

When multiple-step-processing approach is used to deliver bioactives into food, it is important to ensure that the delivery system is capable of conserving their structure and protect bioactive after incorporation into the formulation of the final food product. This demands good characterization of the physical and chemical conditions involved during the processing, storage and consumption of the final food product, as well as the influence of these conditions on the stability of delivery system. In spite of this challenging task, the approach must still provide a simple, efficient and cost–effective solution compared to direct addition of bioactives. Therefore, although multiple-step-processing approach has been the state of the art to design functional foods, its layered structure involving several processes makes it complex and limits its implementation to the conventional food products.

1.4 One–step extrusion processing: A novel approach to the delivery of lipophilic bioactives

Extrusion is a highly integrated low–cost process with many unique advantages. These include energy efficiency, the lack of process effluents, and versatility with respect to ingredient selection and the shapes and textures of products that can be produced (Guy, 2001). Other than being used for encapsulation applications (as discussed in the previous section), the extrusion technology is a conventional food process (often named extrusion cooking) applied to a large number of food applications nowadays. It is a high–

temperature, short–time process in which starch and/or protein based food materials are plasticized, cooked and in some cases expanded by a combination of moisture, pressure, temperature and shear. The latter does not only gelatinize and therefore makes starch digestible, but also leads to molecular transformations and chemical reactions. Typically, starch–based foods such as ready–to–eat cereals, pastas, salty and sweet snacks are produced by extrusion cooking and are highly appreciated by consumers (Guy, 2001).

The multifunctional nature of extruders allows combining several unit operations, which can be manipulated to provide desired processing temperature and shear or elongational rate profiles by varying extrusion parameters, e.g. screw design and speed, barrel heating, feed rate or moisture/plasticiser concentration. Therefore, the processing steps involved in the conventional approach ((i.e. emulsification, microencapsulation and final food processing) to design functional foods can be reduced to only one integrated processing step. A schematic illustration of such a process is given in Figure 1.4. In the feeding zone, the screw configuration is such that the matrix and water are conveyed and mixed at a low pressure to form a homogenous feed. In the subsequent zone, an increase in pressure along with shear and temperature, achieved by kneading blocks and reverse elements, leads to melting/cooking of the matrix. In the final part of the barrel, the lipophilic carrier (e.g. triglycerides) comprising bioactives is incorporated into the plasticized matrix and dispersed into small droplets. At the end of the extruder, the melt is forced to flow through an orifice of a die, which is followed by shaping/expanding and cooling to solidify the structure and form a glassy matrix, therefore, restricting the molecular diffusion (Yilmaz et al., 2001; Lakkis, 2007).

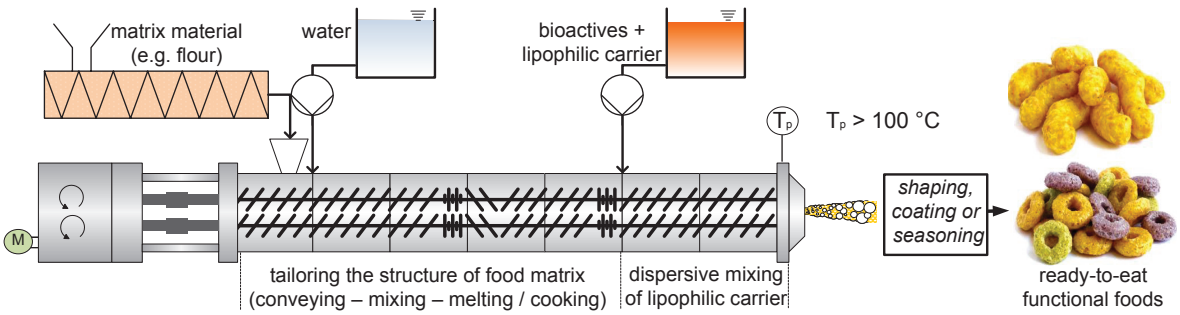

Figure 1.4: Illustration of one–step extrusion process for design of ready–to–eat functional foods.

This multifunctional character of an extruder gives rise to many unique advantages regarding the design of functional food products, namely:

i. **Stability:** Elimination of extra processing steps (i.e. emulsification, microencapsulation) reduces the variety of environmental / processing stresses which may have detrimental effect on the encapsulated bioactives. Furthermore, the modular design of the screws and the possibility of applying different profiles of process parameters or incorporating some ingredients at different points of the extrusion process offer the flexibility to account for thermal or mechanical sensitivity of bioactives.

ii. **Controlled release:** It is known that the starch structure, such as crystallinity and molecular size distribution, has strong influence on its release characteristics (Ispas–Szabo et al., 2000; Tolstoguzov, 2003; Lakkis, 2007). In the first part of the extruder, the starch structure and therefore the release chracteristics can be tailored, whereas in the second part of the extruder, the droplet size of the dispersed phase (i.e. lipophilic carrier) can be altered according to the specific requirements of each bioactive by varying the process parameters, such as screw speed and/or configuration.

iii. **Raw material:** Starch based matrices (e.g. wheat or maize flours) are the most commonly used materials in extrusion cooking (Guy, 2001). Starch and its derivatives are also widely used in the encapsulation of various food components because of its unique attributes (Lakkis, 2007). Starch is a non–allergenic, low–cost ingredient, and well perceived by consumers. It is an excellent barrier for oxygen, available in various molecular sizes, and has desirable physicochemical properties such as solubility, melting and phase change (Lakkis, 2007).

iv. **Simplicity:** There is no need for extra emulsification or encapsulation processes, which greatly simplifies the process control and shortens the time necessary for the process and product development.

v. **Versatility:** Extrusion process has the capability of producing a wide range of food products and is remarkably versatile in being able to accommodate the new demands of consumers.

Despite all these advantages, the extrusion process possesses several challenges regarding the design of functional foods. The production of directly expanded ready–to–eat products requires processing under elevated temperatures (>100 °C) and shear in order to gelatinize

the starch and make products thus digestible. These are also necessary to expand the matrix and obtain the desired texture. Since most of the bioactives are susceptible to these stresses, it is crucial to investigate the retention of lipophilic bioactives under various thermal and mechanical stresses applied to produce directly expanded ready–to–eat starch based products by an extruder. It is especially important to differentiate between the influence of mechanical and thermal stresses for the sake of better control on the product characteristics.

Another important concern is the control on dispersed phase morphology. For most lipophilic bioactives, it is favorable to dissolve the bioactive in a lipid based delivery system (e.g. triglycerides) and disperse this solution into small droplets to improve the stability, bioavailability and palatability of the bioactives (Horn, 1989; Grolier et al., 1995; Horn and Rieger, 2001; Borel, 2003; Ribeiro et al., 2006; Parker et al., 2007; Gonnet et al., 2010). Since these lipophilic carriers are immiscible with hydrophilic starch biopolymers, an effective dispersive mixing is crucial to incorporate the lipophilic bioactives and to achieve the desired dispersed phase morphology in the starch matrix, i.e., size and shape of the dispersed phase. Such a task is very challenging, since it demands a good control of the stresses present inside the extruder, which are composed of both shear and elongational stresses and vary with the actual position of the screws (Cheng and Manas–Zloczower, 1997).

Furthermore, plasticized starch shows complex rheological behavior, namely shear thinning and viscoelastic behavior (Vansoest et al., 1996; Della Valle et al., 1998). Droplet formation in viscoelastic matrices are known to differ from Newtonian systems which are well characterized (Tucker and Moldenaers, 2002). Therefore, it is necessary to determine the influence of more fundamental parameters such as shear stress, shear rate and viscosity on the formation of lipid droplets in plasticized starch that mostly includes two simultaneous mechanisms, i.e. droplet breakup and coalescence.

Although there are several studies examining the relationships between structure, rheology, extrusion process, and product characteristics of plasticized starch (e.g. Averous, 2000; Della Valle et al., 1997; Lai and Kokini, 1991; Willett et al., 1995; van den Einde et al., 2003), there is a lack of studies on these concerns regarding the dispersive mixing in a plasticized starch in an extrusion processing.

In general, it is necessary to have a good understanding of the interrelations between the

extrusion parameters and the key system parameters and the resulting product quality attributes, as schematically illustrated in Figure 1.5. Such a mechanistic insight into extrusion processing will allow innovative and advanced solutions for delivery of lipophilic bioactives through food products.

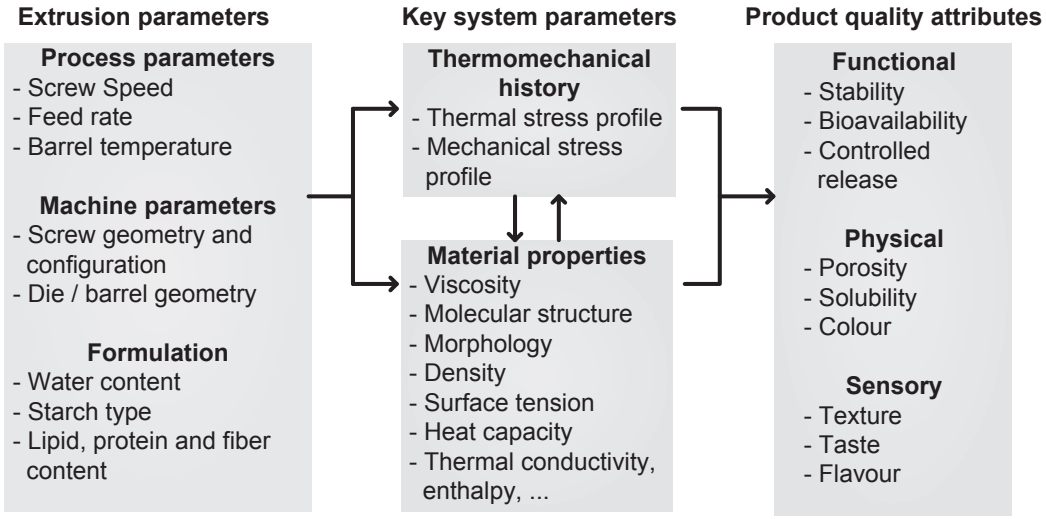

Figure 1.5: Overview of the interrelation between product quality attributes, extrusion and key system parameters.

1.5 Objective and outline of this thesis

The overall objective of this thesis is to develop an understanding of the dispersive mixing of oil in plasticized starch by extrusion processing with respect to the design of ready–to–eat functional foods.

Therefore, a special effort lies on investigating the stability of lipophilic bioactives dissolved in oil under various extrusion conditions, with the purpose being to define the mixing zone of the extruder, in which the bioactives show the highest retention.

In particular, this thesis aims at developing mechanistic methods that will characterize the dispersive mixing in extrusion processing by using computational and experimental approaches. These methods have to be able to characterize the droplet breakup and coalescence at various extrusion conditions by taking into account the main governing mechanisms. The structure of this thesis is outlined in Figure 1.6.

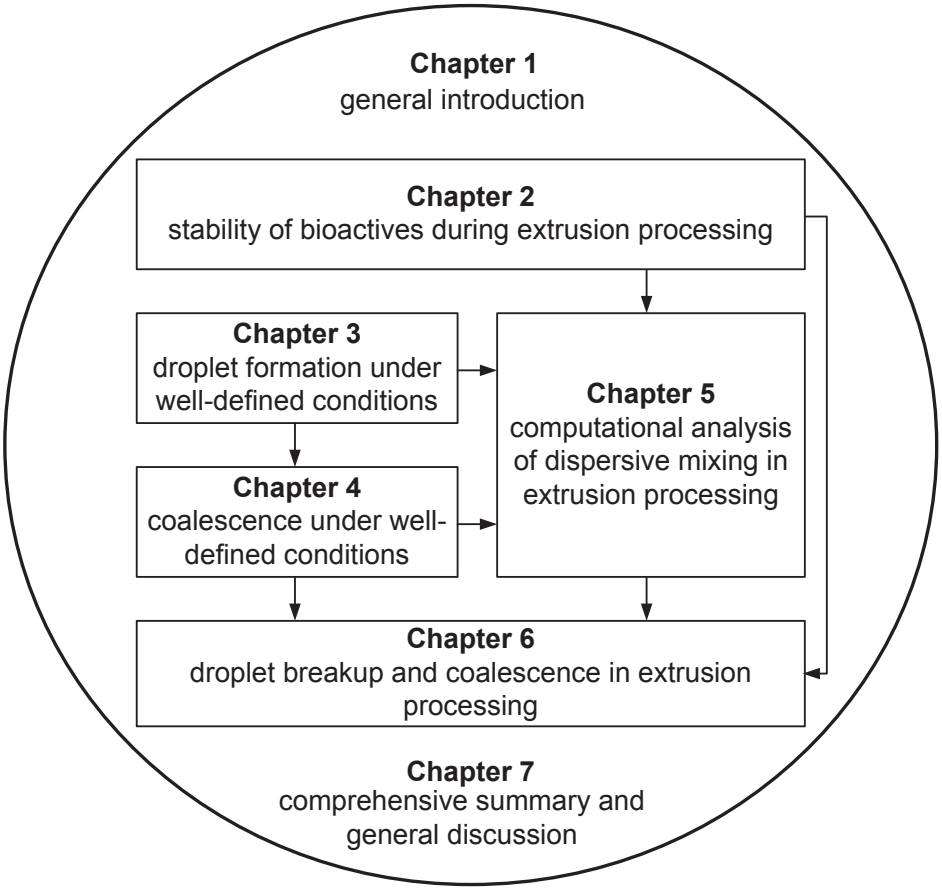

Figure 1.6: Overview of the structure of this thesis and the coherence between the chapters.

Chapter 2 deals with the retention of oil–dispersed β–carotene as a model lipophilic bioactive during extrusion processing of directly expanded starch based products. In particular, the principal applicability of extrusion processing on formulation of sensitive bioactives is verified. Insight is acquired on the influence of various extrusion conditions by using different dosing points, screw speeds and barrel temperatures. The effect of thermal and mechanical stresses on the retention of β–carotene molecules is differentiated. In the range of process parameters investigated, a mixing zone allowing the highest retention of β–carotene is established.

Chapter 3 describes the effect of defined flow conditions, namely simple shear flow applied by a specific shearing device, on the formation of triglyceride droplets in plasticized starch. The effect of the fundamental parameters such as shear stress, shear rate and viscosity on dispersed phase morphology is studied. The differences between plasticized

starch and Newtonian matrices are discussed by comparing the results with predictions from theory developed for emulsification processes.

Chapter 4 unveils the occurrence of coalescence affecting the droplet formation discussed in Chapter 3. The dimensionless numbers necessary to quantify the intensity of coalescence in well defined flow conditions are introduced. The intensity of coalescence at varying oil concentration, shear rate and viscosity are investigated. A model necessary to characterize oil droplet breakup in plasticized starch is developed.

Chapter 5 introduces a method to simulate the flow of plasticized starch in a mixing zone of a co–rotating twin screw extruder (established in Chapter 2) by using computational fluid dynamics (CFD). Influence of the rheological data measured online and the associated rheological models on the sensitivity of the simulation is presented. Computational results are compared with the results from experimental measurements. The local flow characteristics regarding the droplet breakup are investigated and the model presented in Chapter 4 is implemented into the simulation to evaluate the dispersive mixing efficiency.

In **Chapter 6**, the droplet breakup and coalescence in plasticized starch are investigated for complex extrusion conditions. For this, the methods and insights described in the preceding chapters are applied. In addition, a new method quantifying the intensity of coalescence during extrusion processing is presented. The influence of process characteristics relevant for droplet breakup and coalescence such as screw speed, screw configuration, flow rate, oil content and matrix viscosity are elucidated. The results obtained are further used to demonstrate how to enhance the dispersive mixing efficiency of extrusion processing.

Finally, **Chapter 7** provides a comprehensive summary and general discussion of the preceding chapters by linking the associated approaches and main findings. Furthermore, the scientific and practical implications of the main findings as well as the limitations of the current study are discussed. At the end, the main conclusions of this thesis and outlook are presented.

References

Augustin, M. A., & Sanguansri, L. (2008). Encapsulation of bioactives. In Aguilera, J. M. & Lillford, P. J. (Eds.), *Food Materials Science* (pp. 577–601). Springer.

Averous, L. (2000). Properties of thermoplastic blends: starch–polycaprolactone. *Polymer*, 41(11), 4157–4167.

Awad, A. B., & Fink, C. S. (2000). Phytosterols as anticancer dietary domponents: Evidence and mechanism of action. *Journal of Nutrition* 130, 2127–2130.

Barbosa–Cánovas G. V., Ortega–Rivas E., & Juliano P, Y. H. (2005). *Food powders. Physical properties, processing, and functionality*. New York, NY: Kluwer Academic/Plenum Publishers.

Block, G., Patterson, B., & Subar, A. (1992). Fruit, vegetables, and cancer prevention: a review of the epidemiological evidence. *Nutrition and Cancer*, 18(1), 1–29.

Borel, P. (2003). Factors affecting intestinal absorption of highly lipophilic food microconstituents (fat–soluble vitamins, carotenoids and phytosterols). *Clinical Chemistry and Laboratory Medicine*, 41(8), 979–94.

Cheng, H., & Manas–Zloczower, I. (1997). Study of mixing efficiency in kneading discs of co–rotating twin–screw extruders. *Polymer Engineering and Science*, 37(6), 1082–1090.

Della Valle, G., Vergnes, B., & Colonna, P. (1997). Relations between rheological properties of molten starches and their expansion behaviour in extrusion. *Journal of Food Engineering*, 31(3), 277–295.

Della Valle, G., Buleon, A., Carreau, P. J., Lavoie, P. A., & Vergnes, B. (1998). Relationship between structure and viscoelastic behavior of plasticized starch. *Journal of Rheology*, 42(3), 507.

Dickinson, E. (2010). Double emulsions stabilized by food biopolymers. *Food Biophysics*, 6(1), 1–11.

Dickinson, E. (2009). Hydrocolloids as emulsifiers and emulsion stabilizers. *Food Hydrocolloids*, 23(6), 1473–1482.

Dillard, C., & German, J. (2000). Phytochemicals: nutraceuticals and human health. *Journal of the Science of Food and Agriculture*, 1756.

Engel, R. & Schubert, H., 2005. Formulation of phytosterols in emulsions for increased dose response in functional foods. Innovative Food Science & Emerging Technologies, 6(2), pp.233–237.

Garti, N., & Amar, Y. (2008). Micro– and nano–emulsions for delivery of functional food ingredients. In Nissim Garti (Ed.), *Delivery and controlled release of bioactives in foods and nutraceuticals* (pp. 149–183). Cambridge, UK.

Garti, N. (2008). *Delivery and controlled release of bioactives in foods and nutraceuticals* (p. 478). Woodhead Publishing.

Gharsallaoui, A, Roudaut, G., Chambin, O., Voilley, A., & Saurel, R. (2007). Applications of spray–drying in microencapsulation of food ingredients: An overview. *Food Research International*, 40(9), 1107–1121.

Giovannucci, E., Ascherio, A., Rimm, E. B., Stampfer, M. J., Colditz, G. A., & Willett, W. C. (1995). Intake of carotenoids and retino in relation to risk of prostate cancer. *Journal of the National Cancer Institute*, 87(23), 1767.

Gonnet, M., Lethuaut, L., & Boury, F. (2010). New trends in encapsulation of liposoluble vitamins. *Journal of Controlled Release*, 146(3), 276–90.

Gouin, S. (2004). Microencapsulation: industrial appraisal of existing technologies and trends. *Trends in Food Dcience & Technology*, 15(7–8), 330–347.

Grolier, P., Agoudavi, S., & Azais–Braesco, V. (1995). Comparative bioavailability of diet–, oil– and emulsion–based preparations of vitamin A and β–carotene in rat. *Nutrition Research*, 15(10), 1507–1516.

Guy, R. (2001). *Extrusion Cooking: Technologies and Applications* (p. 288). Woodhead Publishing Ltd.

Guzey, D., & McClements, D. J. (2006). Formation, stability and properties of multilayer emulsions for application in the food industry. *Advances in Colloid and Interface Science*, 128–130(2006), 227–48.

Heinonen, M., Haila, K., Lampi, A. M., & Piironen, V. (1997). Inhibition of oxidation in 10% oil–in–water emulsions by β–carotene with α– and γ—tocopherols. *Journal of the American Oil Chemist's Society*, 74(9), 1047–1052.

Horn, D. (1989). Preparation and characterization of microdisperse bioavailable carotenoid hydrosols. *Die Angewandte Makromolekulare Chemie*, 166(1), 139–153.

Horn, D., & Rieger, J. (2001). Organic nanoparticles in the aqueous phase–theory, experiment, and use. *Angewandte Chemie International Edition*, 40(23), 4330–4361.

Ispas–Szabo, P., Ravenelle, F., Hassan, I., Preda, M., & Mateescu, M. a. (2000). Structure–properties relationship in cross–linked high–amylose starch for use in controlled drug release. *Carbohydrate Research*, 323(1–4), 163–75.

Jones, P. J. H., & Abumweis, S. S. (2009). Phytosterols as functional food ingredients: linkages to cardiovascular disease and cancer. *Current Opinion in Clinical Nutrition and Metabolic Care*, 12(2), 147–51.

Kaur, C., & Kapoor, H. (2008). Antioxidants in fruits and vegetables: the millenniumt's health. *International Journal of Food Science & Engineering*, 703–725.

Krinsky, N., Mayne, S., & Sies, H. (2004). *Carotenoids in health and disease*. CRC.

Kris–Etherton, P. M. (2002). Fish Consumption, Fish Oil, Omega–3 Fatty Acids, and Cardiovascular Disease. *Circulation*, 106(21), 2747–2757.

Kulås, E., Olsen, E., & Ackman, R. G. (2003). Oxidations of fish lipids and its inhibition with tocopherols. In A. Kamal–Eldin (Ed.), *Lipid Oxidation Pathways*. AOCS Publishing.

Lai, L., & Kokini, J. (1991). Physicochemical changes and rheological properties of starch during extrusion (a review). *Biotechnology Progress*, 7(3), 251–266.

Lakkis, J. (2007). *Encapsulation and controlled release technologies in food systems*. Ames, Iowa, USA: Blackwell Publishing.

Lengerich, B. V. (2001). Embedding and encapsulation of sensitive components into a matrix to obtain discrete controlled release particles.

Livney, Y. D. (2010). Milk proteins as vehicles for bioactives. *Current Opinion in Colloid & Interface Science*, 15(1–2), 73–83.

Lobstein, T., Baur, L., & Uauy, R. (2004). Obesity in children and young people: a crisis in public health. *Obesity Reviews*, 5, 4–85.

Madene, A., Jacquot, M., Scher, J., & Desobry, S. (2006). Flavour encapsulation and controlled release – a review. *International Journal of Food Science and Technology*, 41(1), 1–21.

Mayne, S. T. (1996). Beta–carotene, carotenoids, and disease prevention in humans. *The FASEB Journal*, 10(7), 690.

McClements, D. J., Decker, E. A, & Weiss, J. (2007). Emulsion–based delivery systems for lipophilic bioactive components. *Journal of Food Science*, 72(8), 109–24.

McClements, D. J. (2012). Crystals and crystallization in oil–in–water emulsions: implications for emulsion–based delivery systems. *Advances in Colloid and Interface Science*, 174, 1–30.

McClements, D. J., Decker, E. A., Park, Y., & Weiss, J. (2009). Structural design principles for delivery of bioactive components in nutraceuticals and functional foods. *Critical Reviews in Food Science and Nutrition* (Vol. 49, pp. 577–606).

Mente, A., de Koning, L., Shannon, H. S., & Anand, S. S. (2009). A systematic review of the evidence supporting a causal link between dietary factors and coronary heart disease. *Archives of Internal Medicine*, 169(7), 659–69.

Mozaffarian, D., Hao, T., Rimm, E. B., Willett, W. C., & Hu, F. B. (2011). Changes in diet and lifestyle and long–term weight gain in women and men. *The New England Journal of Medicine*, 364(25), 2392–404.

Parker, R. S., Swanson, J. E., You, C.-S., Edwards, A. J., & Huang, T. (2007). Bioavailability of carotenoids in human subjects. *Proceedings of the Nutrition Society*, 58(01), 155–162.

Porter, C. J. H., Trevaskis, N. L., & Charman, W. N. (2007). Lipids and lipid–based formulations: optimizing the oral delivery of lipophilic drugs. *Nature Reviews. Drug Discovery*, 6(3), 231–48.

Pouton, C. W. (2006). Formulation of poorly water–soluble drugs for oral administration: physicochemical and physiological issues and the lipid formulation classification system. *European Journal of Pharmaceutical Sciences*, 29(3–4), 278–287.

Ribeiro, H. S., Ax, K., & Schubert, H. (2003). Stability of lycopene emulsions in food systems. *Journal of Food Science*, 68(9).

Ribeiro, H. S., Guerrero, J. M. M., Briviba, K., Rechkemmer, G., Schuchmann, H. P., & Schubert, H. (2006). Cellular uptake of carotenoid–loaded oil–in–water emulsions in colon carcinoma cells in vitro. *Journal of Agricultural and Food Chemistry*, 54(25), p.9366.

Sagalowicz, L., & Leser, M. E. (2010). Delivery systems for liquid food products. *Current Opinion in Colloid & Interface Science*, 15(1–2), 61–72.

Sanguansri, L., & Augustin, M. A. (2010). New technologies for functional food manufacture. In J. Smith & E. Charter (Eds.), *Functional Food Product Development*.

Simopoulos, A. P. (1991). Omega–3 fatty acids in health and disease and in growth and development. *The American Journal of Clinical Nutrition*, 54(3), 438–63.

Steinmetz, K. A., & Potter, J. D. (1996). Vegetables, Fruit, and Cancer Prevention: A Review. *Journal of the American Dietetic Association*, 96(10), 1027–1039.

Tolstoguzov, V. (2003). Thermodynamic considerations of starch functionality in foods. *Carbohydrate Polymers*, 51(1), 99–111.

Tucker, C.L. & Moldenaers, P., 2002. Microstructural Evolution in Polymer Blends. *Annual Review of Fluid Mechanics*, 34(1), pp.177–210.

Turgeon, S. L., Schmitt, C., & Sanchez, C. (2007). Protein–polysaccharide complexes and coacervates. *Current Opinion in Colloid & Interface Science*, 12(4–5), 166–178.

WHO, & FAO Expert Consultation. (2003). Diet, nutrition and the prevention of chronic diseases. *WHO Technical Report Series*, 916.

Wildman, R. E. C. (2001). *Handbook of nutraceuticals and functional foods*. Boca Raton, FL: CRC Press.

Willett, J. L., Jasberg, B. K., & Swanson, C. L. (1995). Rheology of thermoplastic starch: Effects of temperature, moisture content, and additives on melt viscosity. *Polymer Engineering and Science*, 35(2), 202–210.

Xianquan, S., Shi, J., Kakuda, Y., & Yueming, J. (2005). Stability of lycopene during food processing and storage. *Journal of Medicinal Food*, 8(4), 413–22.

Yilmaz, G., Jongboom, R. O. J., Feil, H., & Hennink, W. E. (2001). Encapsulation of sunflower oil in starch matrices via extrusion: effect of the interfacial properties and processing conditions on the formation of dispersed phase morphologies. *Carbohydrate Polymers*, 45(4), 403–410.

Zuidam, N. J., & Shimoni, E. (2009). Overview of microencapsulates for use in food products or processes and methods to make them. *Encapsulation Technologies for Active Food Ingredients and Food Processing* (p. 400). Springer.

van den Einde, R. M., van der Goot, A. J., & Boom, R. M. (2003). Understanding Molecular Weight Reduction of Starch During Heating–shearing Processes. *Journal of Food Science*, 68(8), 2396–2404.

Vansoest, J., Benes, K., Dewit, D., & Vliegenthart, J. (1996). The influence of starch molecular mass on the properties of extruded thermoplastic starch. *Polymer*, 37(16), 3543–3552.

2 Retention of β–carotene as a model substance for lipophilic phytochemical during extrusion cooking

This chapter is published as: Emin, M. A., Mayer–Miebach, E., & Schuchmann, H. P. (2012). Retention of β–carotene as a model substance for lipophilic phytochemicals during extrusion cooking. *LWT – Food Science and Technology*, 48(2), 302–307.

Abstract

Incorporation of phytochemicals, such as lipophilic bioactives, into starch based food products via extrusion has become a very attractive process in the last decades. However during extrusion cooking, phytochemicals are exposed to high temperatures and high mechanical stresses accelerating oxygen or light induced as well as other chemical reactions or structural changes (i.e. isomerisation). In order to investigate processing losses due to the sensitivity of phytochemicals, oil–dispersed β–carotene as a model for lipophilic phytochemicals (e.g. carotenoids, tocopherols) was incorporated into an extrusion cooked cereal based product. Process induced stresses were varied by using different dosing points, screw speeds and barrel temperatures. An initial loss of about 30% β–carotene due to oxidative/thermal degradation was found for all process conditions investigated. Maximum retention was achieved, if the β–carotene was incorporated at the end of the extruder. Increasing the melt temperature from 135 °C to 170 °C didn't show any influence on the β–carotene retention. Increasing the screw speed from 300 to 500 1/min increased the retention significantly ($P < 0.05$) by about 25%. These results suggest that β–carotene losses are mainly affected by the generated mechanical stress in extrusion rather than by thermal stress.

2.1 Introduction

Beyond maintaining the nutritional quality, adding health–promoting and/or disease–preventing properties to food during processing is a potentially important area of research. Especially, the addition of lipophilic phytochemicals (e.g. carotenoids, phytosterols) into food products promises potential health benefits such as preventing cardiovascular diseases and some cancers (Giovannucci et al., 1995; Mayne, 1996; Steinmetz and Potter, 1996; Awad and Fink, 2000; Krinsky et al., 2004). The bioavailability of such phytochemicals mainly depends on e.g. the overall size and shape of the molecule (Britton, 1995), the solubility in oil (Dimitrov et al., 1988; Horn, 1989) and the droplet size distribution of oil dispersions (Ribeiro et al., 2006). Carotenoids are often used in foods, not only for their bioactive potential, but also for their coloring properties, making products more attractive to consumers.

Extrusion is a highly integrated low–cost process with many unique advantages for encapsulation, such as its energy efficiency, the lack of process effluents, and its versatility with respect to ingredient selection and the shapes and textures of products that can be produced (Guy, 2001). Extruders are multifunctional systems combining several unit operations, which can be manipulated to provide desired processing temperature and shear or elongational rate profiles by varying e.g. screw design and speed, barrel heating, feed rate or moisture/plasticiser concentration. It is a high–temperature, short–time process in which starchy and/or proteinacious food materials are plasticised, cooked and in some cases puffed/expanded by a combination of moisture, pressure, heating and mechanical shear. The latter do not only gelatinize starch and make products thus digestible, but also result in molecular transformations and chemical reactions.

The complex multivariate nature of the extrusion processing presents many challenges, particularly with respect to the stability of the phytochemicals, since they are exposed to thermal as well as mechanical stress during extrusion cooking. Although these problems were addressed in several studies before (Marty and Berset, 1988; Beetner et al., 1974; Guzman–Tello and Cheftel, 1990; Ilo and Berghofer 1998; Cha, Suparno et al., 2003), the mechanisms behind the deterioration during the extrusion processing is not yet well understood. Furthermore, to the best of our knowledge, the previous studies didn't consider to incorporate the lipophilic phytochemicals, as e.g. carotenoids, phytosterols, tocopherols, through a lipophilic carrier (e.g. triglycerides), which is essential to improve

their bioavailability (Dimitrov et al., 1988; Horn, 1989). Likewise, the influence of the dosing point on retention of lipophilic phytochemicals is not described in literature, yet. It is, however, expected to play an important role on the retention of sensitive phytochemicals, as the residence time and exposed thermal/mechanical stresses are highly influenced by the dosing point.

The objective of this study is to investigate the stability of β–carotene added as triglyceride–based solution to a high temperature short time (HTST) extrusion cooking of a starch based matrix with respect to the formulation and dosing point with an effort to differentiate the influences of thermal and mechanical stresses separately.

2.2 Materials and methods

2.2.1 Materials and reagents

Native maize starch C*Gel 03401 at 10 g/100 g moisture content (wet basis) was obtained from Cargill, Germany. It will be referred to as "starch" throughout the paper. Medium chain triglyceride oil (MCT–oil) was obtained from Schumann & Sohn, Germany. Synthetic β–carotene (98.9%; HPLC) was kindly supplied by BASF (Ludwigshafen, Germany). All chemicals used for extraction and HPLC analysis were purchased from Merck/VWR, Darmstadt, Germany, except otherwise stated.

2.2.2 Extrusion processing

Experiments were conducted using a co–rotating high speed twin–screw extruder ZSK 26 Mc (Coperion, Stuttgart, Germany) consisting of 7 barrels with length to diameter ratio of 29, screw and die diameter of 26 and 3 mm, respectively. The extrusion experiments were performed varying screw speed from 300 1/min to 800 1/min and melt temperature from 135 °C to 170 °C. The temperature of the starch melt was regulated by changing the barrel temperature. At the first part of the extruder, starch (10 kg/h) was mixed with water (1 kg/h) which was then plasticised under thermal and mechanical stresses generated by rotation of the screws. An illustration of the experimental set–up, screw geometry and feeding points can be seen in Figure 2.1. Synthetic β–carotene was mixed with MCT–oil to a concentration of 2 mg/ml. This β–carotene–in–oil solution was incorporated into the

extruder at two different dosing points A, B (Figure 2.1). The temperature of the melt was kept constant within the last 3 barrels of the extruder which was monitored by inline mounted temperature sensors. Therefore, average values of the temperatures measured by sensors T2 and T3 were used as the melt temperature throughout this study. At the end of the extruder, the last 2 barrels were fully filled due to the pressure generated at the extrusion die which was verified by inline mounted pressure sensors. Each experiment was conducted three times. The obtained samples were stored in evacuated plastic packages at -80 °C until the day of analysis.

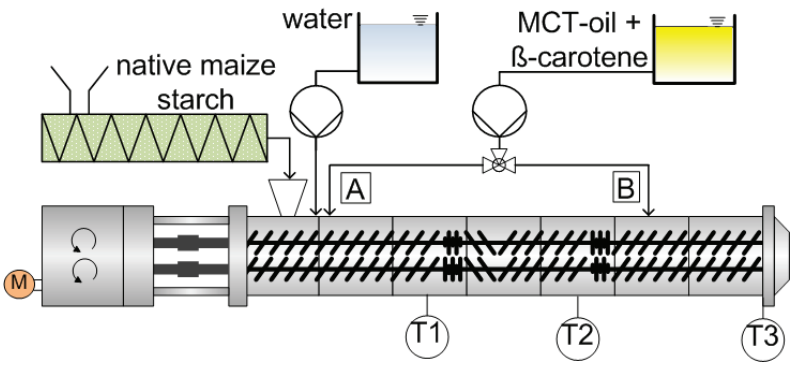

Figure 2.1: Schematic illustration of experimental set-up. β–carotene–in–oil solution was incorporated into the extruder at two different dosing points A, B. The temperature of the melt was monitored by inline mounted temperature sensors T1, T2 and T3.

2.2.3 Rheological measurements

Rheological data of the plasticized starch within the extruder were determined online by a multiple step slit die rheometer (Horvat et al., 2009). The extruder thermomechanically transforms the starch, whose rheological properties can be calculated from the pressure drop of the flow in the slit–die which is measured using flush–mounted transducers. Various shear rates necessary to obtain a viscosity curve were generated by increasing the cross section of the slit–die without any disturbance on extrusion process parameters, thus keeping the thermomechanical history of the product constant. The shear stress τ (Pa) can be calculated by Eq. 2.1

$$\tau = (\Delta P/L) \times (H/2) \tag{2.1}$$

where ΔP is the pressure drop per distance (Pa), L is the distance between two pressure sensors (mm) and H is the slit height (mm). The apparent shear rate $\dot{\gamma}_{app}$ (s^{-1}) was calculated at three different steps of the multiple step slit die rheometer by Eq. 2.2

$$\dot{\gamma}_{app} = 6Q/(B \times h^2) \tag{2.2}$$

where Q is the volumetric mass flow (mm^3/s), B is the width of the slit (mm) and h is the slit height (mm). The apparent viscosity η_{app} (Pa·s) was calculated using Eq. 2.3

$$\eta_{app} = \tau/\dot{\gamma}_{app} \tag{2.3}$$

Measured viscosity data were fitted to a power law model, which has been reported by other authors for extrusion–plasticized starch (Padmanabhan, 1991; Vergnes et al., 1993)

$$\eta_{app} = K \times \dot{\gamma}_{app}^{n-1} \tag{2.4}$$

where K is the consistency and n is the power law index. Values of n are between 0 and 1 for thermoplastics. For n < 1, the viscosity decreases with increasing shear rate; such materials are called shear thinning. Values for the power law index n and the consistency K were obtained from the linear regression analysis of a double logarithmic plot of Eq. 2 vs Eq. 3.

2.2.4 Extraction and analysis of β–carotene

Extruded samples were extracted twice. Aliquots of 10 g were rehydrated with 75 mL of ultrapure water (Milli–Q Advantage A10, Millipore, Schwalbach, Germany) for 30 min at room temperature and homogenised (Ultra Turrax, IKA–Werke, Staufen, Germany). 150 mL of ice–cold tetrahydrofuran containing 0.1 g/100 mL butylated hydroxytoluene (Acros Organics/VWR, Darmstadt, Germany) (THF/BHT) were added slowly under continuous stirring. After further incubation for 10 min, the extraction mixture was re–extracted with petroleum ether until colourless (as checked visually) and discarded. The β–carotene containing organic phase was washed with water, dried overnight at 8 °C using anhydrous sodium sulphate, filtered and evaporated to dryness at 40 °C under reduced pressure (Rotavapor R–205, Büchi, Essen, Germany), flushed with nitrogen

gas and stored at -86 °C until HPLC–analysis. All experiments were carried out under subdued light to prevent photo–degradation and isomerisation.

For HPLC analysis, all extracts were re–dissolved in THF/BHT and measured twice according to a modified method described by Emenhiser et al., (1995) using an HPLC equipment (LaChrom Elite, VWR/Hitachi, Darmstadt, Germany) consisting of a quarternary pump, an auto–sampler, a column oven and a photodiode array detector combined with a software for controlling, data acquisition and analysis (EZChrom Elite, VWR/Hitachi, Darmstadt). All–trans–β–carotene and the 9–cis, 13–cis and 15–cis isomers were separated on a C30 reversed phase column (250 mm $\times$ 4.6 mm; 5 μm) (YMC Europe, Dinslaken, Germany) at 27 °C using a linear gradient of methyl t–butyl ether (MTBE) in methanol for 50 min (starting phase composition: 81 mL/100 mL methanol, 15 mL/100 mL MTBE, 4 mL/100 mL water, end phase composition: 36 mL/100mL methanol, 60 mL/100 mL MTBE, 4 mL/ 100 mL water) at a flow rate of 1 mL/min. The isomers were identified based on retention time and specific absorption spectra (Britton, 1995). All–trans–β–carotene ($\geqslant$ 97%; UV) (Fluka/Sigma–Aldrich, München, Germany) was used as calibration standard for quantification. Results are given as mean values with the corresponding standard deviations.

2.2.5 Statistical analysis

Results are expressed as mean values $\pm$ standard deviations of triplicate trials in minimum. Statistical analysis was performed using the ANOVA procedure (SigmaPlot 11.0, Systat Software GmbH, Erkrath, Germany) with significance levels set at $P < 0.05$).

2.3 Results and discussion

2.3.1 Stability of β–carotene during pre–mixing, extraction and HPLC analysis

To examine the stability of β–carotene during pre–mixing, extraction and HPLC analysis, we mixed the β–carotene–in–oil solution intensely to plasticised starch without applying thermal or mechanical stress. For this purpose, the β–carotene–in–oil solution was incorporated into plasticized starch at the end of the extruder and mixed at extremely

mild process conditions: No extruder die was used, screw speed (180 1/min) and barrel temperature (25 °C) were kept low and water content (47 g/100 g) was kept high. Medium chain triglyceride oil (MCT–oil) was chosen, because it does not form lipid–amylose complexes when mixed with starch (Schweizer et al., 1986; French et al., 1963).

According to HPLC analysis, 74.9 ± 2.8 mg of total β–carotene was extracted per kg extrusion mixture on a dry mass base (mg/kg dm) which is about 97 ± 3.6 g/100 g of the amount given originally to the sample.

β–carotene used in this study was comprised of all–trans, 9–cis, 13–cis and 15–cis isomers that represented 85.6 ± 6.7, 4.4 ± 0.2, 2.2 ± 0.2 and 13.1 ± 0.9 g/100 g of the total mass, respectively. Extracted β–carotene had very similar amounts of all–trans, 9–cis, 13–cis and 15–cis isomers which were 84.9 ± 2.3, 4.9 ± 0.6, 5.7 ± 0.4, 4.5 ± 1.3 g/100 g, respectively. This proves that β–carotene was stable during mixing with the MCT–oil and maize starch as well as during the extraction procedure and the HPLC measurement.

2.3.2 Stability of β–carotene during extrusion processing as a function of the dosing point

The β–carotene–in–oil solution was incorporated into the extruder at two different dosing points, which are shown as A and B in Figure 2.1. The starch differs in structure at these dosing points, namely not yet plasticised (at point A) and plasticised (at point B). Screw speed, water content and oil content were kept constant at 500 1/min, 18 g/100 g and 4 g/100 g, respectively. Melt temperature was kept at the range of 150 ± 10 °C.

If the β–carotene–in–oil solution is incorporated after starch plastification (Figure 2.1, B), the total β–carotene and all–trans isomer contents were reduced to 52.7 ± 4.9 and 28.7 ± 3.1 mg/kg dm, respectively, equivalent to retentions (c/c_0) of 0.70 and 0.45 (Table 2.1). On the other hand, there is an increase in 9–cis, 13–cis and 15–cis isomers, which indicates the isomerisation of all–trans isomer to cis–isomers. Both, contents and retentions of β–carotene are given in Table 2.1a, b. The overall loss of about 30% of total β–carotene content is explicable by mainly oxidative degradation of β–carotene to almost volatile final reaction products (Marty and Berset, 1990). However, literature data concerning an application of β–carotene after starch plastification during extrusion cooking are not available, yet.

Table 2.1: β–carotene contents (a) and retentions (c/c_0) (b) after extrusion cooking (feed rate 11 kg/h, screw speed 500 1/min, water content 18 g/100 g, oil content 4 g/100 g, melt temperature range 150 $\pm$ 10 °C) incorporated at different dosing points (A, B). Initial β–carotene contents (c_0) were 74.9 $\pm$ 2.8, 63.6 $\pm$ 0.7, 3.6 $\pm$ 0.6, 4.3 $\pm$ 0.5 and 3.4 $\pm$ 1.1 for total contents and all–trans, 9–, 13– and 15–cis isomers, respectively.

feeding point	total	all–trans	9–cis	13–cis	15–cis
	a) β–carotene content [mg/kg dm]				
A	39.7 $\pm$ 9.5	19.8 $\pm$ 6.3	5.3 $\pm$ 2.2	10.6 $\pm$ 2.6	4.0 $\pm$ 0.5
B	52.7 $\pm$ 4.9	28.7 $\pm$ 3.1	6.0 $\pm$ 2.8	13.2 $\pm$ 2.1	4.9 $\pm$ 0.7
	b) β–carotene retention c/c_0[-]				
A	0.53 $\pm$ 0.13[a]	0.31 $\pm$ 0.10[a]	1.45 $\pm$ 0.64[a]	2.45 $\pm$ 0.60[a]	1.19 $\pm$ 0.16[a]
B	0.70 $\pm$ 0.07[b]	0.45 $\pm$ 0.05[b]	1.64 $\pm$ 0.76[a]	3.06 $\pm$ 0.48[a]	1.45 $\pm$ 0.20[b]

[a,b] All values are means $\pm$ standard deviations of triplicate trials. Means with different letters within the same column are significantly different ($P < 0.05$).

If, according to common practice, the β–carotene–in–oil solution is incorporated at the beginning of the extrusion process (Figure 2.1, A), the total β–carotene and all–trans isomer retention (c/c_0) is 0.53 and 0.31, respectively (Table 2.1). This overall loss of about 70% of all–trans–β–carotene determined is in accordance with literature data although extrusion cooking conditions were not identical. A degradation of all–trans–β–carotene in the range of 65% was reported by Guzman–Tello and Cheftel (1990), who extruded synthetic all–trans–β–carotene mixed directly with wheat flour (twin screw extruder, feed rate 30 kg/h, water content 18.6 g/100 g, screw speed of 150 1/min, barrel temperatures 150 °C). According to Lee et al., 1978), approximately 74% of β–carotene mixed into white maize meal was degraded. Marty and Berset (1986) reported that the extrusion cooking at 180 °C was a more drastic treatment for β–carotene than simple heating for a long period (2 h) at the same temperature. According to their data, all–trans–β–carotene retention (c/c_0) was about 0.08 during extrusion cooking, while 85% and 92.5% of the initial concentration remained from thermal treatment in presence/absence of oxygen, respectively.

Degradation of β–carotene during extrusion processing resulted from oxidation driven by thermal and mechanical stresses (Marty and Berset 1986). When the solution is incorporated at the end of the extruder, the β–carotene molecules are exposed to mechanical and

thermal stresses for a shorter time resulting in a 10% higher retention of the total content as compared to an application prior to starch plastification. Furthermore, due to structural changes and increase in the melt temperature, the viscosity of the starch matrix decreases during its flow in the extruder. This means that, at the end of the extruder, β–carotene molecules are not only exposed to the mechanical stress for shorter time, but also the extent of these stresses is lower.

Based on the promising results for the β–carotene incorporation at the end of the extruder and due to the lack of information in literature for this approach, the influences of thermal and mechanical stresses were investigated experimentally and discussed in the next sections.

2.3.3 Influence of melt temperature on β–carotene retention

Over the whole range of investigated melt temperatures a 35 °C rise in temperature didn't have any influence on the total β–carotene content with about 75% retention. Figure 2.2 shows the retention of β–carotene (c/c_0) as a function of the melt temperature during extrusion processing. The β–carotene–in–oil solution was incorporated into the extruder after starch plastification (Figure 2.1, B). Initial β–carotene contents (c_0) were 74.9 $\pm$ 2.8, 63.6 $\pm$ 0.7, 11.3 $\pm$ 2.1 for total content, all–trans and total cis–isomers, respectively. Due to the variation of barrel temperatures between 80 °C and 170 °C, the temperature of starch melt was varied in the range of 135 to 170 °C. The screw speed, water content and feed rate were kept constant at 500 1/min, 18 g/100 g and 11 kg/h. The retention of all–trans–β–carotene (c/c_0) remains constant at a level of about 0.50 at all varied melt temperatures (Figure 2.2). Likewise, the isomerisation of the all–trans isomer due to temperature increase is negligible. Nevertheless, retention of total cis–isomer (c/c_0) varies between 1.75 to 2.50 at the range of investigated melt temperature; suggesting that the isomerisation takes place due the initial thermal degradation as proposed by Sweeney and Marsh (1971) and Chandler and Schwartz (1988). Here, it is noteworthy to mention that the viscosity of the starch matrix decreases with an increasing temperature (Della Valle, 1996). This leads to a decrease in applied mechanical stress at higher melt temperatures, even if the screw speed is kept constant. Since increasing the melt temperature has a contrary effect on the thermal and mechanical stresses, a concrete conclusion regarding the influence of thermal stress on β–carotene retention remains challenging to draw.

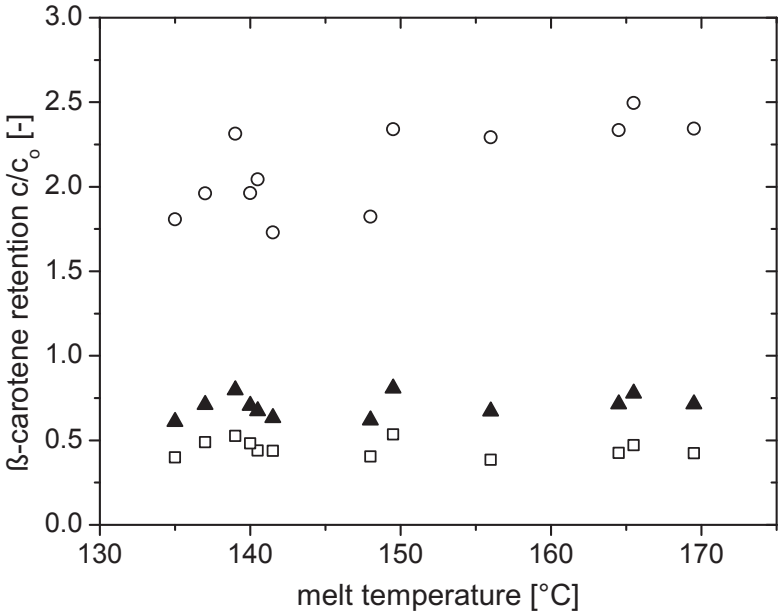

Figure 2.2: Retention (c/c_0) of total β–carotene (▲), all-trans (□) and total cis isomers (○) during extrusion processing of native maize starch at varying melt temperature with β–carotene solution incorporated after starch plastification (screw speed 500 1/min, water content 18 g/100 g, oil content 4 g/100 g, feed rate 11 kg/h).

2.3.4 Influence of screw speed on β–carotene retention

β–carotene contents and retentions of the samples extruded at 3 different screw speeds of 300, 500 and 800 1/min are given in Table 2.2a,b. Feed rate and water content were kept constant at 11 kg/h and 18 g/100 g, respectively. Melt temperature was kept constant at 145 $\pm$ 5 °C. Dosing point and initial concentration of β–carotene were the same as during the experiments with varied melt temperatures. Mean total β–carotene retentions (c/c_0) of 0.45, 0.71 and 0.65 resulted from screw speeds of 300, 500 and 800 1/min, respectively. The results suggest that the retention of β–carotene could be significantly ($P < 0.05$) increased by about 26% by just increasing the screw speed from 300 to 500 1/min (Table 2.2). When the screw speed increased further to 800 1/min, a slight but statistically not significant decrease of 6% in β–carotene retention was observed. Nevertheless it is still 20% higher compared to the samples extruded at 300 1/min. The ratio of all–trans to total cis–isomers remained constant at 55:45 during screw speed variation.

At the end of the extruder, barrels are fully filled with plasticised starch as it was measured by inline pressure sensors (data not shown). The mean residence time t_m at the fully filled

Table 2.2: β–carotene contents (a) and retentions (c/c_0) (b) after extrusion cooking of maize starch at various screw speeds (feed rate 11 kg/h, water content 18 g/100 g, oil content 4 g/100 g, melt temperature range 145 $\pm$ 5 °C). Initial β–carotene contents (c_0) were 74.9 $\pm$ 2.8, 63.6 $\pm$ 0.7, 3.6 $\pm$ 0.6, 4.3 $\pm$ 0.5 and 3.4 $\pm$ 1.1 for total contents and all–trans, 9–, 13– and 15–cis isomers, respectively.

screw speed [1/min]	total	all–trans	9–cis	13–cis	15–cis
	a) β–carotene content [mg/kg dm]				
300	33.9 $\pm$ 9.3	18.1 $\pm$ 5.7	3.6 $\pm$ 1.6	7.4 $\pm$ 3.3	4.7 $\pm$ 1.5
500	53.4 $\pm$ 6.6	30.3 $\pm$ 3.6	4.3 $\pm$ 0.6	13.5 $\pm$ 2.4	5.3 $\pm$ 0.6
800	48.7 $\pm$ 6.6	26.6 $\pm$ 4.3	5.1 $\pm$ 2.5	12.0 $\pm$ 1.0	5.0 $\pm$ 0.6
	b) β–carotene retention c/c_0[-]				
300	0.45 $\pm$ 0.12[a]	0.29 $\pm$ 0.09[a]	0.99 $\pm$ 0.45[a]	1.72 $\pm$ 0.76[a]	1.39 $\pm$ 0.44[a]
500	0.71 $\pm$ 0.09[b]	0.48 $\pm$ 0.06[b]	1.18 $\pm$ 0.17[a]	3.13 $\pm$ 0.55[b]	1.56 $\pm$ 0.17[a]
800	0.65 $\pm$ 0.09[b]	0.42 $\pm$ 0.07[b]	1.40 $\pm$ 0.69[a]	2.79 $\pm$ 0.24[b]	1.48 $\pm$ 0.18[a]

[a,b] All values are means $\pm$ standard deviations of triplicate trials. Means with different letters within the same column are significantly different ($P < 0.05$).

section of the extruder depends only on the feed rate of the matrix Q and free volume of the extruder barrel V.

$$t_m = V/Q \tag{2.5}$$

Since the flow rate was kept constant during the experiments, the mean residence times of the samples were also constant at the fully filled section of the extruder. However, the variance of the residence time distribution depends on the screw speed and expected to decrease with increasing screw speed (Carneiro et al., 2004). Nevertheless, such a change in the variance alone cannot explain the increased retention of β–carotene at 500 1/min, since further increase in screw speed up to 800 1/min does not lead to higher retention of the β–carotenee. Thermal degradation is, therefore, not expected to be the reason for the increasing β–carotene retentions at higher screw speeds, since the temperature was also kept constant.

In contrast, the applied mechanical stress changes as the shear rate and matrix viscosity changes with screw speed, and therefore are expected to play an important role in β–

carotene degradation. This is discussed in the next section in detail.

2.3.5 Influence of rheological properties and flow characteristics on β–carotene retention

Plasticised starch extruded at 300, 500 and 800 1/min (feed rate, water content, melt temperatures identical to the experiments concerning β–carotene stability) showed shear thinning behaviour (Table 2.3), since power law indices (n) are well below 1 (see section 2.2.3). Increasing screw speed led to increasing n values indicating that the matrices show less shear thinning behaviour when extruded at higher screw speeds. More relevantly, the consistency value (K) was decreased significantly when the screw speed was increased suggesting that the viscosity of the matrix decreases with an increasing screw speed. Van den Einde et al., (2004) showed that the transformation of starch molecules under mechanical stress only depends on the applied maximum stress. With the screw geometry selected for the present study, the maximum stress is to be generated at the reverse screw elements located at the fifth barrel. It was therefore expected that the molecular structure, and thus, the viscosity of the starch further doesn't change at the end of extruder (where dosing point B is located), which was confirmed by the measured rheological data obtained by the online slit die rheometer (data not presented here).

During an extrusion process maximum mechanical stress is generated at the clearence between the screw elements and the barrel wall where the flow is dominated by shear flow (Emin et al., 2011). Hence, the maximum shear stress τ_{max} can be calculated from

Table 2.3: Rheological properties of plasticised starch matrices and generated maximum shear stress during the extrusion processing at various screw speeds (feed rate 11 kg/h, moisture content 18 g/100 g, melt temperature 145 $\pm$ 5 °C).

screw speed N (1/min)	power law index n	consistency K (Pa·s)	maximum shear rate $\dot{\gamma}_{max}$ (1/s)	maximum shear stress τ_{max} (kPa)
300	0.329	14716	567	141.5
500	0.344	8366.2	945	125.2
800	0.52	3311.7	1512	80.00

the maximum shear rate $\dot{\gamma}_{max}$ as long as the viscosity of matrix η_{matrix} is known.

$$\dot{\gamma}_{max} = \pi \times d \times (N/60)/\delta \tag{2.6}$$

$$\tau_{max} = \dot{\gamma}_{max} \times \eta_{matrix} \tag{2.7}$$

where d is the diameter of screws (m), N is the screw speed (rpm) and δ is the flight clearance (m).

The results given in table 2.3 suggest that the maximum shear stress was decreased when the screw speed was increased from 300 1/min to 500 1/min from 141.5 kPa to 125.2 kPa. Although the screw speeds were higher, the viscosity of the starch matrix was lower at 500 1/min which led to lower maximum shear stress. In our previous study (Emin et al., 2011), we simulated the flow of the plasticised starch matrix at the end of the twin screw extruder (screw speed of 200 and 400 1/min, feed rate of 11 kg/h) and showed that almost all of the droplets flowing in the extruder are exposed to maximum shear stress at least one time until the end of their flow. Therefore, we expect that the β–carotene molecules dissolved in MCT–oil droplets were exposed lower shear stress at 500 than 300 1/min, which is consequently the reason of higher β–carotene retention at 500 1/min.

On the other hand, the maximum shear stress generated at 800 1/min is lower than at 500 1/min but the β–carotene retention is slightly but not significantly changed (i.e. 6% decrease) when the screw speed is increased from 500 1/min to 800 1/min. This can be explained by the frequency of the exposure to the maximum shear stress which might increase at higher screw speeds. However, a more detailed study, for instance using computational fluid dynamics simulation, is necessary to understand better the flow patterns and resulting shear stress–time profile during extrusion cooking. Nevertheless, measured and calculated results suggest that the retention of β–carotene at the end of extruder is mainly affected by the generated mechanical rather than by thermal stress.

2.4 Conclusions

With respect to the stability during extrusion cooking, it is favourable to incorporate bioactive phytochemicals such as β–carotene only after the plastification of the starch (i.e. at the end of the extruder). In that way, β–carotene retention could be increased by 10%. This could be explained by a shorter exposure time to thermal and mechanical stresses

and, especially, by lower absolute values of the mechanical (shear) stress.

It is further reported that a minimal loss in β–carotene of about 30% was found in all samples being extrusion cooked. Beyond that, β–carotene degradation was independent of temperature in the range of melt temperatures investigated (135 – 170 °C): In this range, the retention of total contents was always at about 70%. On the other hand, it is shown that the retention of β–carotene could be significantly ($P < 0.05$) increased by about 25% by increasing the screw speed from 300 to 500 1/min. This could be explained by decreased mechanical stress at higher screw speeds, which were calculated using online measurements of the matrix viscosity.

Although the complete differentiation of the influences of thermal and mechanical stress remains still challenging, it has been shown that the retention of β–carotene, when incorporated after starch plastification at the end of extruder, is mainly affected by the generated mechanical stress rather than the thermal stress.

Nomenclature

c_0	initial β–carotene content	c/c_0	β–carotene retention
B	width of the slit	ΔP	pressure drop
h	slit height	Q	volumetric flow rate
τ	shear stress	L	distance between pressure sensors
η_{app}	apparent viscosity	$\dot{\gamma}_{app}$	apparent shear rate
K	consistency	n	power law index

2.5 References

Awad, A. B., & Fink, C. S. (2000). Phytosterols as anticancer dietary domponents: Evidence and mechanism of action. *Journal of Nutrition* 130, 2127–2130.

Beetner, G., Tsao, T., Frey, A., & Harper, J. (1974). Degradation of thiamine and riboflavin during extrusion processing. *Journal of Food Science*, 39(1), 207–208.

Britton, G. (1995). Structure and properties of carotenoids in relation to function. *The FASEB Journal*, 9(15), 1551.

Carneiro, O. S., Covas, J. A., Ferreira, J. A. & Cerqueira, M. F. (2004). On–line monitoring of the residence time distribution along a kneading block of a twin-screw extruder. *Polymer Testing*, 23, 925–937.

Cha, J. Y., Suparno, M., Dolan, K. D., & Ng, P. K. W. (2003). Modeling thermal and mechanical effects on retention of thiamin in extruded foods. *Journal of Food Science*, 68(8), 2488–2489.

Chandler, L. A., & Schwartz, S. J. (1988). Isomerization and Losses of trans–β–carotene in Sweet Potatoes as Affected by Processing Treatments. *Journal of Agricultural and Food Chemistry*, 36, 129–133.

Della Valle, G. (1996). Influence of amylose content on the viscous behavior of low hydrated molten starches. *Journal of Rheology*, 40(3), 347.

Dimitrov, N., Meyer, C., Ullrey, D., & Chenoweth, W. (1988). Bioavailability of β–carotene in humans. *American Journal of Clinical Nutrition*, 298–304.

Emenhiser, C., Sander, L., & Schwartz, S. (1995). Capability of a polymeric C30 station-

ary phase to resolve cis-trans carotenoid isomers in reversed-phase liquid chromatography. *Journal of Chromatography A*, 707(2), 205–216.

Emin, M. A., Köhler, K., Schlender, M., & Schuchmann, H.P. (2011). Characterization of Mixing in Food Extrusion and Emulsification Processes by Using CFD. (W. E. Nagel, D. B. Kröner, & M. M. Resch, Eds.)*High Performance Computing in Science and Engineering'10*, 443–462. Berlin, Heidelberg: Springer.

French, D., Pulley, A.O. & Whelan, W.J., (1963). Starch fractionation by hydrophobic complex formation. *Starch–Stärke*, 15(10), 349–354.

Giovannucci, E., Ascherio, A., Rimm, E. B., Stampfer, M. J., Colditz, G. A., & Willett, W. C. (1995). Intake of carotenoids and retino in relation to risk of prostate cancer. *Journal of The National Cancer Institute*, 87(23), 1767.

Guy, R. (2001). *Extrusion Cooking: Technologies and Applications* (p. 288). Woodhead Publishing Ltd.

Guzman-Tello, R., & Cheftel, J. (1990). Colour loss during extrusion cooking of β–carotene-wheat flour mixes as an indicator of the intensity of thermal and oxidative processing. *International Journal of Food Science and Technology*, 25(4), 420–434.

Horn, D. (1989). Preparation and characterization of microdisperse bioavailable carotenoid hydrosols. *Die Angewandte Makromolekulare Chemie*, 166(1), 139–153.

Horvat, M., Emin, M. A., Schuchmann, H.P., Hochstein, B., & Willenbacher, N. (2009). A multiple–step online–slit-die rheometer for investigations of the influence of extrusion process parameters on the rheological behaviour of starch-based food products. *Proceedings of the 5th International Symposium on Food Rheology and Structure*, ETH Zürich, 474–475.

Ilo, S., & Berghofer, E. (1998). Kinetics of thermomechanical destruction of thiamin during extrusion cooking. *Journal of Food Science*, 63(2), 312–316.

Krinsky, N., Mayne, S., & Sies, H. (2004). *Carotenoids in health and disease*. CRC Press.

Lee, T. C., Chen, T., Alid, G., & Chichester, C. 0. (1978). Stability of vitamin A and provitamin A in extrusion cooking processing. *AICHE Symposium Series* 74, 172, 192–195.

Marty, C., & Berset, C. (1986). Degradation of trans–β–carotene during Heating in

Sealed Glass Tubes and Extrusion Cooking. *Journal of Food Science*, 51(3), 698–702.

Marty, C., & Berset, C. (1988). Degradation Products of Trans–β–carotene produced during Extrusion Cooking. *Journal of Food Science*, 53(6), 1880–1886.

Marty, C. & Berset, C. (1990). Factors affecting the thermal degradation of all–trans–β–carotene. *Journal of Agricultural and Food Chemistry*, 38(4),1063–1067.

Mayne, S. T. (1996). β–carotene, carotenoids, and disease prevention in humans. *The FASEB Journal*, 10(7), 690.

Padmanabhan, M. (1991). Flow behavior and exit pressures of corn meal under high–shear–high–temperature extrusion conditions using a slit diea). *Journal of Rheology*, 35(3), 315.

Ribeiro, H. S., Guerrero, J. M. M., Briviba, K., Rechkemmer, G., Schuchmann, H. P., & Schubert, H. (2006). Cellular uptake of carotenoid-loaded oil-in-water emulsions in colon carcinoma cells in vitro. *Journal of Agricultural and Food Chemistry*, 54(25), 9366–9.

Schweizer, T.F., Reimann, S., Solms, J., Eliasson, A.C. & Asp, N.G. (1986). Influence of drum-drying and twin-screw extrusion cooking on wheat carbohydrates, II, effect of lipids on physical properties, degradation and complex formation of starch in wheat flour. *Journal of Cereal Science*, 4(3), 249–260.

Steinmetz, K. A., & Potter, J. D. (1996). Vegetables, Fruit, and Cancer Prevention:: A Review. *Journal of the American Dietetic Association*, 96(10), 1027–1039.

Sweeney, J. P., & Marsh, A. C. (1971). Effect of processing on provitamin A in vegetables. *Journal of the American Dietetic Association*, 59(3), 238–43.

Van den Einde, R.M., Akkermans, C., van der Goot, A.J. & Boom, R.M. (2004). Molecular breakdown of corn starch by thermal and mechanical effects. *Carbohydrate Polymers*, 56(4), 415–422.

Vergnes, B., Della Valle, G., & Tayeb, J. (1993). A specific slit die rheometer for extruded starchy products. Design, validation and application to maize starch. *Rheologica Acta*, 32(5), 465–476.

3 Formation of oil droplets in plasticized starch matrix in simple shear flow

This chapter is published as: Emin, M. A., Hardt, N., van der Goot, A. J., & Schuchmann, H. P. (2012). Formation of oil droplets in plasticized starch matrix in simple shear flow. *Journal of Food Engineering*, 112(3), 200–207.

Abstract

This paper describes the effect of simple shear flow on the formation of triglyceride oil droplets in a plasticized starch matrix. An in–house developed shearing device was used that enabled the application of controlled shear flow and rheological characterization of the native maize starch–triglyceride blends at shear stresses of up to 37 kPa. Due to the high viscosity of starch matrix, the viscosity ratio of the continuous starch phase and the dispersed triglyceride phase varied between 10^{-7} and 10^{-5}. It was possible to create small droplets with a droplet diameter of 2.1 μm using simple shear flow only. An increase in shear rate had no influence on droplet diameter. However, an increase in oil content led to a vast increase in droplet diameter indicating the occurrence of coalescence. The results further show that the maximum stable droplet size in plasticized starch is significantly smaller (up to 100 times) than the predicted values for a Newtonian matrix. The differences of plasticized starch to Newtonian matrices are discussed in detail.

3.1 Introduction

Incorporation of functional hydrophobic components into extruded starch based products has gained interest by food industry as well as by chemical, pharmaceutical, and medical industries (Shogren et al., 1993; Ellis et al., 1998; Yilmaz et al., 2001; Mano et al., 2003). The properties of such products do not only depend on the functional components' distribution in the matrix, but also on the microstructure obtained during processing. For most hydrophobic components (e.g. bioactive lipids, flavors, antimicrobials, antioxidants or drugs), it is favorable to dissolve the hydrophobic component in a lipid based delivery system and disperse this solution into small droplets to improve the stability, bioavailability and palatability of the functional component (Horn, 1989; Horn and Rieger, 2001; Ribeiro et al., 2006). Especially small droplets (< 1 μm) are qualified to enhance bioavailability of the encapsulated substances (Ribeiro et al., 2006) due to hindered crystallization inside the small droplets (Horn and Rieger, 2001). Starch has several attributes that make it favorable for encapsulation applications. Starch is a non–allergenic, low–cost ingredient, and well perceived by consumers. It is available in various molecular sizes, and has desirable physicochemical properties such as solubility, melting and phase change (Lakkis, 2007). Physicochemical properties being important for target release characteristics can be adapted by the molecular structure of the matrix (Wing et al., 1988; Freiberg and Zhu, 2004). However, starch is a hydrophilic biopolymer, which is not compatible with hydrophobic components. As a consequence the desired components cannot be dissolved in the starch matrix. That is why an effective mixing process is required to disperse the hydrophobic components into sufficiently small droplets in the starch matrix.

Extrusion is a versatile process used to mix and disperse liquids into highly viscous matrices, such as starch. The lipid–based delivery system containing the bioactives is dispersed into the starch, which is plasticized by the heat and shear provided by the extruder. When passing and leaving the extruder die, the dispersion is shaped and solidified upon cooling and water evaporation, bringing the starch matrix into the glassy state, restricting the molecular diffusion and improving stability (Yilmaz et al., 2001; Lakkis, 2007).

Despite the abundant literature on the relationships between structure, rheology, extrusion process, and product characteristics of plasticized starch (e.g., Lai and Kokini, 1991;

Willett et al., 1995; Della Valle et al., 1997; Averous, 2000; van den Einde et al., 2003), there is a lack of studies on droplet breakup and coalescence in a plasticized starch matrix. To the best of our knowledge, there is only one study on the droplet formation in plasticized starch matrix through extrusion, which was conducted by Yilmaz et al. (2001). They studied the influence of several extrusion parameters such as screw speed, screw geometry and emulsifier content on the emulsification of sunflower oil in plasticized maize starch. This study gives a good insight on the relation between the process parameters and final droplet morphology. However, to understand the mechanisms behind the droplet formation, the influence of more fundamental physical parameters like shear stress, shear rate and total deformation has to be investigated in more detail. This is challenging due to the fact that the stresses present inside the extruder vary with the actual position inside the machine and are composed of both shear and elongational stresses (Cheng and Manas–Zloczower, 1997). Furthermore, the final droplet size might not only result from droplet breakup but also from coalescence. The use of controlled flow conditions could provide the understanding of the droplet formation process in plasticized starch matrices. Unfortunately, conventional rheometer is not sufficient for this purpose, due to the limited shear stresses that this apparatus can apply to the material. That is why a dedicated shearing device is developed that allows controlled deformation of highly viscous matrices (Peighambardoust et al., 2004; van den Einde et al., 2004; Habeych et al., 2008).

The aim of this study is therefore to investigate the formation of triglyceride droplets in a plasticized starch matrix in simple shear flow using a dedicated shearing device. The droplet sizes obtained will be compared with predictions from theory developed for emulsification processes.

3.2 Materials and Methods

3.2.1 Materials

Native maize starch, C*Gel 03401, was obtained from Cargill, Germany. It will be referred to as “starch” throughout the paper. Medium chain triglyceride oil (MCT–oil) was obtained from Schumann & Sohn, Germany. MCT–oil was chosen, because it does not form lipid–amylose complexes when mixed with starch (French et al., 1963;

Schweizer et al., 1986). To make the oil droplets visible under confocal laser scanning microscopy (CLSM), Nile Red (purchased from Sigma–Aldrich, Germany) was used as a lipophilic fluorescent dye.

3.2.2 Methods

3.2.2.1 Shear cell

One of the main challenges concerning a study on droplet formation in plasticized starch is the necessity of elevated temperature and pressure to plasticize the starch, and to prevent the evaporation of water. Furthermore, high torque levels ($>$ 200 Nm) have to be realized due to the high viscosity of plasticized starch. Under these experimental circumstances, traditional rheometers are hardly applicable.

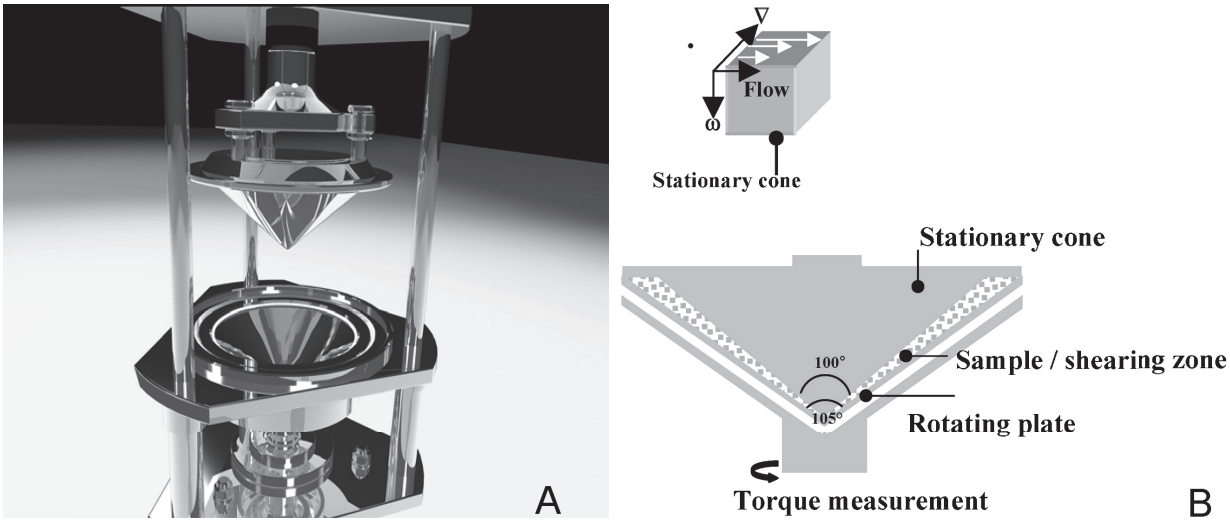

Figure 3.1: The shear cell device. (A) Animation and (B) schematic overview of the shear cell device. Cone angle = 100 °, angle between cone and plate (shearing zone), θ = 2.5°(Habeych et al., 2008).

The shear–cell, an in–house built device of Wageningen University (The Netherlands), was designed to process biopolymeric systems under simple shear flow (Habeych et al., 2008). The shear cell and its extents are demonstrated in Figure 3.1. Thickness of the product layer inside the shear cell device is kept small compared to the diameter of

the cones to apply a linear shear rate profile at relatively low rotational speeds, thereby avoiding circular flow. The circulating lower cone is connected to a Brabender Do–corder unit with an interface and controller unit (PL2100, Brabender Measurement and Control Systems, Duisburg, Germany) to monitor the torque and the rotational speed. The upper cone is kept rotationally immobile, while it is vertically connected to a hydraulic pump to pressurize the shear cell up to 400 kPa. Both cones are heated electrically, and the upper cone is equipped with a water cooling system. A gear box is used between the Brabender unit and the shear cell to provide a fivefold speed reduction allowing higher torque values at low shear rates. The shear cell is designed to generate shear stresses up to 200 kPa with the shear rates up to 120 s^{-1}. The temperature of the material is measured by a set of thermocouples located at different positions in the upper cone. Furthermore, the contact surface of both cones is roughened (serrated) to avoid wall slip. Thus starch can be plasticized at low water contents (similar to those found in extrusion processing) and conduct experiments at controlled flow and temperature conditions.

3.2.2.2 Sample preparation

Nile red was dissolved in MCT–oil at a concentration of 0.033 mg/ml to visualize droplets under confocal laser scanning microscopy (CLSM). Before the shear cell treatment, 260 g of a starch–water–oil pre–mixture was prepared by slowly adding water and stained oil into the starch, while the mass was stirred with a spatula. An overfilling or underfilling of the shear cell causes uneven distribution of the shear stresses that could be detected from fluctuations at the measured values. Therefore, the filling mass of 260 g was determined with preliminary experiments by varying the filling mass and measuring the shear stress profiles of the conducted shear cell treatments.

After filling the sample into the lower cone, the device was closed by the upper cone and a constant pressure of 400 kPa was applied allowing working above evaporation temperature of the water. Subsequently, the sample was heated from room temperature to technically–possible maximum temperature (113 °C) at a heating rate of 6 °C/min. This temperature was then kept for 5 min to allow for an even distribution of temperature and relaxation of material before processing. Thermal degradation of the starch during this stage was assumed to be rather small according to results by van den Einde et al. (2004).

After temperature was constant at 113 °C, the experiments were conducted by increasing

the shear rate linearly from zero shear to the desired shear rate (i.e. 5 s^{-1}, 24 s^{-1} or 120 s^{-1}) in one minute. Then, the shear rate was kept constant for another 4 min and the generated torque was recorded by a computer. Directly after the end of treatment, the samples were cooled down to room temperature in the shear cell at a cooling rate of about 10 °C/min. The samples were then stored at 4 °C in a refrigerator until further analysis. Table 3.1 summarizes the experimental parameters used.

Table 3.1: Experimental Parameters.

Parameter	Unit	Range
Water content	% (dry basis)	50 – 100
Oil content	% (dry basis)	0.5, 2, 4
Shear rate	s^{-1}	5, 24, 120
Temperature	°C	113

3.2.2.3 Rheological evaluation

The design of the shear cell is based on a cone–plate rheometer, likewise with a cone angle of 2.5°and adjacent tip of the upper cone to the lower cone. This geometry ensures the generation of constant shear rates $\dot{\gamma}$ all over the shear cell, which can be calculated from the rotational speed ω and the angle α of the lower cone:

$$\dot{\gamma} = \omega/\alpha \tag{3.1}$$

The engine torque M monitored by the Brabender control unit then gives the shear stress τ:

$$\tau = 3M/2\pi r^3 \tag{3.2}$$

where r is the cone radius of the shear cell. Due to the sealing design of the shear cell, the outer rim of the upper cone contacts the lower cone. Before filling the sample, the shear cell was therefore calibrated by measuring the empty torque value at the shear rate applied. From these values, the apparent viscosity of blend η_b is calculated according to:

$$\eta_b = \tau/\dot{\gamma} \tag{3.3}$$

Therefore, the apparent viscosity of the blend (i.e. mixture of plasticized starch and MCT–oil) was measured simultaneously during the shear cell treatment.

The apparent viscosity of the MCT–oil was measured with a conventional Anton Paar Physica MCR301 rheometer with a cone and plate geometry (CP50–1/TG–SN15821) at a gap width of 0.049 mm. Measurements were conducted at the same conditions as during the shear cell treatment: The temperature was set to 113 °C and the shear rate ranged from 1 to 120 s^{-1}. MCT oil showed Newtonian behavior at the range of measurements with a viscosity of 0.0028 ± 1.5% Pa·s.

3.2.2.4 Droplet size distribution

The droplet size distributions of MCT–oil in plasticized starch were analyzed by confocal laser scanning microscopy and image processing software. For the analysis, four specimens with a dimension of 15×7×0.11 mm were cut from each sample using a blade and a microtome. Because of the sealing design of the shear cell, the exerted shear rate, and thus, the shear stress on the outer rim of the sample was expected to be slightly different from the rest of the sample. The specimens were therefore taken cautiously from different locations, namely 2 and 5 cm away from the outer rim of the sample at which the sample's thickness are about 5 and 4 mm, respectively. This way the influence of geometrical confinement on droplet breakup is also evaluated. Each specimen was then placed on a separate glass slide that was wetted with distilled water and closed with a cover slide. The oil had already been stained with Nile Red before sample processing in the shear cell. The CLSM used was a Zeiss LSM 510–META 18 (Zeiss, Oberkochen, Germany), which consisted of an Axiovert 200M. A 63× Plan–Apochromat/1.4 oil immersion lens was chosen to take the images. Nile Red was excited with an Argon–laser at the wavelength of 514 nm and the emitted light was filtered by a LP 560 filter. From each specimen, 10 images with a dimension of 202×202 μm were taken from different locations. To assure that the previous cutting procedure of the specimens did not influence the droplet sizes, images were taken at the depth of 20 to 100 μm within the specimens by changing the focal point of the lens. In general, 40 images from each sample were taken. The images obtained were further analyzed using digital image processing software (ImageJ software, National Institutes of Health, USA). Droplet area and diameter were analyzed.

CLSM–images are generated by using the light emitted from certain slice thickness (e.g. 1

μm). As droplets are not always "cut" at the biggest diameter (in the middle of the sphere), the apparent size distribution of the droplets observed at the surface is not identical with the real size distribution. A conversion of their diameter distribution into that of the original spheres is problematic. This problem is known as the "tomato salad problem". Several authors proposed algorithms to solve this problem (Fleischer, 1994; Gegner et al., 2004). Scott (1990) as well as Sundararaj et al. (1995) found errors of less than 10% with and without consideration of this problem. The correction algorithm was therefore not used in this study. Depending on the process parameters, 8000 to 20000 droplets per sample were counted. The results are plotted as an area–weighted cumulative size distribution (Q_2) and density distribution (q_2). The droplet sizes of $D_{90,2}$, $D_{50,2}$ and D_{max} (i.e. maximum droplet size) were determined from the cumulative area–weighted size distribution (Q_2). $D_{90,2}$ and $D_{50,2}$ refer the droplet size bigger than all droplets forming 90% and 50% of total droplet area, respectively.

3.3 Theoretical background

One of the most important parameters to describe the droplet behavior under flow is a dimensionless number called the capillary number (Ca) (Taylor, 1932; 1934). The capillary number represents the ratio between the deforming viscous forces and the shape conserving interfacial forces:

$$Ca = \tau/(2\sigma/D) \tag{3.4}$$

where τ is the shear stress, σ is the interfacial tension between the droplet and matrix phase, and D is the diameter of the droplet. The capillary number corresponding to the critical value at which the droplet becomes unstable and breaks is called the critical capillary number (Ca_{crit}). The critical capillary number depends on the viscosity ratio (λ), which is a dimensionless parameter describing the ratio between the viscosities of the dispersed phase and the continuous phase. This dependency was established and validated for Newtonian systems (Grace, 1982; Bentley and Leal, 1986; Debruijn, 1991). The authors found that droplet breakup in a simple shear flow occurs most favorably at an intermediate range of $0.1 < \lambda < 1$. At lower λ values – as found for the systems investigated here –, Cacrit steadily increases with decreasing λ values. No breakup is possible at $\lambda > 4$. Empirical fit to Grace's data at $\lambda < 0.1$ was given by Hinch and Acrivos

(1980):

$$Ca_{crit} = 0.17 \cdot \lambda^{-0.55} \tag{3.5}$$

3.4 Results and Discussion

3.4.1 Rheological Behavior of Plasticized Starch

A quantitative analysis of droplet breakup under simple shear requires the knowledge of the rheological properties of the droplet and the continuous phase. For concentrated systems, the breakup of a droplet in a concentrated emulsion is determined by the average blend viscosity η_b rather than the continuous phase η_c viscosity (Armbruster, 1990; Jansen et al., 2001).

The apparent viscosity of the blend was derived from torque measurements obtained during the shear cell treatments as described in section 3.2.2. When a starch suspension is heated, different conversion processes (i.e. gelatinization, melting) take place that change the structural order of the starch granule irreversibly. These processes are affected by temperature, the amount of water present, and applied mechanical forces like shearing. If the starch is not only treated thermally but also mechanically, molecular degradation will happen most likely (Brümmer et al., 2002; van den Einde et al., 2004). During this study, we observed that the degradation of the starch lead to a decrease in apparent blend viscosity up to 12% during 4 minutes of shearing treatment at which the shear rate was kept constant. The extent of this effect depended on process conditions (i.e. water content, oil content, shear rate). Therefore, the average values of the measured shear stresses were used for the calculations.

The influence of water content and shear rate on the apparent blend viscosity is depicted in Figure 3.2. The results show a shear thinning behavior of the blend in the investigated shear rate range. This rheological behavior is typical for polymer solutions (Dealy and Larson, 2006) and expected, as starch is a mixture of two (bio–) polymers with amylose and amylopectin, respectively, being the monomers.

Increasing water content leads to a decrease in the apparent blend viscosity as expected. The results are in accordance with previous studies conducted on native maize starch (i.e. Vergnes and Villemaire, 1987; Willett et al., 1995; Xie et al., 2009). It is here noteworthy

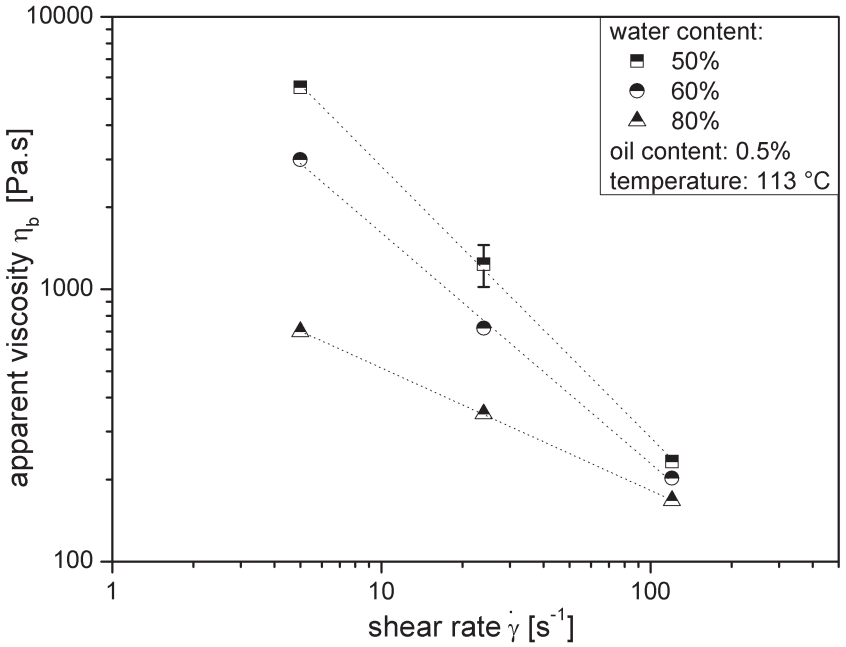

Figure 3.2: Flow curves of the blends with water content of 50, 60 and 80% at constant temperature of 113 °C.

to mention that in contrast to many synthetic polymers, the starch molecules, especially amylopectin molecules, which are longer in molar mass and branched, are susceptible to the stresses applied (Brümmer et al., 2002; van den Einde et al., 2004). Decrease in the apparent blend viscosity at higher shear rates is, therefore, not only driven by the shear thinning behavior typically found for polymer molecules aligning in a shear field, but also by the degradation of the starch molecules and decrease in molar mass due to higher stresses.

The typical standard deviation of the experimental value is given for the experiment with 50% water content at shear rate of 24 s^{-1}. For its evaluation the experiment was repeated three times.

A perfectly even distribution of the pre–mixture into the lower cone of the shear cell was challenging. This affected the reproducibility of the experiments up to 15% by means of shear stress deviation measured at the triplicate experiment. However, the effects of variations in moisture content or other changes in process parameters were notably larger.

The apparent viscosity of the blend as a function of oil content is given in Figure 3.3 for three different water contents (50, 60 and 80%). The shear rate was kept constant at

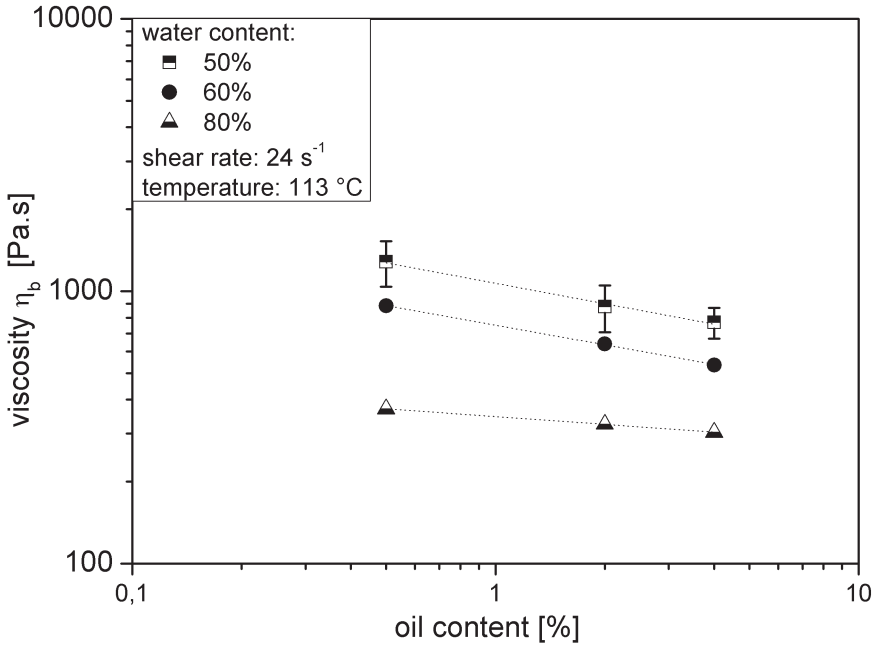

Figure 3.3: Influence of the oil content on the apparent viscosity of the blends with water content of 50, 60 and 80% at constant temperature of 113 °C.

24 s^{-1} during these measurements and the oil content was varied from 0.5 to 4%. The results for 50% water content are the means of triplicate trials. It is clear from Figure 3.3 that the apparent blend viscosity decreases with increasing oil content independent of the water content. Similar results were also found by Dautant et al. (2007) who worked on rice flour with lipid contents of 3% to 7% by using a slit die rheometer. The influence of the oil content is not as strong as the one of the water content, which is cause by the fact that oil is dispersed in the matrix, while water is able to act a plasticizer. The dependency of the apparent blend viscosity on oil content is moderate for higher water contents at which the apparent blend viscosity is low.

Table 3.2 shows the viscosity of native maize starch measured at previous studies (i.e. Vergnes and Villemaire, 1987; Willett et al., 1995; Xie et al., 2009) by different methods. To facilitate the comparison of experimental values, only the viscosities measured at the relevant process conditions and shear rate of 5 s^{-1} are presented. However, the thermomechanical treatment of the starch prior to the rheological measurements remains still different. Willett et al. (1995) and Xie et al. (2009) measured the viscosity of pre-extruded and pelletized starch during a second extrusion step. Vergnes and Villemaire

(1987), however, used a pre–shearing device for a defined pre–treatment of the starch. Despite the different methods and thermomechanical treatments, the results are in the same range.

Table 3.2: Viscosity of native maize starch measured by different methods ($\dot{\gamma}$ = 5 s^{-1}).

Reference	Temperature [°C]	Moisture content [%] (wet basis)	Measurement method	Viscosity η [Pa·s]
Xie et al. 2009	110	27	Slit die	5594
Willett et al. 1995	110	30	Torque rheometer	8120
Vergnes et al. 1987	110	33	Slit die	4298
This study	113	33	Shear cell	5510

3.4.2 Influence of shear rate on droplet formation

Figure 3.4 shows the influence of the shear stress on the droplet size $D_{50,2}$, for shear rates of 5, 24 and 120 s^{-1}. The oil content was kept constant at 0.5%. The applied shear stresses were changed by altering the apparent blend viscosity through the water content of the matrix. The detailed information about the experiments is given in Table 3.3.

At the range of shear stresses applied, droplet sizes ($D_{50,2}$) down to 2.1 μm were measured. Yilmaz et al. (2001) worked on a similar system (i.e. sunflower oil in plasticized maize starch) by using a twin–screw extruder. They showed that the size of dispersed oil droplets varies in the range of 3.3 μm to 35.6 m depending on the process parameters used (e.g. screw speed, screw geometry). It must be noted that they used the mean diameter $D_{1,2}$ for presenting their results which might give significantly lower values than the median of the area weighted size distribution ($D_{50,2}$) used in this study. Nevertheless, smaller droplet sizes are found in the experiments conducted with the shear cell. It is an unexpected result, because in addition to simple shear stresses, elongational stresses are present inside the extruder which are more effective in droplet deformation and breakup (Grace, 1982; Bentley and Leal, 1986). These stresses are, however, inhomogeneous. A possible explanation for the small droplets obtained could be the fact that within the shear cell,

Table 3.3: Viscosity of native maize starch measured by different methods ($\dot{\gamma}$ = 5 s^{-1}).

Shear rate $\dot{\gamma}$ [s^{-1}]	Blend viscosity η_b [kPa·s]	Shear stress τ [kPa]	$D_{50,2}$ [μm]	$D_{90,2}$ [μm]	D_{max} [μm]	Viscosity ratio η_d/η_b [10^{-7}]
5	0.70	3.40	4.5	9.3	17.3	40
5	0.95	4.64	3.7	6.7	13.0	29
5	1.36	6.64	4.8	10.4	16.6	21
5	3.00	14.64	3.9	7.1	15.1	9
5	5.51	26.88	2.9	5.0	11.3	5
24	0.35	8.24	3.9	7.2	16.0	80
24	0.39	9.23	2.9	6.0	13.6	72
24	0.72	17.01	2.5	5.9	15.6	39
24	1.01	23.85	2.1	3.9	18.0	28
24	1.05	24.73	2.8	4.7	10.9	27
24	1.37	32.39	2.6	4.6	12.2	20
24	1.47	34.72	2.2	3.8	7.2	19
120	0.17	20.00	3.4	6.2	13.0	167
120	0.20	24.19	2.8	4.9	11.4	138
120	0.23	27.80	2.9	5.1	9.9	120

the stresses are constant all over the sample during the whole process time. All of the droplets are therefore exposed to the maximum available stress in the flow, which lead to the breakup of the droplet to the maximum diameter that is stable in the flow.

The results in Figure 3.4 suggest that the droplet size is a function of the shear stress. This dependency is, however, very moderate as the droplet size $D_{50,2}$ is only halved (4.8 μm to 2.1 μm) with about ten times increase in the applied shear stress (3.5 kPa to 35 kPa).

At a constant shear stress, the apparent blend viscosity decreased with increasing shear rate. Therefore, it led to a higher viscosity ratio of the blend (Table 3.3). According to Eq. 3.5, the critical capillary number decreases with increasing viscosity ratio. Hence, smaller droplets were expected at the higher shear rates. The results in Figure 3.4, however, show that a change in shear rate did not influence the droplet diameter. One reason might be that the increasing coalescence of droplets becomes more relevant at higher shear rates. The importance of coalescence is further discussed in the following sections.

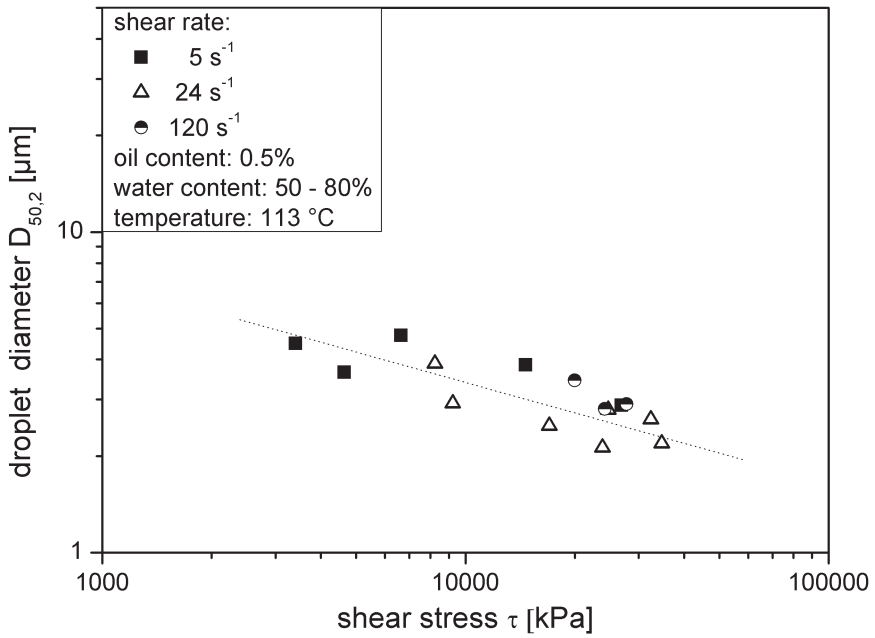

Figure 3.4: Influence of shear stress on droplet diameter ($D_{90,2}$) at shear rates of 5, 24 and 120 s^{-1}.

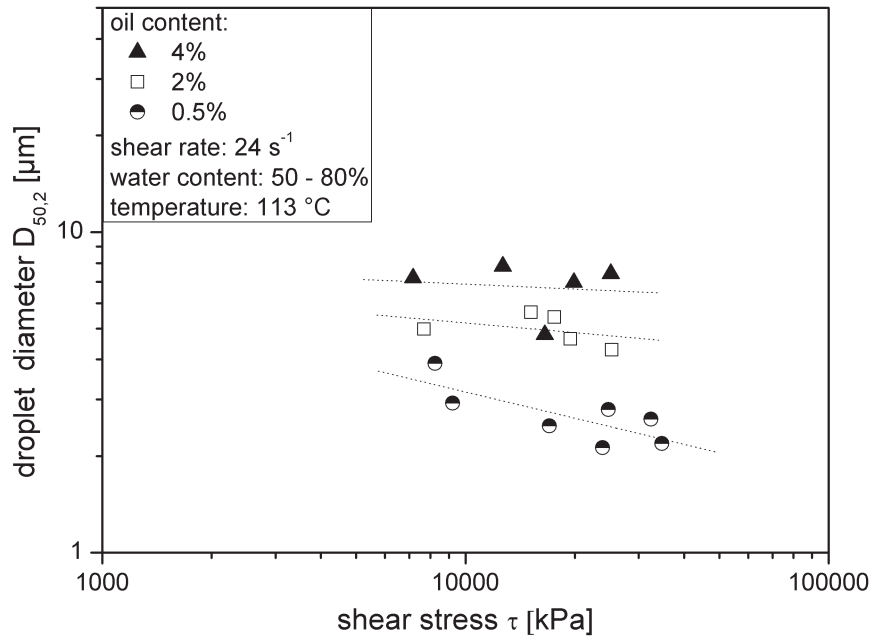

Figure 3.5: Influence of shear stress on droplet diameter at oil contents of 0.5, 2 and 4%.

3.4.3 Influence of oil content on droplet formation

The droplet diameters ($D_{50,2}$) as a function of the applied shear stress are given in Figure 3.5 for different oil contents (0.5%, 2% and 4%). The shear rate during these experiments was kept constant at 24 s^{-1}. The shear stress was varied by altering the water content of the matrix in the range of 50 to 80%.

The results clearly show that increasing the oil content led to bigger droplets. Furthermore, the droplet diameters did not show any negative correlation with the shear stress at oil contents of 2% and 4%. This indicated the occurrence of coalescence during the treatment in the shear cell. Coalescence at low disperse phase contents is seldom reported, as the number of droplets is an important parameter for droplet collision, and thus for the coalescence.

This phenomenon is, therefore, investigated in more detail. The viscosity is known to have an influence on the coalescence rate (Chesters, 1991; Yoon et al., 2005). To investigate the influence of oil content only, the density size distributions of the samples with similar viscosities but different oil contents of 0.5, 2, and 4% were plotted in Figure

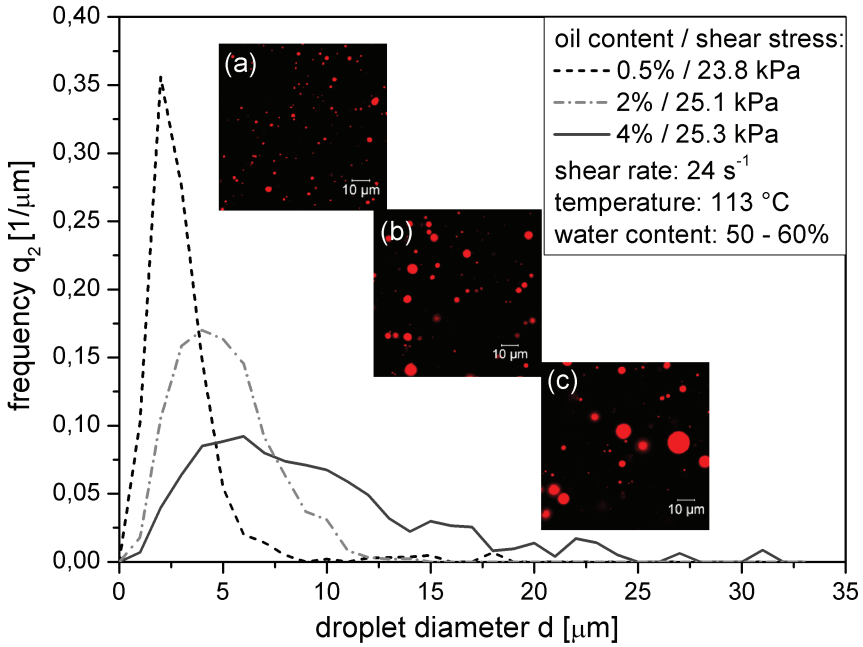

Figure 3.6: Droplet size distributions and CLSM images of the samples with oil contents of (a) 0.5%, (b) 2% and (c) 4%, which were sheared at 23.8 kPa, 25.1 kPa and 25.3 kPa, respectively.

3.6. The shear stresses were similar, because the shear rate was kept constant during these experiments at 24 s^{-1}. In case of a coalescence–free system, similar droplet size distributions of the samples are expected. However, bigger droplets are found with increasing oil content (see Figure 3.6). Moreover, the droplet size distribution gets broader. The CLSM images obtained from these samples are also depicted in Figure 3.6. These images clearly show the influence of increasing oil content on droplet sizes. These findings suggest coalescence of oil droplets, which is expected to increase with higher oil content.

3.4.4 Comparison of breakup in plasticized starch with Newtonian matrices

The critical capillary number defines the maximum droplet size (D_{max}) that is stable under the applied stress (Taylor, 1934):

$$Ca_{crit} = \tau/(2\sigma/D_{max}) \tag{3.6}$$

For Newtonian systems at low viscosity ratios, $\lambda < 0.1$, the maximum stable droplet diameter (D_{max}) can therefore be derived from Eq.3.4 and Eq.3.5:

$$D_{max} = 0.34 \cdot \lambda^{-0.55} \cdot \sigma/\tau \tag{3.7}$$

For the calculation of the maximum stable droplet diameter D_{max}, the interfacial tension between the triglyceride droplets and plasticized starch at the process conditions is necessary. Since the available measurement methods are not applicable to plasticized starch above the water boiling point of 100 °C, the interfacial tension was estimated from the measurements conducted by Yilmaz et al. (1999). Yilmaz et al. (1999) measured the interfacial tension of oil droplets in maize starch paste using a tensiometer, fitted with a platinum ring attachment. The measurements were carried out at 70 °C and the measured value was 13.29 mN/m. In our study, shearing experiments were conducted at higher temperature of 113 °C, at which the interfacial tension is expected to be lower. Based on the temperature dependency of the interfacial tension in polymer melts given in literature (Roe, 1968; Kamal et al., 1994; Robeson, 2007), the value of 10 mN/m was estimated. As no emulsifiers or interfacial active molecules were added to the formula,

the interfacial tension is assumed to be constant during the experiments. This must not necessarily be the case, since the water content was altered in the range of 50% to 80%. The error resulting from this was estimated to be up to 20% of the absolute value of the interfacial tension based on the measurements of Yilmaz et al. (1999).

Figure 3.7 gives the maximum stable droplet diameter versus shear stress calculated from Eq 3.2. For comparison, the maximum droplet diameters measured in our experiments at shear rates of 5, 24 and 120 s^{-1} are also plotted in the same figure. During the experiments, the shearing time was kept long enough (240 s) to ensure that the droplet sizes reach an equilibrium. The oil content was kept low at 0.5% to minimize the probability of coalescence. The detailed information about the experiments is given in Table 3.3.

The maximum droplet diameter found experimentally varied between 7 μm and 17 μm at the investigated range of shear rate and shear stress. The predicted maximum droplet diameter is, however, significantly bigger compared to the experimental results. The difference is about 10 times for the shear rate of 120 s^{-1} and increases up to about 100 times for the shear rate of 5 s^{-1}.

A major aspect to be critically analyzed is the rheological characteristics of the phases. The critical capillary number used to calculate the predicted values are obtained from Newtonian systems (Grace, 1982). Plasticized starch matrix, however, is known to depict non–Newtonian, namely shear–thinning and viscoelastic behavior (Vansoest et al., 1996; Della Valle et al., 1998). Droplet breakup mechanism in a viscoelastic matrix is known to differ from the Newtonian case. Despite the vast amount of studies on this aspect, the picture is still incomplete: Already in 1972, Flumerfelt reported that a viscoelastic matrix stabilizes a Newtonian droplet against breakup leading to a higher critical capillary number than the corresponding Newtonian one. However, Elmendorp and Maalcke (1985) observed that increasing the normal stress in a shear–thinning polymer solution increases the deformation of a Newtonian droplet. Moreover, Mighri et al. (1998) showed that matrix elasticity increases the deformation of a droplet indirectly supporting the results of Elmendorp and Maalcke (1985). Most recent studies presented clear evidence that a Newtonian droplet deforms less if the matrix is viscoelastic (Guido et al., 2003; Sibillo et al., 2004; Verhulst et al., 2007; Verhulst et al., 2009). These results seemingly contradict each other, and the physical mechanisms behind the observed behavior remain unknown. A Newtonian droplet in a viscoelastic matrix is not only subjected to the viscous but also

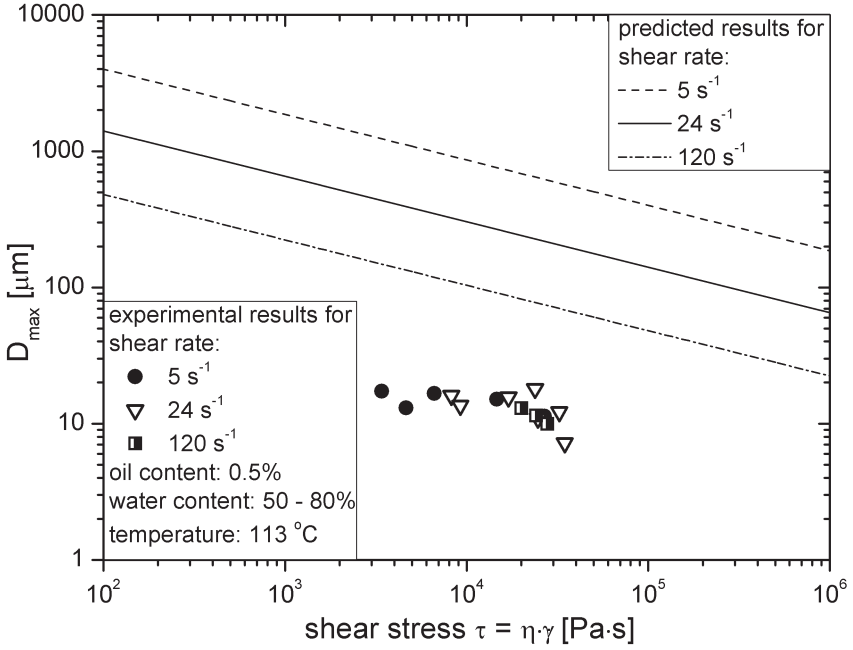

Figure 3.7: Influence of shear stress and shear rate on the maximum stable droplet size predicted by Eq. 3.7 and measured in the experiments.

to the elastic forces of the matrix. The viscoelastic effects comprise the contribution of these stresses at the droplet interface as well as the modification of the flow by the stresses over the entire domain, which eventually has an influence on the droplet deformation (Ramaswamy and Leal, 1999; Yue et al., 2005). It is also noteworthy to mention that not only the rheological character of the matrix and the disperse phase but also the flow history and the viscosity ratio affect the contribution of the viscoelastic stresses at the interface (Verhulst et al., 2009). The experiments in this study are conducted at remarkably high shear stresses up to 35 kPa and at very low viscosity ratios (10^{-7} to 10^{-5}) compared to the here mentioned studies. Therefore, the comparison of the results with other studies in the literature must be taken carefully.

Besides the rheological properties of the matrix, the geometrical confinement has an influence on the droplet breakup (Van Puyvelde et al., 2008). Here, the specimens for the CLSM measurements were taken at 2 cm and 5 cm away from the outer rim where the sample thickness is 5 mm and 4 mm, respectively. The effect of the geometrical confinement is evaluated by comparing these specimens. Such an effect is, however, not observed (results not shown), probably because of sufficiently long distances between the

cones at these sampling locations.

Another reason for these major deviations from the theoretical predicted values could arise from the molecular structure of the plasticized starch. Native starch is mainly composed of two macromolecules – amylose and amylopectin –, which are organized in "starch granules", semi–crystalline structures of about 1 – 100 μm size. Native starch is practically insoluble in cold water. However, when a starch suspension is heated, different conversion processes (i.e. gelatinization, melting) take place that change the structural order of the starch granule irreversibly. During our experiments, the starch granules that could not melt completely might lead to instabilities in the flow, which in turn, might lead to easier breakup of the droplets. However, we must stress that, at the experimental procedure chosen (i.e. high temperature, high water content, long waiting time before the treatment), the starch granules are expected to melt completely (Lai and Kokini, 1991).

Furthermore, the results depicted in Figure 3.7 indicate that the applied shear rate has no influence on the experimental maximum droplet diameter, whereas the theory predicts that an increasing shear rate leads to lower droplet diameters because of higher viscosity ratios at higher shear rates. This is another hint for droplet coalescence happening during treatment in the shear cell, as already discussed in section 3.4.2 and 3.4.3. It is known that the shear rate has a strong influence on the coalescence rate (Janssen, 1993; Sundararaj and Macosko, 1995). Increasing shear rate might increase the coalescence rate (Sundararaj and Macosko, 1995), which could explain the experimental results. It is, however, clear that additional work will be required before a complete understanding of this phenomenon occurs.

3.5 Conclusions

The application of simple shear flow, using an in–house developed shearing device, resulted in the formation of triglyceride oil droplets down to 2.1 μm in a plasticized starch matrix. To do so, shear stresses up to 37 kPa had to be applied. It was found that increasing shear rate had no influence on droplet diameter at the shear rate ranges investigated. An increase in oil content led to an increase in droplet diameter. The latter results suggest the possibility that coalescence takes place even at low oil contents (2%). Additional work is, however, necessary to prove this phenomenon.

When the droplet sizes obtained are compared with predicted values for a Newtonian matrix, it was found that the maximum stable droplet sizes in plasticized starch are significantly smaller (factor of 10 to 100) than the predicted values for a Newtonian matrix. This difference might be related to the non-Newtonian behavior of the system evaluated. The prediction requires the rheological characterization of both phases. The shearing device was used successfully to characterize the highly viscous starch matrix, which could not be characterized with conventional rheometers, due to the fact that those devices cannot deliver sufficiently high torque.

Overall it was concluded that the use of simple shear flow conditions using a shearing device allowed successful investigation of the droplet formation in plasticized starch matrices, while keeping the complexity of the system as close as possible to those found in the industrial food extrusion processing.

Compared to the previous studies conducted with an extruder, smaller droplet sizes were found using simple shear flow conditions. This effect is unexpected and emphasizes the necessity of well–defined flow conditions in the industrial processes to obtain better predictable droplet morphology.

Nomenclature

Ca	capillary number	M	engine torque
Ca_{crit}	critical capillary number	Q_2	cumulative area-weighted size distribution
D_{50}	50^{th} percentile of cumulative area-weighted droplet size distribution	q_2	density area-weighted size distribution
D_{max}	maximum droplet diameter	r	cone radius of the shear cell
$\dot{\gamma}$	shear rate	R_{crit}	critical radius
τ	shear stress	R_{max}	maximum radius
ω	rotational speed	η_b	apparent blend viscosity
τ	shear stress	σ	interfacial tension
α	angle of the lower cone of the shear cell	λ	viscosity ratio

3.6 References

Armbruster, H. (1990). *Untersuchungen zum kontinuierlichen Emulgierprozess in Kolloidmühlen*. Doctoral Thesis. Karlsruhe University.

Averous, L. (2000). Properties of thermoplastic blends: starch–polycaprolactone. *Polymer*, 41(11), 4157–4167.

Bentley, B., & Leal, L. (1986). An experimental investigation of drop deformation and breakup in steady, two–dimensional linear flows. *Journal of Fluid Mechanics*, 167, 241–283.

Brümmer, T., Meuser, F., Lengerich, B. V., & Niemann, C. (2002). Effect of extrusion cooking on molecular parameters of corn starch. *Starch – Stärke*, 54, 1–8.

Cheng, H. & Manas–Zloczower, I. (1997). Study of mixing efficiency in kneading discs of co–rotating twin–screw extruders. *Polymer Engineering and Science*, 37(6), 1082–1090.

Chesters, A. K. (1991). The modelling of coalescence processes in fluid–liquid dispersions: a review of current understanding. *Chemical Engineering Research & Design*, 69(A4), 259–270.

Dautant, F. J., Simancas, K., Sandoval, A. J., & Müller, A. J. (2007). Effect of temperature,

moisture and lipid content on the rheological properties of rice flour. *Journal of Food Engineering*, 78, 1159–1166.

Dealy, J. M., & Larson, R. G. (2006). *Structure and Rheology of Molten polymers: From Structure to Flow Behavior and Back Again* (p. 516). Hanser Verlag.

Debruijn, R. A. (1991). *Deformation and breakup of drops in simple shear flows*. Doctoral Thesis. Eindhoven University, The Netherlands.

Della Valle, G., Vergnes, B. & Colonna, P. (1997). Relations between rheological properties of molten starches and their expansion behaviour in extrusion. *Journal of Food Engineering*, 31(3), 277–295.

Della Valle, G., Buleon, A., Carreau, P. J., Lavoie, P. A., & Vergnes, B. (1998). Relationship between structure and viscoelastic behavior of plasticized starch. *Journal of Rheology*, 42(3), 507.

Ellis, R. P., Cochrane, M. P., Dale, M. F. B., Duffus, C. M., Lynn, A., Morrison, I. M., Prentice, R. D. M., Swanston, J. S., & Tiller S. A. (1998). Starch production and industrial use. *Journal of the Science of Food and Agriculture*, 77(3), 289–311.

Elmendorp, J. J., & Maalcke, R. J. (1985). A study on polymer blending microrheology: Part 1. *Polymer Engineering and Science*, 25(16), 1041–1047.

Fleischer, K. (1994). The tomato salad problem reconsidered. *Biometrical Journal*, 36(2), 193–203.

Flumerfelt, R. (1972). Drop breakup in simple shear fields of viscoleastic fluids. *Industrial & Engineering Chemistry Fundamentals*, 11(3), 312–318.

Freiberg, S., & Zhu, X. X. (2004). Polymer microspheres for controlled drug release. *International Journal of Pharmaceutics*, 282(1–2), 1–18.

French, D., Pulley, A. O., & Whelan, W. J. (1963). Starch fractionation by hydrophobic complex formation. *Starch–Stärke*, 15(10), 349–354.

Gegner, J., Henninger, C., & Öchsner, A. (2004). Stereologische Analyse und Modelierung von Objektverteilungen aus Schnittbildern. *Materialwissenschaft und Werkstofftechnik*, 35(1), 36–44.

Grace, H. P. (1982). Dispersion phenomena in high viscosity immiscible fluid systems and application of static mixers as dispersion devices in such systems. *Chemical Engineering Communications*, 14(3–6), 225–277.

Guido, S., Simeone, M., & Greco, F. (2003). Effects of matrix viscoelasticity on drop deformation in dilute polymer blends under slow shear flow. *Polymer*, 44(2), 467–471.

Habeych, E., Dekkers, B., van der Goot, A. J. & Boom, R. M. (2008). Starch–zein blends formed by shear flow. *Chemical Engineering Science*, 63(21), 5229–5238.

Hinch, E. J., & Acrivos, A. (1980). Long slender drops in a simple shear flow. *Journal of Fluid Mechanics*, 98(02), 305.

Horn, D. (1989). Preparation and characterization of microdisperse bioavailable carotenoid hydrosols. *Die Angewandte Makromolekulare Chemie*, 166(1), 139–153.

Horn, D., & Rieger, J. (2001). Organic nanoparticles in the aqueous phase–theory, experiment, and use. *Angewandte Chemie International Edition*, 40(23), 4330–4361.

Jansen, K. M. B., Agterof, W. G. M., & Mellema, J. (2001). Droplet breakup in concentrated emulsions. *Journal of Rheology*, 45, 227.

Janssen, J. (1993). *Dynamics of liquid–liquid mixing*. Doctoral Thesis. Eindhoven University of Technology, The Netherlands.

Kamal, M. R., Lai–Fook, R., & Demarquette, N. R. (1994). Interfacial tension in polymer melts. Part II: Effects of temperature and molecular weight on interfacial tension. *Polymer Engineering and Science*, 34(24), 1834–1839.

Lai, L., & Kokini, J. (1991). Physicochemical changes and rheological properties of starch during extrusion (a review). *Biotechnology Progress*, 7(3), 251–266.

Lakkis, J. (2007). *Encapsulation and Controlled Release Technologies in Food Systems*. Ames, Iowa, USA: Blackwell Publishing.

Mano, J. F., Koniarova, D., & Reis, R. L. (2003). Thermal properties of thermoplastic starch/synthetic polymer blends with potential biomedical applicability. *Journal of Materials Science. Materials in Medicine*, 14(2), 127–35.

Mighri, F., Carreau, P. J., & Ajji, A. (1998). Influence of elastic properties on drop deformation and breakup in shear flow. *Journal of Rheology*, 42(6), 1477.

Peighambardoust, S. H., van der Goot, A. J., Hamer, R. J. & Boom, R. M. (2004). A new method to study simple shear processing of wheat gluten–starch mixtures. *Cereal Chemistry*, 81(6), 714–721.

Ramaswamy, S., & Leal, L. G. (1999). The deformation of a Newtonian drop in the uniaxial extensional flow of a viscoelastic liquid. *Journal of Non–Newtonian Fluid*

Mechanics, 88(1–2), 149–172.

Ribeiro, H. S., Guerrero, J. M. M., Briviba, K., Rechkemmer, G., Schuchmann, H. P., & Schubert, H. (2006). Cellular uptake of carotenoid–loaded oil–in–water emulsions in colon carcinoma cells in vitro. *Journal of Agricultural and Food Chemistry*, 54(25), 9366–9.

Robeson, L. M. (2007). *Polymer blends: A comprehensive review* (p. 470). Hanser Verlag.

Roe, R. J. (1968). Surface tension of polymer liquids. *The Journal of Physical Chemistry*, 72(6), 2013–2017.

Schweizer, T. F., Reimann, S., Solms, J., Eliasson, A. C., & Asp, N. G. (1986). Influence of drum–drying and twin–screw extrusion cooking on wheat carbohydrates, II, effect of lipids on physical properties, degradation and complex formation of starch in wheat flour. *Journal of Cereal Science*, 4(3), 249–260.

Scott, C. I. (1990). *Characterization of the reactive polymer blending process*. Doctroral Thesis. University of Minnesota, USA.

Shogren, R. L., Fanta, G. F., & Doane, W. M. (1993). Development of starch based plastics – A reexamination of selected polymer systems in historical perspective. *Starch – Stärke*, 45(8), 276–280.

Sibillo, V., Simeone, M., & Guido, S. (2004). Break–up of a Newtonian drop in a viscoelastic matrix under simple shear flow. *Rheologica Acta*, 43(5), 449–456.

Sundararaj, U. & Macosko, C.W. (1995). Drop breakup and coalescence in polymer blends: the effects of concentration and compatibilization. *Macromolecules*, 28(8), 2647–2657.

Sundararaj, U., Dori, Y., & Macosko, C. W. (1995). Sheet formation in immiscible polymer blends: model experiments on initial blend morphology. *Polymer*, 36(10), 1957–1968.

Taylor, G. I. (1932). The viscosity of a fluid containing small drops of another fluid. *Proceedings of the Royal Society of London. Series A*, 138(834), 41–48.

Taylor, G. I. (1934). The formation of emulsions in definable fields of flow. *Proceedings of the Royal Society of London. Series A*, 146(858), 501–523.

van den Einde, R. M., Akkermans, C., van der Goot, A. J., & Boom, R. M. (2004).

Molecular breakdown of corn starch by thermal and mechanical effects. *Carbohydrate Polymers*, 56(4), 415–422.

van den Einde, R. M., van der Goot, A. J., & Boom, R. M. (2003). Understanding molecular weight reduction of starch during heating–shearing processes. *Journal of Food Science*, 68(8), 2396–2404.

Van Puyvelde, P., Vananroye, A., Cardinaels, R., & Moldenaers, P. (2008). Review on morphology development of immiscible blends in confined shear flow. *Polymer*, 49(25), 5363–5372.

Vansoest, J., Benes, K., Dewit, D., & Vliegenthart, J. (1996). The influence of starch molecular mass on the properties of extruded thermoplastic starch. *Polymer*, 37(16), 3543–3552.

Vergnes, B., & Villemaire, J. P. (1987). Rheological behaviour of low moisture molten maize starch. *Rheologica Acta*, 576, 570–576.

Verhulst, K, Cardinaels, R., Moldenaers, P., Afkhami, S., & Renardy, Y. (2009). Influence of viscoelasticity on drop deformation and orientation in shear flow. Part 2: Dynamics. *Journal of Non–Newtonian Fluid Mechanics*, 156(1–2), 44–57.

Verhulst, K., Moldenaers, P., & Minale, M. (2007). Drop shape dynamics of a Newtonian drop in a non–Newtonian matrix during transient and steady shear flow. *Journal of Rheology*, 51(2), 261.

Willett, J. L., Jasberg, B. K., & Swanson, C. L. (1995). Rheology of thermoplastic starch: Effects of temperature, moisture content, and additives on melt viscosity. *Polymer Engineering and Science*, 35(2), 202–210.

Wing, R. E., Maiti, S., & Doane, W. M. (1988). Amylose content of starch controls the release of encapsulated bioactive agents. *Journal of Controlled Release*, 7(1), 33–37.

Xie, F., Yu, L., Su, B., Liu, P., Wang, J., Liu, H., & Cheng, L. (2009). Rheological properties of starches with different amylose/amylopectin ratios. *Journal of Cereal Science*, 49(3), 371–377.

Yilmaz, G., Jongboom, R. O. J., van Soest, J. J. G. & Feil, H. (1999). Effect of glycerol on the morphology of starch–sunflower oil composites. *Carbohydrate Polymers*, 38(1), 33–39.

Yilmaz, G., Jongboom, R. O. J., Feil, H., & Hennink, W. E. (2001). Encapsulation of

sunflower oil in starch matrices via extrusion: effect of the interfacial properties and processing conditions on the formation of dispersed phase morphologies. *Carbohydrate Polymers*, 45(4), 403–410.

Yoon, Y., Borrell, M., Park, C. C., & Leal, L. G. (2005). Viscosity ratio effects on the coalescence of two equal–sized drops in a two–dimensional linear flow. *Journal of Fluid Mechanics*, 525, 355–379.

Yue, P., Feng, J. J., Liu, C., & Shen, J. (2005). Viscoelastic effects on drop deformation in steady shear. *Journal of Fluid Mechanics*, 540(1), 427.

4 Coalescence of oil droplets in plasticized starch matrix in simple shear flow

This chapter is published as: Emin, M. A., Schmidt, U., van der Goot, A. J., & Schuchmann, H. P. (2012). Coalescence of oil droplets in plasticized starch matrix in simple shear flow. *Journal of Food Engineering*, 113(3), 453-460.

Abstract

The formation of oil droplets in plasticized starch matrices is studied by using well-defined conditions similar to extrusion. A method based on double staining and confocal scanning microscopy was developed to investigate the role of coalescence during droplet formation. The results indicate that coalescence takes place at all process conditions studied. The apparent critical capillary number was used to quantify the coalescence intensity and to separate the influence of interdependent process parameters on the coalescence. The intensity of coalescence increased with shear rate and oil content whereas an increase in blend viscosity reduced the extent of coalescence. Besides, the results showed that the critical dispersed phase concentration (ϕ_c), below which no coalescence takes place, depends on applied shear rate and decreases with increasing shear rate.

4.1 Introduction

Extrusion cooking is a thermomechanical process that is applied for a large number of food applications nowadays. Typically, starch–based foods such as ready–to–eat cereals, salty and sweet snacks are produced by extrusion cooking and are highly appreciated by consumers. With the number of extruded products increasing, interest has grown in further understanding and controlling the physicochemical, functional and nutritionally relevant effects of extrusion processing on food materials (Killeit, 1994; Singh et al., 2007). The prevention or reduction of nutrient destruction as well as a fortification of the products with functional ingredients are of special interest. The fortification of extruded products with lipophilic bioactives by encapsulating those within the food matrix is a new and promising extrusion application leading to potential health benefits such as preventing cancer or coronary heart diseases (Giovannucci et al., 1995; Steinmetz and Potter, 1996; Awad and Fink, 2000; Krinsky et al., 2004; McClements et al., 2009).

For the encapsulation of lipophilic bioactives, a lipophilic carrier, such as triglycerides is required. Triglyceride droplets, especially those of small sizes (e.g. < 1 μm) are known to encapsulate high concentrations of bioactive substances (Horn, 1989; Horn and Rieger, 2001; Ribeiro et al., 2006). The use of oil droplets as a delivery system should also result in additional stabilizing effects (McClements, 2005) as diffusion is retarded. Hence, in many cases, it is favourable to dissolve the lipophilic components in a lipid carrier and to disperse this carrier into small droplets, thereby improving the stability, bioavailability and palatability of the bioactives. In terms of process intensification, the unit operation of dispersion can be integrated into an extrusion process to eliminate an extra emulsification step. However, such a complex process demands a high degree of understanding of the mechanisms taking place in order to efficiently design processes and products.

Laminar flow is the dominating flow regime in an extruder. Here, shear and elongational stresses are responsible for droplet formation (Cheng and Manas–Zloczower, 1997). The droplet sizes obtained also depend on the viscosity ratio between dispersed phase (i.e. lipophilic components) and matrix phase (i.e. plasticized starch matrix) (Taylor, 1934; Grace, 1982). Hence, the knowledge of dispersion mechanisms in laminar flow is essential to control final emulsion characteristics, which in turn determine the bioavailability and stability of lipophilic bioactives. However, in extruders, stresses (i.e. shear and elongational stresses) vary strongly and are difficult to quantify. To differentiate between

the influence of simple shear and elongation, experiments under controlled stresses are necessary.

In our previous study (Emin et al., 2012[1]), we performed experiments with a dedicated shearing device to investigate the formation of oil (middle chain triglycerides) droplets in plasticized starch matrices under extrusion–like conditions. It was shown that breakup alone was not sufficient to explain the final droplet size at process conditions investigated (e.g. shear rate, oil content, water content). The hypothesis is that the final droplet size distribution is not only determined by droplet breakup, but also by droplet coalescence.

Although coalescence of droplets in emulsification processes has been studied extensively for several decades so far (Chesters, 1991; Minale et al., 1998; Lyu et al., 2000; Rother and Davis, 2001; Yang et al., 2001), droplet collision and coalescence in concentrated, and non–Newtonian emulsions, such as oil in plasticized starch still poses many open questions (Leal, 2004; Fischer and Erni, 2007). To the best of our knowledge, there is no coalescence–study conducted on plasticized starch matrix. A prerequisite for realizing such a study is the necessity of defined flow conditions applied under elevated temperature ($>$ 100 °C) plasticizing the starch and elevated pressure ($>$ water vapour pressure) preventing the evaporation of water (Emin et al. 2012). Unfortunately, conventional rheometers can handle only limited amount of torque that is insufficient for this purpose. Hence, a dedicated shearing device is developed that allows controlled deformation of highly viscous matrices (Peighambardoust et al., 2004; van den Einde et al., 2004; Habeych et al., 2008)

The aim of this study is to investigate the extent of coalescence of triglyceride droplets in a plasticized starch matrix using simple shear flow. Occurrence of coalescence will be discussed both qualitatively and quantitatively using a double staining method and non–dimensional numbers, respectively.

4.2 Background

The capillary number (Ca) and viscosity ratio (λ) are two important parameters for describing droplet deformation and breakup in flow (Taylor, 1932; 1934). The capillary number (Ca) defines the ratio of deforming viscous forces to shape conserving interfacial

[1] presented in this thesis as Chapter 3

forces:

$$Ca = \tau/(\sigma/R) \tag{4.1}$$

where τ is the shear stress, σ is the interfacial tension between the droplet and matrix phase, and R is the radius of the droplet. The droplet becomes unstable and breaks when the capillary number exceeds a certain value that is called the critical capillary number (Ca_{crit}). The critical capillary number is a function of the viscosity ratio (λ) which describes the ratio between the dispersed phase viscosity (η_d) and the viscosity of the continuous phase (η_c). For concentrated systems, the breakup of a droplet is determined by the average blend viscosity (η_b) rather than the continuous phase viscosity (η_c) (Armbruster, 1990; Jansen et al., 2001). The dependency of the critical capillary number on the viscosity ratio was established and validated for Newtonian systems consisting of a single drop in a Newtonian matrix (Grace, 1982; Debruijn, 1991). It was found that in simple shear flow, breakup is not possible for $\lambda > 4$, whereas it occurs most favourably at an intermediate range of $0.1 < \lambda < 1$. At lower values of λ, Ca_{crit} steadily increases with decreasing λ values making the droplet breakup more difficult (though less pronounced as for $\lambda > 4$). The system comprising plasticized starch and oil as studied here has low λ–values (10^{-7} to 10^{-4}) because the viscosity of the starch matrix is much larger than the oil viscosity.

In a coalescence–free flow, adequate exertion of shear stress results in the breakup of the droplets until their critical radius R_{crit} (Taylor, 1934). At this droplet size, the capillary number is right below the critical value Ca_{crit} where the interfacial forces start to dominate, and thus no further droplet breakup is possible. Thus, the critical capillary number can be calculated, if the applied constant shear stress and the consequently formed maximum droplet size is known (Taylor, 1934):

$$Ca_{crit} = \tau \cdot R_{crit}/\sigma \tag{4.2}$$

However, in concentrated blends in which coalescence occurs, the steady–state morphology is generally considered to be the result of a dynamic equilibrium between breakup and coalescence of the droplets (Roland and Böhm 1984; Elmendorp and Van Der Vegt 1986). In other words, the maximum droplet radius formed after adequate exertion of

shear stress is not only driven by breakup but also by coalescence. Once a droplet exceeds a critical size due to coalescence, it becomes unstable and breaks up again (Ramic et al., 2000).

When the flow is stopped (as in most of the industrial applications), the droplets that just coalesced are expected to remain larger than the critical droplet radius $R_{max} > R_{crit}$ (Sundararaj and Macosko, 1995). The critical capillary number calculated from this maximum droplet radius would therefore lead to an overestimation of the critical capillary number, Ca_{crit} (Everaert, 1999). Prediction of maximum stable droplet sizes using Eq. 4.2 is therefore limited to infinitely diluted monodisperse systems at which $\phi_d < \phi_c$, where ϕ_d is the dispersed phase concentration, and ϕ_c is the critical dispersed phase concentration below which no coalescence takes place (Elmendorp and Van Der Vegt, 1986; Utracki and Shi, 1992). Elmendorp and Van der Vegt (1986) showed that even a dispersed phase ϕ_d concentration of 0.5% can give rise to flow induced coalescence. Therefore, coalescence plays an important role at the development of final dispersed phase morphology in most applications of technical relevance.

4.3 Materials and Methods

4.3.1 Materials

Native maize starch (C*Gel 03401) with a moisture content of 11% was received from Cargill, Germany. It will be referred to as "starch" throughout the paper. Medium chain triglyceride oil (MCT–oil, purchased from Schumann & Sohn, Germany) was used throughout the experiments. Nile Red (lipophilic fluorescent dye) as well as Tween 20 (emulsifier), both of analytical grades, were obtained from Sigma–Aldrich, Germany. DiD ($DiIC_{18}(5)$, a lipophilic fluorescent dye) was purchased from Promokine, Germany.

4.3.2 Shear cell and experimental procedure

Experiments were conducted with a shear cell designed especially to work on plasticized starch (Habeych et al., 2008). The shear cell and its extents are demonstrated in Figure 4.1. To develop a simple shear flow, the gap between the upper and lower cone is kept small compared to their diameters (i.e. angle upper cone =105 °, α lower cone = 100

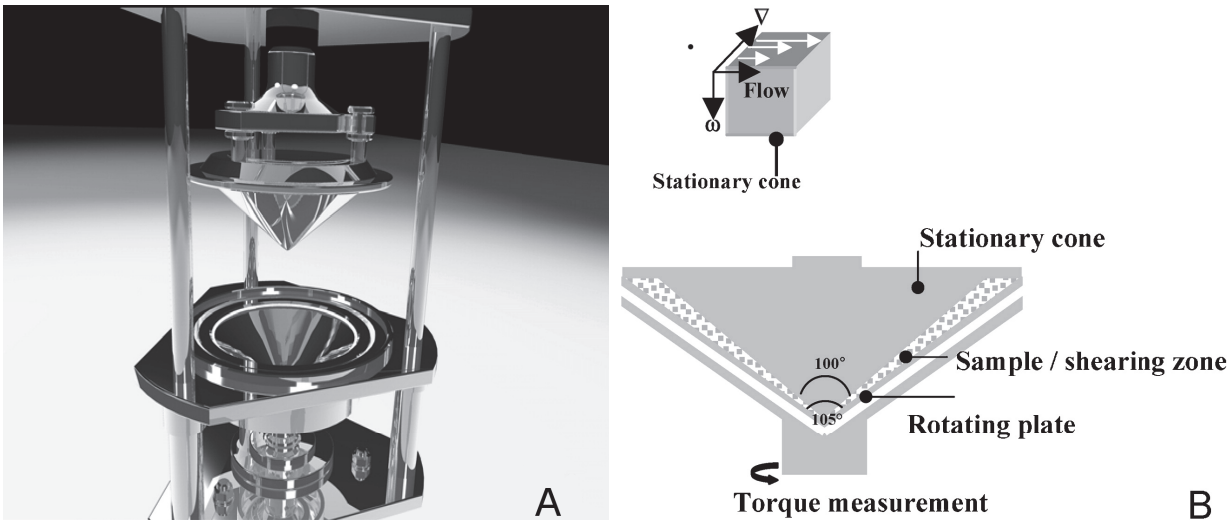

Figure 4.1: The shear cell device. (A) Animation and (B) schematic overview of the shear cell device. Cone angle = 100 °, angle between cone and plate (shearing zone), θ = 2.5°(Habeych et al., 2008).

°). In this way, circular flow is avoided and ideal flow conditions (i.e. simple shear flow) are ensured. The circulating lower cone is attached to a Brabender Do–Corder 330 (Brabender OHG, Duisburg, Germany) to enable shear rate control and to monitor the torque. The stationary upper cone is vertically connected to a hydraulic pump to pressurize the shear cell up to 400 kPa. Both cones are equipped with electrical heaters while only the upper one also comprises a water cooling system. The temperature of the material is measured with a set of thermocouples located in the upper cone. The contact surface of both cones is roughened (serrated) to avoid wall slip.

For the investigation of droplet formation, two slightly different experimental procedures were applied. The procedure for breakup experiments was as follows: Fluorescent dye (Nile Red) was dissolved in MCT–oil at a concentration of 0.033 mg/ml to enable the visibility of droplets in confocal laser scanning microscopy (CLSM). Before the shear cell processing, a homogeneous mixture of starch, water and oil was prepared by slowly adding water and stained oil into the starch, while the mixture was stirred with a spatula. The filling mass of 260 g was determined at preliminary experiments by varying the filling mass and examining the shear stress profiles.

After filling the sample into the lower cone , the shear cell was closed by upper cone and a pressure of 400 kPa was applied and kept constant during the experiments. The

pressure applied allowed working at higher temperatures by avoiding water evaporation. The sample was heated from room to process temperature (113 °C) at a heating rate of about 6 °C/min. Before shearing, the material was given a resting time of 5 minutes to allow for an even distribution of temperature and relaxation of material before processing.

After starting the process, the shear rate was increased linearly from zero shear to the set shear rate in one minute and kept constant at that value for another 4 minutes. The generated torque was recorded by a computer. Directly after the shearing process, the sample was cooled inside the shear cell to room temperature at a cooling rate of about 10 °C/min. The samples were then kept at 4 °C in a refrigerator until further analysis. For the coalescence experiments, the pre–mixture was divided into two portions. The MCT–oil in these portions were stained separately with Nile Red and DiD, respectively. These lipophilic dyes have different excitation/emission spectra, and can therefore be observed separately under the CLSM. The portions were then placed into the two halves of the rotating lower cone. The experiments were then performed as for the breakup experiments.

4.3.3 Rheological measurements

The apparent viscosity of the blend (η_b) was measured simultaneously during shear cell experiments and calculated from the generated shear rate ($\dot{\gamma}$) and the monitored shear stress (τ).

$$\eta_b = \tau/\dot{\gamma} \tag{4.3}$$

A cone angle of 2.5°of the shear cell and the tip of the upper cone adjacent to the lower one ensured the generation of constant shear rates in the shearing zone.

$$\dot{\gamma} = \omega/\alpha \tag{4.4}$$

where ω is the rotational speed and α is the angle of the lower cone. The engine torque M recorded by the control unit which gives the shear stress (τ):

$$\tau = 3M/2\pi r^3 \tag{4.5}$$

where r is the cone radius of the shear cell. Due to the sealing design of the shear cell, the outer rim of the upper cone has to contact the lower cone. Before filling the sample, the shear cell was thus calibrated by measuring the empty torque value at the shear rate applied.

The viscosity of MCT–oil was measured with a conventional rheometer, because the exhibited viscosity is too low to be measured within the shear cell. The rheometer used was an Anton Paar Physica MCR301 rheometer with a cone and plate geometry (CP50–1/TG–SN15821) and a gap width of 0.049 mm. Measurements were conducted at process temperature (113 °C) with a shear rate ranging from 1 to 120 s^{-1} which cover the conditions as during the shear cell experiments. The oil showed Newtonian behaviour with a viscosity of 0.0028 $\pm$ 0.000042 Pa·s

4.3.4 CLSM and droplet size measurement

A confocal laser scanning microscope (CLSM) and image processing software were used to measure the droplet size distributions of MCT–oil in plasticized starch. For the measurements, four specimens with a dimension of 15×7×0.11 mm were cut from each sample using a blade and a microtome. Due to the sealing design of the shear cell, the exerted shear stress on the outer rim of the sample was expected to be slightly different from the rest of the sample. Hence, the specimens were taken 2 and 5 cm away from the outer rim of the sample. Each specimen was placed on a separate glass slide, wetted with distilled water and closed with a cover slide. A Zeiss LSM 510–META 18 (Zeiss, Oberkochen, Germany) with an Axiovert 200M and equipped with a 63× Plan–Apochromat/1.4 oil immersion lens was used as CLSM for taking images. Nile Red was excited with an Argon–laser at the wavelength of 514 nm and the emitted light was filtered by a LP 560. DiD was excited with a He/Ne–laser at 633 nm and the emitted light was filtered by a LP 650 filter. The samples stained with both dyes were analyzed by multi–channel tracking to enable the visibility of the dyes, and thus the droplets, separately. The pinhole of the microscope was set to 96 μm. From each specimen, 10 images with a dimension of 202×202 μm were taken from different locations. The images were taken at a depth of 20 to 100 μm within the specimens to prevent the possible influence of the previous cutting procedure on the droplet sizes. From each sample, 40 images were taken. The obtained images were further analyzed by digital

image processing software (ImageJ, National Institutes of Health, USA). Depending on the droplet sizes, about 8000 to 20000 droplets per sample were counted. The results were plotted as an area–weighted cumulative size distribution (Q_2) and density distribution (q_2). Characteristic droplet sizes of $D_{90,2}$, $D_{50,2}$ and D_{max} (i.e. maximum droplet size) were determined from the cumulative area–weighted size distribution (Q_2). $D_{90,2}$ and $D_{50,2}$ refer the droplet size bigger than all droplets forming 90% and 50% of total droplet area, respectively.

4.4 Results and Discussion

4.4.1 Influence of oil content and shear rate on final droplet size

Figure 4.2 shows the influence of shear stress on final droplet diameter (i.e. $D_{90,2}$) for varying oil content and shear rate. The viscosity, and therefore the shear stress were altered by changing the water content in the range of 50 to 100% dry basis. To see the influence of oil content alone, the shear rate was kept constant at 24 s^{-1} and the oil content varied in the range of 0.5 to 4% dry basis (open symbols). Table 4.1 outlines the process variables, viscosity ratios and the final droplet sizes for varying oil contents in details.

Figure 4.2 clearly shows that increasing oil content leads to bigger droplets. Since shear rate was kept constant at these experiments, the blends possessing similar viscosities were sheared at similar shear stresses. Therefore, the final droplet sizes in these samples are expected to be similar. However, from Table 4.1 (e.g. sample 5, 12 and 17), it is evident that this is not the case. The droplet size increases with increasing oil content. These results suggest that coalescence of oil droplets took place under those conditions.

An increase in shear rate had no clear influence on the final droplet size (Figure 4.2, square symbols). This also hints in the direction of coalescence taking place in this system, because at higher shear rates, samples having similar viscosities are exposed to higher shear stresses. In a coalescence free system, this is expected to lead to smaller droplets since higher shear stresses lead to higher capillary numbers. However, this decrease in droplet size is not observed.

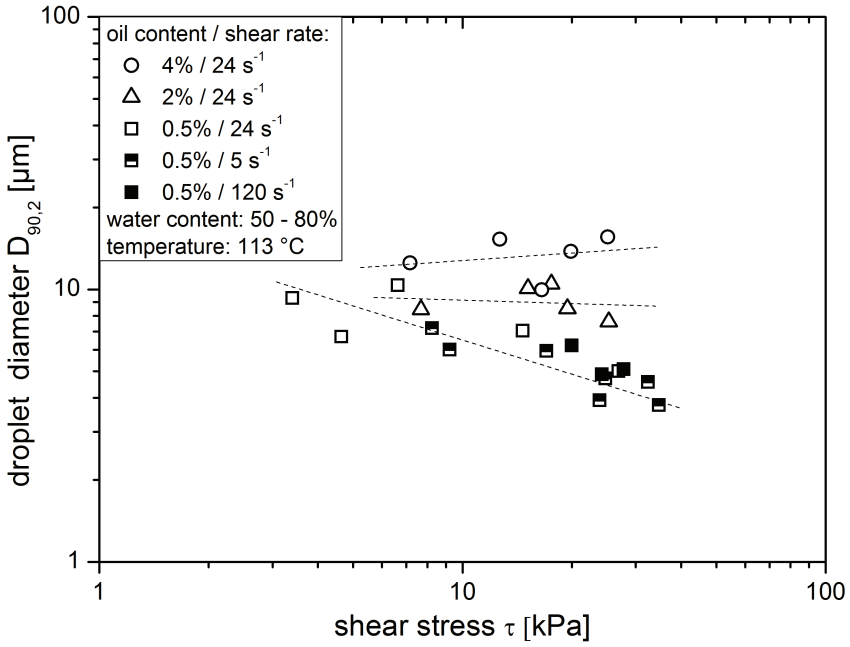

Figure 4.2: Influence of shear stress on the characteristic droplet diameter $_{D90,2}$ at oil contents of 0.5, 2 and 4% and shear rates of 5, 24 and 120 s^{-1}. The lines are included to guide the eyes.

4.4.2 Occurrence of coalescence

To verify the hypothesis that coalescence of oil droplets occurred in our experiments, we have used a double staining method that is described in section 4.2.2 in details. In this method, the oil droplets stained separately with two different fluorescent dyes and placed separately into the two halves of shear cell. The dyes used have different emission wavelengths, which makes them visible under the CLSM separately. The images obtained from CLSM for the samples sheared at 24 s^1 with an oil content of 4% are given in Figure 4.3.

Figure 4.3a and Figure 4.3b show the emitted light from the droplets stained with Nile red and DiD, respectively while Figure 4.3c shows the emitted lights from both fluorescent dyes. In the latter case, the droplets formed through coalescence appear pink due to red and blue colours reflected at the same time. Figure 4.3 shows that nearly all droplets were coalesced. Likewise, the blends sheared at different process conditions ($\dot{\gamma}$ = 5 to 120 s^{-1}, ϕ_d = 0.5 to 4%) showed the same results (images not shown).

The oil content was further decreased to determine the critical dispersed phase concen-

Table 4.1: The effect of oil content on process variables and characteristic droplet diameters. The shear rate content was kept constant at 24 s^{-1}. MCT oil having a viscosity of 2.8 mPa·s is used for the calculation of viscosity ratio.

Sample no.	Oil content [%]	Apparent blend viscosity η_b [kPa·s]	Shear stress τ [kPa]	$D_{50,2}$ [μm]	$D_{90,2}$ [μm]	D_{max} [μm]	Viscosity ratio η_d/η_b [10^{-7}]
1	0.5	0.35	8.24	3.9	7.2	16.0	80.3
2	0.5	0.39	9.23	2.9	6.0	13.6	71.6
3	0.5	0.72	17.01	2.5	5.9	15.6	38.9
4	0.5	1.01	23.85	2.1	3.9	18.0	27.8
5	0.5	1.05	24.73	2.8	4.7	10.9	26.7
6	0.5	1.37	32.39	2.6	4.6	12.2	20.4
7	0.5	1.47	34.72	2.2	3.8	7.2	19.1
8	2	0.33	7.69	5.0	8.4	20.1	86.1
9	2	0.64	15.14	5.6	10.1	16.8	43.7
10	2	0.74	17.55	5.4	10.5	19.3	37.7
11	2	0.82	19.47	4.6	8.5	21.9	34.0
12	2	1.07	25.29	4.3	7.6	13.9	26.2
13	4	0.30	7.17	7.2	12.5	22.3	92.4
14	4	0.54	12.68	7.8	15.3	32.7	52.3
15	4	0.70	16.54	4.8	10.0	18.2	40.0
16	4	0.84	19.87	7.0	13.8	24.7	33.3
17	4	1.06	25.13	7.4	15.6	30.6	26.4

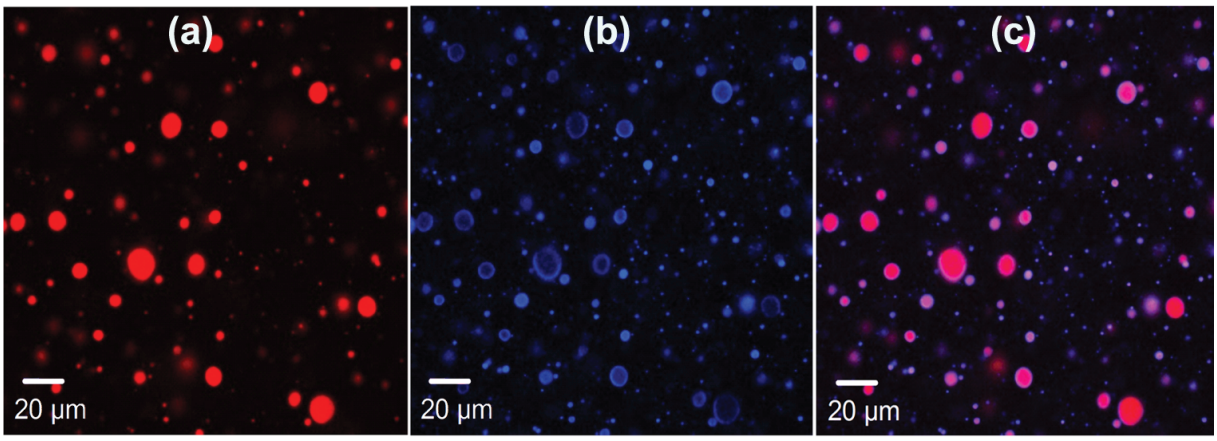

Figure 4.3: CLSM images of the sample sheared for 5 minutes. Water content: 50%, shear rate: 24 s^{-1}, oil content 4%.

tration, ϕ_c, below which no coalescence takes place. Qualitative analyses of the CLSM images showed that coalescence takes place even at an oil content of 0.05% (images not shown). Unfortunately, further decrease of the oil content below 0.05% was not possible due to scarce amount of droplets captured by CLSM imaging. On the other hand, quantitative analyses (i.e. droplet size measurements) were only possible for the samples with oil content of 0.5%, and above. Although the occurrence of coalescence looks unexpected at such a low dispersed phase concentrations and high blend viscosities, Elmendorp and Van der Vegt, (1986) found similar results for a polymer/polymer system. They compared their experimental results with the theoretical predictions and found that the measured droplet size approached the value predicted by breakup theory as the dispersed phase concentration was decreased. However, even at dispersed phase concentration of 0.25%, they showed that the effect of coalescence on droplet size is still visible, as the droplet size is still bigger than the predicted size.

These results depict that coalescence of triglyceride oil droplets takes place in plasticized starch matrices at a significant degree. However, the mechanism and time scale of coalescence is not possible to deduce from these images. Coalescence only occurs if at least two droplets collide and the film between those two droplets drains during their contact time (Chesters 1991; Janssen 1993; Leal 2004). Collisions of droplets do not only occur in flow but also under quiescent conditions. Such collisions are induced by Brownian motion, or diffusion due to concentration fluctuation, etc. (Fortelny and Koval, 1988; Sundararaj and Macosko, 1995). Coalescence of droplets in plasticized polymers is also reported in synthetic polymer processing, especially during annealing (Sundararaj and Macosko, 1995).

Due to the intrinsic nature of the experiments conducted in this study, cooling of the plasticized starch after shearing below its glass transition temperature (50 to 80 °C) took up to approximately 6 minutes depending on the water content of the blend. Therefore, the question arises as to whether the droplets coalesced during shearing or during cooling down at quiescent conditions in shear cell. To answer this question, we repeated the experiments with a shorter shearing time (i.e. 15 seconds), while the cooling rate of the blend, and therefore the time spent under quiescent conditions were kept constant. The corresponding CLSM images are given in Figure 4.4. From Figure 4.4c, the distinct red and pink droplets show that coalescence took also place but at a rate significantly reduced. Besides pink (i.e. coalesced) droplets also red and blue ones were found. These results

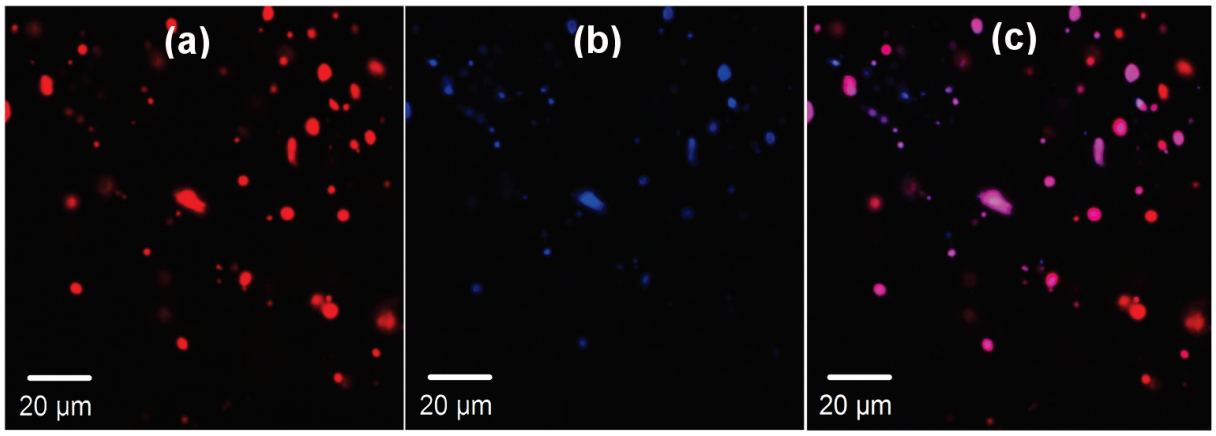

Figure 4.4: CLSM images of the sample sheared for 15 seconds. Water content: 50%, shear rate: 24 s^{-1}, oil content 0.5%.

suggest that coalescence of triglyceride droplets in plasticized starch matrix is mainly dominated by coalescence in shear flow.

4.4.3 Critical capillary number

As described in section 4.2, the critical capillary number can be calculated from Eq. 4.2, provided that the applied shear stress and the resulting maximum stable droplet size are known. However, to avoid an overestimation of critical capillary number, the influence of coalescence on final droplet size must be completely eliminated. Theoretically, this can be done by using a single droplet or oil content below critical dispersed phase concentration (ϕ_c) below which droplets will not collide with each other at all. Unfortunately, this is not applicable in practice since the droplets would be very difficult or even impossible to detect manually with CLSM. Nevertheless, plotting this "overestimated critical capillary number" (from now on named apparent critical capillary number, Ca_{app}) versus viscosity ratio gives clear information on coalescence, because it includes the influence of viscosities and shear stress on final droplet size at the same time.

For the calculation of the apparent critical capillary number from Eq. 4.2, the interfacial tension between the triglyceride droplets and plasticized starch is necessary. In our previous study (i.e. Emin et al., 2012), the interfacial tension was estimated to be 10 ± 2 mN/m at the process conditions investigated. In Figure 4.5, apparent critical capillary number is plotted as a function of the viscosity ratio for varying oil content and shear rate of 0.5 to 4% and 5 to 120 s^{-1}, respectively. The results show that increasing shear rate and

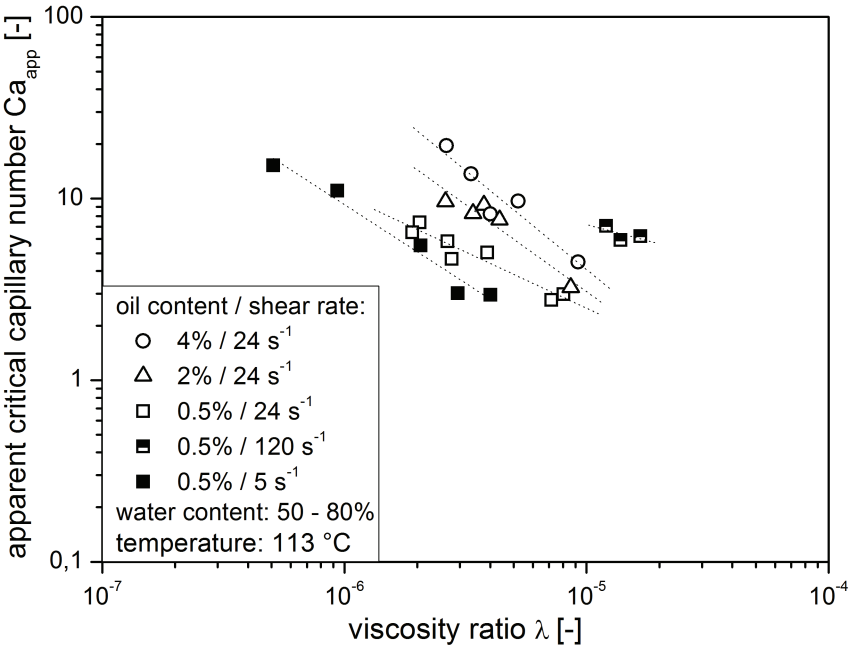

Figure 4.5: Influence of oil content and shear rate as well as viscosity ratio on the apparent critical capillary number. The lines are included to guide the eyes.

oil content lead to higher apparent critical capillary numbers. In other words, coalescence rates increase with increasing oil content and shear rate. The sample with 0.5% oil content being sheared at 5 s^{-1} showed the lowest apparent critical capillary number. As coalescence was detected via image analysis even below this oil content, a further decrease of the oil content and the shear rate is expected to decrease the coalescence and therefore the apparent critical capillary number further. As stated above, a further decrease of oil content or shear rate could not be realised technically by this experimental setup. Lower shear rates were technically not possible to achieve with the system used and at oil contents below 0.5%, the number of droplets measured by CLSM was not sufficient for statistically reliable results.

To stabilize the droplets in flow and prevent coalescence, emulsifiers can be used. We have therefore conducted few experiments in which an emulsifier (i.e. Tween 20) at a concentration of 0.5% dry basis was used. The obtained results are compared with those of the samples comprising no emulsifiers. The influence of emulsifier on final droplet size distributions are plotted in Figure 4.6a for the blend with oil content of 2% sheared at 120 s^{-1} and in Figure 4.6b for the blend with oil content of 0.5% sheared at 24 s^{-1}.

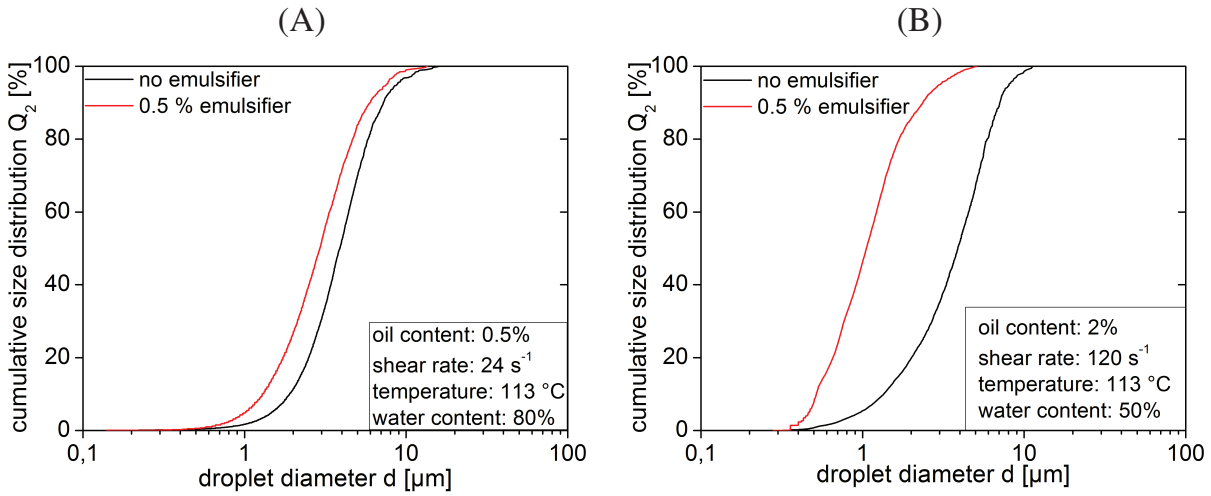

Figure 4.6: Influence of emulsifier on the droplet size distribution: (A) oil content: 2%, shear rate: 120 s^{-1}, (B) oil content: 0.5%, shear rate: 24 s^{-1}.

The addition of emulsifier in the blend containing a higher oil content and sheared at higher shear rate (Figure 4.6a) led to a significant decrease in droplet size (D_{max} from 11.3 μm to 5.1 μm). In contrast, droplet size of the blend having lower oil content and sheared at lower shear rate (Figure 4.6b) changed very slightly (D_{max} from 12.2 μm to 9.4 μm). These results together with the results in Figure 4.5 suggest that the influence of coalescence on final droplet size in the blends are minimized reasonably at the oil content of 0.5% and the shear rate of 5 s^{-1}. Consequently, the apparent critical capillary number of the blends processed at this process condition is expected to be close to the true critical capillary number. The function of this critical capillary number on viscosity ratio at the range investigated was thus obtained from the curve (ϕ_d= 0.5%, $\dot{\gamma}$ = 5 s^{-1}) plotted in Figure 4.5 as:

$$Ca_{crit} = 6 \cdot 10^{-5} \cdot (\lambda)^{-0.86} \tag{4.6}$$

with coefficient of determination (R^2) of 0.967 and p–value < 0.005.

4.4.4 Coalescence intensity

Besides the qualitative analysis, it is important to quantify the influence of coalescence on droplet formation. This allows for investigating the impact of different process parameters

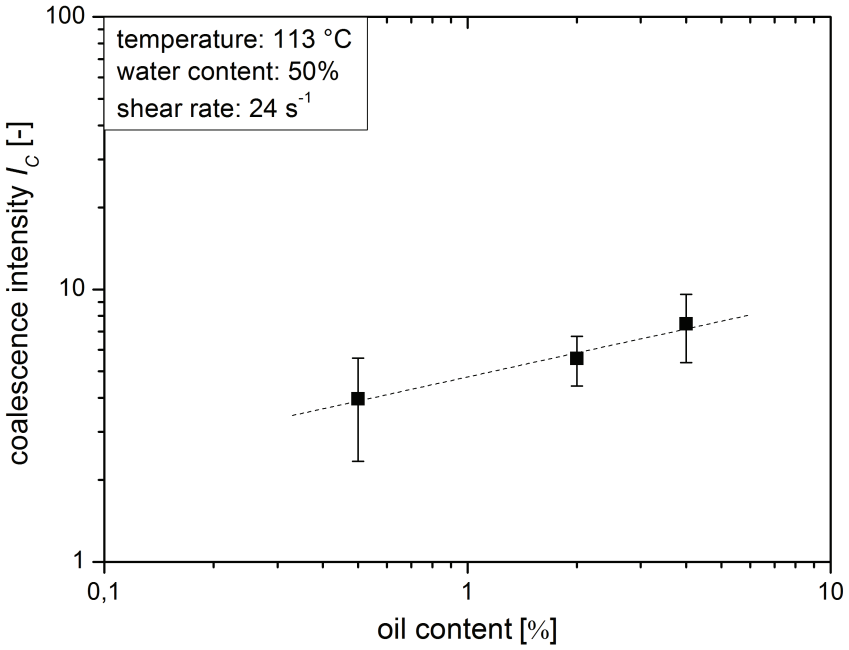

Figure 4.7: Influence of the oil content on the coalescence intensity. The results and the corresponding standard deviations are from triplicate experiments. The lines are included to guide the eyes.

(e.g. oil content, shear rate, viscosity) on this phenomenon. An analysis of the droplet size alone is not sufficient as process parameters such as blend viscosity or applied shear stress varies at the same time. Hence, non–dimensional analysis of the results is necessary. The critical droplet radius (R_{crit}) can be calculated from Eq. 4.2 and Eq. 4.6:

$$R_{crit} = 6 \cdot 10^{-5} \cdot (\lambda)^{-0.86} \cdot \sigma/\tau \tag{4.7}$$

The ratio of this calculated critical radius to the measured maximum droplet radius (R_{max}) in a blend gives a qualitative measure for the intensity at which coalescence influences the final droplet size. It is named as coalescence intensity (I_C):

$$I_C = R_{max}/R_{crit} \tag{4.8}$$

Figure 4.7 depicts the coalescence intensity versus the oil content for the shear rate of 24 s^{-1}. The results show that the coalescence intensity increases with increasing oil content. This is an expected result as the number of droplets in the blend and therefore

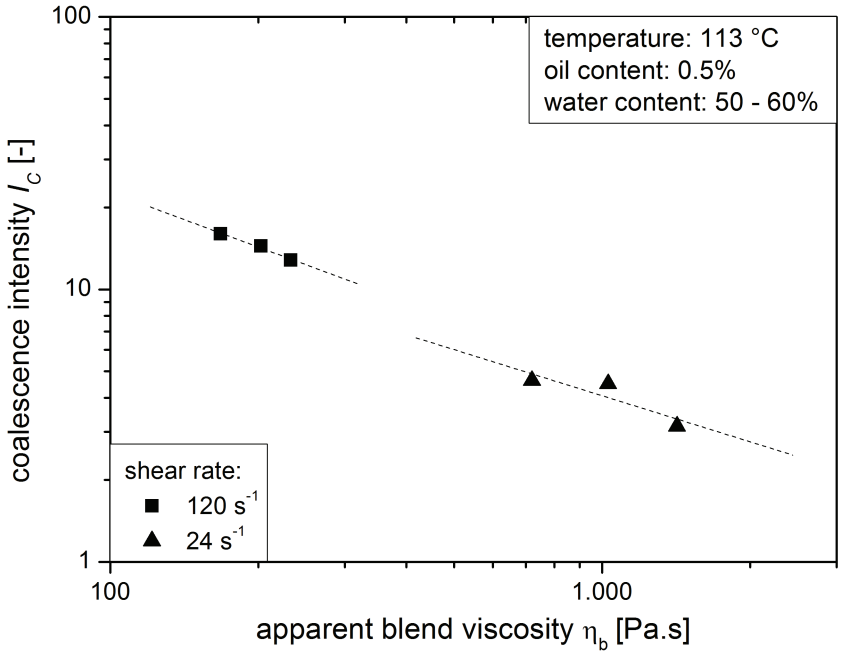

Figure 4.8: Influence of matrix viscosity on the coalescence intensity at two different shear rates of 120 s^{-1} and 24 s^{-1}. The lines are included to guide the eyes.

the frequency of their collision increases with increasing oil content (Chesters, 1991; Elmendorp and Van Der Vegt, 1986; Janssen, 1993; Sundararaj and Macosko, 1995). Even at oil content of 0.5%, the coalescence intensity is about 4 showing that the final droplet size in the blend is about 4 times bigger than in a coalescence–free system. This means that the critical dispersed phase concentration (ϕ_c) depends on applied shear rate and decreases with increasing shear rate in the range investigated.

Figure 4.8 shows the influence of apparent blend viscosity and shear rate on coalescence intensity. It is evident that increasing blend viscosity leads to less coalescence irrespective of the shear rate applied. In addition to blend viscosity, the viscosity ratio, the droplet size and the shear stress are also parameters that influence the intensity of coalescence (Elmendorp and Van Der Vegt, 1986; Chesters, 1991; Janssen, 1993; Yoon et al., 2005). As they vary during these experiments, the exact reason behind these results is hard to deduce. It is difficult, though, to study shear rate effects independently, because the viscosity of the blend is coupled to the shear rate due to the shear thinning behaviour of the plasticized starch. Increasing shear rate leads to lower blend viscosity as it can be also seen in Figure 4.8. Nevertheless, extrapolation of the results could be used for an

indirect comparison, which in this case indicates that increasing shear rate leads to higher coalescence intensity.

4.5 Conclusions

Use of simple shear flow conditions using a dedicated shearing device allowed investigating the coalescence phenomena of triglyceride droplets in plasticized starch matrices. The system studied here reflects the typical conditions found in industrial food extrusion processing (i.e. apparent blend viscosity up to 1500 Pa·s, temperature >100 °C, and shear rate up to 120 s^{-1}). A double staining method in combination with CLSM was introduced and the occurrence of coalescence was demonstrated visually. Even at very low oil content (i.e. 0.05% dry basis) and very high blend viscosity (i.e. 1500 Pa·s), droplet coalescence was observed.

Droplet sizes resulting from breakup and coalescence were used to calculate the critical capillary number. This number was called "apparent critical capillary number", as it included the influence of coalescence on the final droplet sizes. Therefore, it was used to quantify the coalescence intensity as a function of process and material parameters. An increase in shear rate and oil content led to increased coalescence intensity whereas an increase in blend viscosity decreased it. Moreover, the results show that critical dispersed phase concentration (ϕ_c), below which no coalescence takes place, depends on the applied shear rate and decreases with increasing shear rate at the range investigated.

Nomenclature

Ca	capillary number	M	engine torque
Ca_{app}	apparent critical capillary number	Q_2	cumulative area-weighted size distribution
Ca_{crit}	critical capillary number	r	cone radius of the shear cell
D_{50}	50^{th} percentile of cumulative area-weighted droplet size distribution	R_{crit}	critical radius
D_{90}	90^{th} percentile of cumulative area-weighted droplet size distribution	R_{max}	maximum radius
D_{max}	maximum droplet diameter	η_b	apparent blend viscosity
$\dot{\gamma}$	shear rate	σ	interfacial tension
τ	shear stress	λ	viscosity ratio
ω	rotational speed	ϕ_d	dispersed phase concentration
α	angle of the lower cone of the shear cell	ϕ_c	critical dispersed phase concentration
I_C	coalescence intensity		

4.6 References

Armbruster, H. (1990). *Untersuchungen zum kontinuierlichen Emulgierprozess in Kolloidmühlen*. Doctoral Thesis. Karlsruhe University.

Awad, A. B., & Fink, C. S. (2000). Phytosterols as anticancer dietary domponents: Evidence and mechanism of action. *Journal of Nutrition* 130, 2127–2130.

Cheng, H. & Manas–Zloczower, I. (1997). Study of mixing efficiency in kneading discs of co–rotating twin–screw extruders. *Polymer Engineering and Science*, 37(6), 1082–1090.

Chesters, A. K. (1991). The modelling of coalescence processes in fluid–liquid dispersions: a review of current understanding. *Chemical Engineering Research & Fesign*, 69(A4), 259–270.

Debruijn, R. A. (1991). *Deformation and breakup of drops in simple shear flows*. Eindhoven University.

Emin, M. A., Hardt, N., van der Goot, A. J. & Schuchmann, H. P. (2012). Formation of oil droplets in plasticized starch matrix in simple shear flow. *Journal of Food Engineering*, 112(3), 200-207.

Elmendorp, J. J., & Van Der Vegt, A. K. (1986). A study on polymer blending microrheology: Part IV. The influence of coalescence on blend morphology origination. *Polymer Engineering and Science*, 26(19), 1332–1338.

Everaert, V. (1999). Phase morphology development in immiscible PP/(PS/PPE) blends influence of the melt–viscosity ratio and blend composition. *Polymer*, 40(24), 6627–6644.

Fischer, P., & Erni, P. (2007). Emulsion drops in external flow fields – The role of liquid interfaces. *Current Opinion in Colloid & Interface Science*, 12(4–5), 196–205.

Fortelny, I., & Koval, J. (1988). Theory of coalescence in immiscible polymer blends. *Polymer Composites*, 9(2), 119–124.

Giovannucci, E., Ascherio, A., Rimm, E. B., Stampfer, M. J., Colditz, G. A., & Willett, W. C. (1995). Intake of carotenoids and retino in relation to risk of prostate cancer. *Journal of the National Cancer Institute*, 87(23), 1767.

Grace, H. P. (1982). Dispersion phenomena in high viscosity immiscible fluid systems and application of static mixers as dispersion devices in such systems. *Chemical Engineering Communications*, 14(3–6), 225–277.

Habeych, E., Dekkers, B., van der Goot, A. J., & Boom, R. M. (2008). Starch–zein blends formed by shear flow. *Chemical Engineering Science*, 63(21), 5229–5238.

Horn, D. (1989). Preparation and characterization of microdisperse bioavailable carotenoid hydrosols. *Die Angewandte Makromolekulare Chemie*, 166(1), 139–153.

Horn, D., & Rieger, J. (2001). Organic nanoparticles in the aqueous phase–theory, experiment, and use. *Angewandte Chemie International Edition*, 40(23), 4330–4361.

Jansen, K. M. B., Agterof, W. G. M., & Mellema, J. (2001). Droplet breakup in concentrated emulsions. *Journal of Rheology*, 45(July 2000), 227.

Janssen, J. (1993). emphDynamics of liquid–liquid mixing. Eindhoven University of Technology, The Netherlands.

Killeit, U. (1994). Vitamin retention in extrusion cooking. *Food chemistry*, 49(2), 149–155.

Krinsky, N., Mayne, S., & Sies, H. (2004). *Carotenoids in Health and Disease*. CRC.

Leal, L. G. (2004). Flow induced coalescence of drops in a viscous fluid. *Physics of Fluids*, 16(6), 1833.

Lyu, S.–P., Bates, F. S., & Macosko, C. W. (2000). Coalescence in polymer blends during shearing. *AIChE Journal*, 46(2), 229–238.

McClements, D. J. (2005). *Food emulsions: principles, practices, and techniques* (p. 609). CRC Press.

McClements, D. J., Decker, E. A., Park, Y., & Weiss, J. (2009). Structural design principles for delivery of bioactive components in nutraceuticals and functional foods. *Critical Reviews in Food science and Nutrition*, 49(6), 577–606.

Minale, M., Mewis, J., & Moldenaers, P. (1998). Study of the morphological hysteresis in immiscible polymer blends. *AIChE Journal*, 44(4), 943–950.

Peighambardoust, S. H., van der Goot, A. J., Hamer, R. J., & Boom, R. M. (2004). A New Method to Study Simple Shear Processing of Wheat Gluten–Starch Mixtures. *Cereal Chemistry*, 81(6), 714–721.

Ramic, A., Hudson, S., Jamieson, A., & Manas–Zloczower, I. (2000). Temporary droplet–size hysteresis in immiscible polymer blends. *Polymer*, 41(16), 6263–6270.

Ribeiro, H. S., Guerrero, J. M. M., Briviba, K., Rechkemmer, G., Schuchmann, H. P., & Schubert, H. (2006). Cellular uptake of carotenoid–loaded oil–in–water emulsions in colon carcinoma cells in vitro. *Journal of Agricultural and Food Chemistry*, 54(25), 9366–9.

Roland, C. M., & Böuhm, G. G. A. (1984). Shear–induced coalescence in two–phase polymeric systems. I. Determination from small–angle neutron scattering measurements. *Journal of Polymer Science: Polymer Physics Edition*, 22(1), 79–93.

Rother, M. A., & Davis, R. H. (2001). The effect of slight deformation on droplet coalescence in linear flows. *Physics of Fluids*, 13(5), 1178.

Singh, S., Gamlath, S., & Wakeling, L. (2007). Nutritional aspects of food extrusion: a review. *International Journal of Food Science & Technology*, 42(8), 916–929.

Steinmetz, K. A., & Potter, J. D. (1996). Vegetables, Fruit, and Cancer Prevention: A Review. *Journal of the American Dietetic Association*, 96(10), 1027–1039.

Sundararaj, U., & Macosko, C. W. (1995). Drop breakup and coalescence in polymer blends: the effects of concentration and compatibilization. *Macromolecules*, 28(8),

2647–2657.

Taylor, G. I. (1932). The Viscosity of a Fluid Containing Small Drops of Another Fluid. *Proceedings of the Royal Society of London. Series A*, 138(834), 41–48.

Taylor, G. I. (1934). The formation of emulsions in definable fields of flow. *Proceedings of the Royal Society of London. Series A*, 146(858), 501–523.

Utracki, L. A., & Shi, H. (1992). During Compounding in a Twin–Screw Extruder . Part I: Droplet Dispersion and Coalescence–A Review. emphPolymer Engineering & Science, 32(24).

Yang, H., Park, C. C., Hu, Y. T., & Leal, L. G. (2001). The coalescence of two equal–sized drops in a two–dimensional linear flow. *Physics of Fluids*, 13(5), 1087.

Yoon, Y., Borrell, M., Park, C. C., & Leal, L. G. (2005). Viscosity ratio effects on the coalescence of two equal–sized drops in a two–dimensional linear flow. *Journal of Fluid Mechanics*, 525, 355–379.

van den Einde, R. M., Akkermans, C., van der Goot, A. J., & Boom, R. M. (2004). Molecular breakdown of corn starch by thermal and mechanical effects. *Carbohydrate Polymers*, 56(4), 415–422.

5 Analysis of the dispersive mixing efficiency in a twin–screw extrusion processing of starch based matrix

This chapter is published as: Emin, M. A., & Schuchmann, H. P. (2013). Analysis of the dispersive mixing efficiency in a twin–screw extrusion processing of starch based matrix. *Journal of Food Engineering*, 115(1),132–143.

Abstract

The flow of plasticized maize starch in a co–rotating twin screw extruder was simulated by using computational fluid dynamics (CFD). Sensitivity of the simulation to the selected viscosity model was analyzed. The results suggest that about 16 times increase in zero shear viscosity has no influence on the flow, whereas a slight change in viscosity at the shear thinning region leads to significant increase in pressure drop along the mixing zone of extruder. Simulation results were validated quantitatively by experimental data. Furthermore, the flow type and profile in the extruder were discussed by using the influence of screw speed and screw configuration as exemplary process parameters. To evaluate the dispersive mixing efficiency, material specific critical capillary number was implemented into particle tracking simulations. Maximum shear stress generated at the tip of the screws was used to calculate the maximum capillary ratio, and therefore to determine the dispersive mixing efficiency. The results show that increase in screw speed led to better dispersive mixing, although the generated shear stresses decreased. To investigate the influence of screw geometry, two different screw configurations were simulated. The results show that the dispersive mixing efficiency can be improved by using reverse kneading blocks at which more particles are exposed to high shear stresses

5.1 Introduction

Extrusion is a highly integrated process with many unique advantages for encapsulation applications, such as its energy efficiency, the lack of process effluents, and its versatility with respect to ingredient selection and the shapes and textures of products that can be produced (Lakkis, 2007). Encapsulation of functional hydrophobic components into starch based matrices via extrusion processing is a promising area which has gained growing interest by food industry as well as by chemical, pharmaceutical, and medical industries. For most hydrophobic components (e.g. bioactive lipids, flavors, antimicrobials, antioxidants or drugs), it is favorable to dissolve the hydrophobic component in a lipid based delivery system and disperse this solution into small droplets to improve the stability, bioavailability and palatability of the functional component (Horn, 1989; Horn and Rieger, 2001; Ribeiro et al., 2006). Since starch is a hydrophilic biopolymer, an effective dispersive mixing is crucial to incorporate the hydrophobic components and to achieve the desired dispersed phase morphology in the starch matrix.

In laminar flow, as dominating flow regime in extruders, shear and elongational stresses are responsible for droplet deformation and break–up (Cheng and Manas–Zloczower, 1997). Moreover, the resulting droplet sizes depend on the viscosity ratio between dispersed phase (i.e. hydrophobic components) and continuous phase (i.e. plasticized starch matrix). The knowledge of the shear and elongational stresses inside the extruder is the key to control resulting dispersed phase morphology, and therefore the bioavailability and stability of hydrophobic components encapsulated within the starch matrix. However, the complex geometrical nature of intermeshing twin screw extruders presents many challenges, particularly with respect to inhomogeneous distribution of the stresses in the flow field. Therefore, measurement of the exposed stresses in extruders is a very difficult task and remains challenging.

The approach of this study is to simulate the non–Newtonian flow of plasticized starch in an extruder by using computational fluid dynamics (CFD) which is coupled to the experimental measurements. Furthermore, this study introduces an approach to evaluate the dispersive mixing efficiency by mapping the underlying mixing mechanisms and implementing the fundamental parameters such as capillary number and viscosity ratio into the numerical simulation.

5.2 Fundamentals

5.2.1 Simulation of transitional intermeshing screw elements

In a twin–screw extruder, the flow is three–dimensional (3–D) and unsteady due to the screws' rotation. To model the flow in an extruder channel containing two rotating intermeshing screws, some type of remeshing or moving–mesh technique is required to take into account the time–dependent volume occupied by the fluid. For this purpose, new meshes for each time–step can be created and time–dependent fields are then obtained by interpolation between these meshes (Yang and Manas–Zloczower, 1992; Bravo et al., 2000; Ishikawa et al., 2000; Strutt et al., 2000). However this meshing task is cumbersome and many meshes or very complex meshing tools are generally required in case of a time–dependent geometry. Nevertheless, this quasi–steady state method shows good agreement between numerical and experimental results in terms of velocity and pressure profiles at low screw speeds (Ishikawa et al., 2001).

To simplify the set up of such a simulation and to avoid the use of a remeshing algorithm, flow domains and moving elements can be meshed separately and then superimposed as they would be positioned at any given time. Different authors presented similar techniques based on this principle, such as the mesh superposition technique introduced by Avalosse (1996) and the fictitious domain method proposed by Bertrand et al. (1997). The mesh superposition technique is based on a static mesh corresponding to the flow domain and a dynamic mesh describing the moving screws. At each time step, a procedure identifies the elements of the static mesh that contain elements of the dynamic mesh. The velocity of the moving part is imposed on the nodes of these static elements by means of a penalty technique. For this purpose, a penalty force term, $H(v - v_p)$, has been introduced where H is either zero outside the moving part or 1 within the moving part and v_p is the velocity of the moving part. The term is used by modifying the equation of motion as follows (Avalosse and Rubin, 2000):

$$H(v - v_p) + (1 - H)(-\nabla p + \nabla \cdot T + \rho g - \rho a) = 0 \tag{5.1}$$

where p is pressure, T is the extra–stress tensor, v is the velocity, v_p is the local velocity of the moving part, ρ is the density, ρg is the volume force, and ρa is the acceleration

term. For H = 0, Eq. 5.1 is reduced to the normal Navier–Stokes equations, but when H = 1 the equation degenerates into $v = v_p$. The value of H is determined by the generation of an "inside" field that depends on the position of the moving part. When an element or node is greater than 60% within the moving part, H is given the value of 1. Alsteens et al. (2004) simulated the flow of polyamide in a twin–screw extruder by using the mesh superposition technique and showed that the design of the mesh and the selection of mixed interpolation have a significant influence on the reliability of the obtained results and should be treated carefully for such a simulation. The fictitious domain method proposed by Bertrand et al. (1997) offers similarities with mesh superposition technique. The main difference lies in the fact that, with the fictitious domain method, the kinematics of a moving part is enforced on the control points that describe it by means of Lagrange multipliers and not by a penalty technique.

5.2.2 Droplet formation and dispersive mixing efficiency

Parallel to the advances on computational methods, several studies (e.g. Yang and Manas–Zloczower, 1992; Cheng and Manas–Zloczower, 1997; Ishikawa et al. 2001) focused on devising parameters to evaluate the dispersive mixing efficiency in an extruder by using CFD. Evaluation of the mixing essentially requires fundamental understanding of the morphology development in the multi–phase system studied. When a droplet is suspended in a polymer melt (e.g. oil in plasticized starch) and subjected to laminar flow in a co–rotating twin–screw extruder, it will deform, orient, and possibly break–up into smaller droplets (Elmendorp, 1986; Sundararaj and Macosko, 1995). The capillary number (Ca) and viscosity ratio (p) are two important parameters for describing droplet deformation and breakup in flow (Taylor, 1932; 1934).

$$Ca = \eta_b \cdot \dot{\gamma} \cdot R/\sigma \tag{5.2}$$

$$p = \eta_d/\eta_b \tag{5.3}$$

where η_d and η_b are the dispersed phase and blend viscosity respectively, $\dot{\gamma}$ is the shear rate, R is the initial droplet radius, and σ is the interfacial tension. The capillary number (Ca) may be regarded as the ratio of the deforming viscous stresses to the restoring stresses the latter resulting from the interfacial tensions. It indicates that the larger the

local shear stress $\tau(= \eta_b \cdot \dot{\gamma})$ relative to the interfacial stress $(= \sigma/R)$ is, the more a droplet will deform until it breaks up.

The specific value, at which the droplet breaks–up in a flow field of given shear stress, is called critical capillary number (Ca_{crit}). The dependency of critical capillary number on the viscosity ratio (p) was established and validated for Newtonian systems (Bentley and Leal, 1986; Debruijn, 1991; Grace, 1982). Plasticized starch, however, is a non–Newtonian fluid, in which the droplet breakup is known to differ from Newtonian fluids (Mighri et al., 1998; Yue et al., 2005; Verhulst et al., 2007). Recently, we (Emin et al., 2012a[1]) found that the critical capillary number for the triglyceride droplets suspended in plasticized native maize starch is significantly lower than in Newtonian systems. We also reported a dependency of the critical capillary number (Ca_{crit}) on viscosity ratio (p) for triglyceride droplets suspended in plasticized native maize starch (Emin et al., 2012b[2]):

$$Ca_{crit} = 6 \cdot 10^{-5} \cdot (p)^{-0.86} \tag{5.4}$$

For large capillary numbers ($Ca/Ca_{crit} >> 1$) and for viscosity ratios $(p) < 1$, droplets are stretched into long, slender filaments (Grace, 1982; Janssen, 1993). Local radii are decreased such that the interfacial tension starts playing a role, since it tends to minimize the interfacial area between the two phases. As a consequence, small disturbances present at the interface of the drop filaments grow and finally result in the disintegration of the thread into very small droplets (Grace, 1982; Janssen, 1993). The deformation time plays also an important role on the break–up of the droplets which was reported to decrease with increasing capillary ratios (Ca/Ca_{crit}) (Grace, 1982). Therefore, not only the shear rate or shear stress but also the system specific capillary ratio (Ca/Ca_{crit}) should be taken into account in order to evaluate the dispersive mixing in an extrusion process.

Moreover, the mechanical stress required for droplet breakup depends on the type of the flow, with irrotational flow (i.e. elongational flow) being more effective than simple shear flow (Grace, 1982; Bentley and Leal, 1986). The mixing index λ_{MZ}, introduced by Cheng and Manas–Zloczower (1990), can be considered to be a mapping of the mechanism of

[1] presented in this thesis as Chapter 3
[2] presented in this thesis as Chapter 4

dispersive mixing within the extruder:

$$\lambda_{MZ} = \frac{|d|}{|d| + |\omega|} \tag{5.5}$$

where d is the rate of strain tensor and ω is the vorticity tensor, which are the symmetric and asymmetric components of the velocity gradient tensor. For a mixing index of 0, the system is undergoing purely rotational flow and no effective mixing can occur. A mixing index of 0.5 denotes simple shear flow, while a value of 1.0 denotes irrotational flow (i.e. elongational flow).

Recent studies (i.e. Sibillo et al., 2004; Yue et al., 2005; Verhulst et al., 2009) further showed that the elasticity of the matrix fluid has a significant contribution on the deformation of dispersed droplets, most especially if the applied flow field is transient as in extruders. However, the problems regarding the measurement of elasticity of complex food matrices (e.g. plasticized starch) under extrusion conditions (e.g. high temperature and high pressure) and the constitutive modelling and computational simulation of such a flow in complex geometry of twin–screw extruder still remain very challenging.

5.3 Materials and Methods

5.3.1 Materials

Native maize starch C*Gel 03401 at 10% moisture content (wet basis) was obtained from Cargill, Germany. It will be referred to as “starch” throughout the paper. Medium chain triglyceride oil (MCT–oil) was obtained from Schumann & Sohn, Germany. MCT–oil was chosen, because it does not form lipid–amylose complexes when mixed with starch (French et al., 1963; Schweizer et al., 1986).

5.3.2 Extrusion trials and rheological measurements

To monitor the data necessary for the numerical simulation, experiments were performed using a co–rotating high speed twin–screw extruder ZSK 26 Mc (Coperion, Stuttgart, Germany) consisting of 7 barrels with length to diameter ratio of 29. The extrusion experiments were performed varying screw speed from 300 rpm to 500 rpm. At the

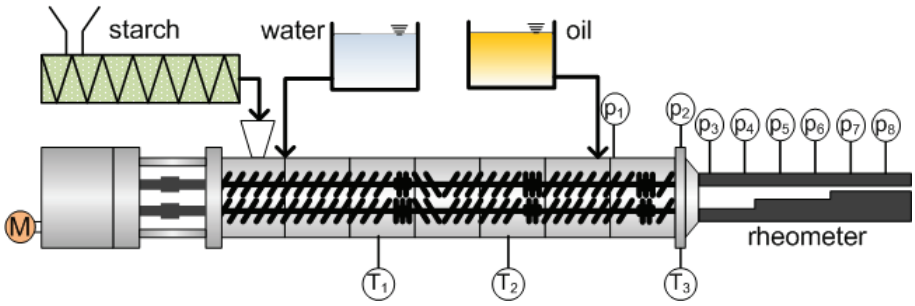

Figure 5.1: Illustration of the experimental set-up.

first part of the extruder, starch (10 kg/h) was mixed with water (18% wet basis) which was then plasticized under thermal and mechanical stresses generated by rotation of the screws. MCT–oil (4% dry basis) was incorporated into the plasticized starch at the last barrel of the extruder. The temperature of the melt was kept constant at 140 °C within the last 3 barrels of the extruder which was regulated by changing the barrel temperature. At the end of the extruder, the last 2 barrels were fully filled due to the pressure generated at the extrusion die which was verified by inline mounted pressure sensors. These two pressure sensors were further used to monitor the pressure difference at this region to validate the simulation results.

Rheological characteristics of the plasticized starch were determined by a multiple step slit die rheometer mounted on the extruder during all the experiments. An illustration of the experimental set–up, screw geometry and feeding points can be seen in Figure 5.1. The rheological properties of the thermomechanically transformed starch can be calculated from the pressure drop of the flow in the slit–die which is measured using flush–mounted transducers. Various shear rates necessary to obtain a viscosity curve were generated by increasing the cross section of the slit–die without any disturbance on extrusion process parameters. Van den Einde et al. (2004) and Liu et al. (2010) showed that the transformation of starch molecules under mechanical stresses only depends on the maximum stress applied. In case of the screw geometry selected for this study, it is expected that the maximum stresses were generated at the inverse screw elements located in the middle of the extruder.. Therefore, it is assumed that the molecular structure, and thus, the viscosity of starch remained unchanged at the end of extruder (mixing zone), which could be measured by online slit die rheometer. The temperature of the rheometer was kept constant at the exit temperature of the starch (i.e. temperature at the end of the

extruder) using a heating jacket. The shear stress τ (Pa) can be calculated by Eq. 5.6:

$$\tau = (\Delta P/L) \times (h/2) \tag{5.6}$$

where ΔP is the pressure drop (Pa) measured at two pressure sensors with the distance L (mm) between them and h is the slit height (mm). The apparent shear rate $\dot{\gamma}_{app}$ (s^{-1}) was calculated at the three different steps by Eq. 5.7 (Eswaran et al., 1963)

$$\dot{\gamma}_{app} = 6Q/(B \times h^2) \tag{5.7}$$

where Q is the volumetric flow rate (mm^3/s), B is the width of the slit (mm). The apparent viscosity η_{app} (Pa·s) was calculated using Eq. 5.8:

$$\eta_{app} = \tau/\dot{\gamma}_{app} \tag{5.8}$$

The Weissenberg–Rabinowitsch correction may be applied to obtain the wall shear rate $\dot{\gamma}_w$ and the true viscosity η_t, respectively, as follows:

$$\dot{\gamma}_w = \frac{1}{3}\{2 + \frac{d\ln(\dot{\gamma}_{app})}{d\ln(\tau_{app})}\}\dot{\gamma}_{app} \tag{5.9}$$

$$\eta_t = \tau/\dot{\gamma}_w \tag{5.10}$$

The apparent viscosity of the MCT–oil was measured with a Anton Paar Physica MCR301 rotational rheometer with a cone and plate geometry (CP50–1/TG–SN15821). Measurements were conducted at the similar conditions as during the extrusion processing: The temperature was set to 140 °C and the shear rate ranged from 1 to 120 s^{-1}. MCT–oil showed Newtonian behavior at the range of measurements with a viscosity of 0.002 ± 0.00003 Pa·s.

5.3.3 CFD Simulation

Lipophilic components are incorporated into plasticized starch matrix most favourably at the end of the extruder for an improved stability of the labile bioactives and for better control on starch conversion (Lakkis, 2007; Emin et al., 2012c[3]). As the goal of this study

[3] presented in this thesis as Chapter 2

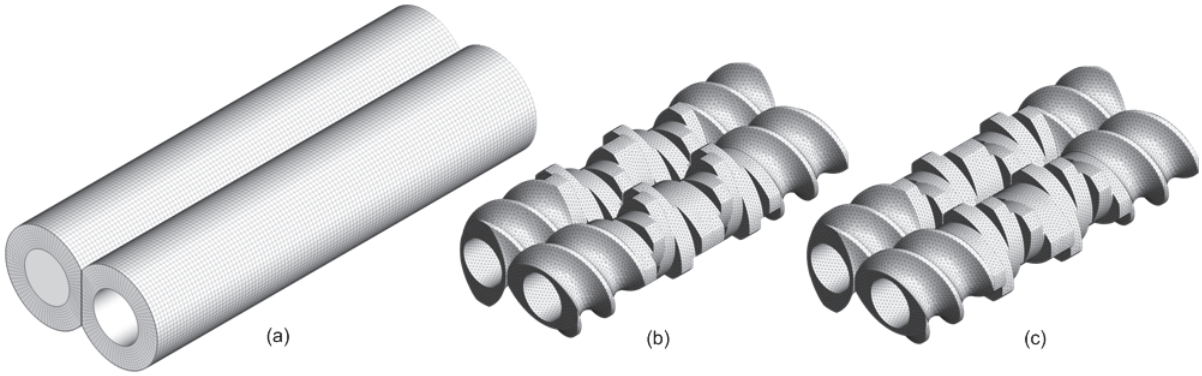

Figure 5.2: Computational domain: (a) barrel and (b) screw configuration 1 (transport elements and reverse kneading blocks) and (c) screw configuration 2 (transport elements and forward kneading blocks).

paper was not to analyze the flow in whole extruder, but to focus on this mixing zone, the analysis was restricted to the flow in the last barrel of the extruder. Two different screw configurations with reverse and forward kneading blocks were used, as shown in Figure 5.2b and Figure 5.2c, respectively. The flow through these elements is assumed to be isothermal in accordance with negligible temperature change of the material at this region. The rheological data of plasticized starch measured with the multiple step online slit die rheometer is fitted to the Bird–Carreau viscosity model

$$\eta_{app} = \eta_0\{1 + (\lambda\dot{\gamma}_{app})^2\}^{\frac{n-1}{2}} \tag{5.11}$$

where η_0 is the zero shear viscosity, λ is the natural time and n is the power law index. At low shear rate ($\dot{\gamma} << 1/\lambda$) Bird–Carreau fluid behaves as a Newtonian fluid and at high shear rate ($\dot{\gamma} >> 1/\lambda$) as a power–law fluid. Since the flow rate of the starch is relatively low (i.e. 11 kg/h), creeping flow is assumed and gravity effects are neglected.
The governing equations regarding a time–dependent, isothermal and incompressible flow of a generalized Newtonian fluid is

$$\rho\frac{Dv}{Dt} = -\nabla p + \nabla \cdot T + \rho g \tag{5.12}$$

$$\nabla \cdot v = 0 \tag{5.13}$$

where D/Dt is the material derivative, v is the velocity, p is the pressure, ρ is the density,

g is the gravity and T is the extra stress tensor defined by:

$$T = 2\eta(\dot{\gamma})d \tag{5.14}$$

with the strain rate tensor d and the kinematic viscosity η. The shear rate $\dot{\gamma}$ is defined as the square root of the second invariant of the strain rate tensor:

$$\dot{\gamma} = \sqrt{2d : d} \tag{5.15}$$

To determine the flow patterns in the extruder, the governing equations were calculated by CFD code ANSYS POLYFLOW 14.0 which is finite element code dedicated to highly viscous flows. The flow in a co–rotating twin–screw extruder is 3–D and unsteady due to moving and intermeshing parts (two rotating intermeshing screws). In order to simplify the set up of such a simulation and to avoid the use of a remeshing algorithm, the mesh superimposition technique introduced by Avalosse (1996) was used. Alsteens et al. (2004) discussed in detail the requirements for the meshing and the mixed interpolations in order to get reliable results out of such a simulation. Mesh refinement and selection of the mixed interpolation were performed accordingly by comparing the pressure evolution along the line Z–Z′ illustrated in Figure 5.3. After performing sensitivity analysis by investigating the influence of mesh design and interpolation method on pressure profile along the extruder, 503000 bricks (i.e. volume elements) for mesh size and enriched mini–element velocity and linear pressure for mixed interpolations were chosen (results are not shown). To capture the high shear rates observed in the clearance between the tip of screws and the barrel wall, the meshes in these zones is composed of three bricks. To be able to set boundary conditions, sufficiently long inlet and outlet channels (i.e. 10mm) were added to the computational domain where fully developed flows can be assumed. Thus, a developed velocity profile is imposed at the inlet section and vanishing normal velocity and tangential force are imposed at the exit section. The geometrical characteristics and the dimensions of the computational domain are depicted in Figure 5.3 and listed in Table 5.1. The XY and XZ cross–sections used to depict the results were taken at the position of line X–X′ and line Z–Z′ given in Figure 5.3, respectively.

Steps of the time dependent simulations were as follows: Firstly, a steady state simulation was performed. Then, the result of the steady state simulation was used as an initial

Table 5.1: Dimensions of the screws and the barrel depicted in Figure 3.

Dimensions (mm)					
A-A′	10	B-B′	48	C-C′	24
X-X′	47.6	Z-Z′	96	D_c	21.1
R_b	13	R_i	8	R_o	12.75

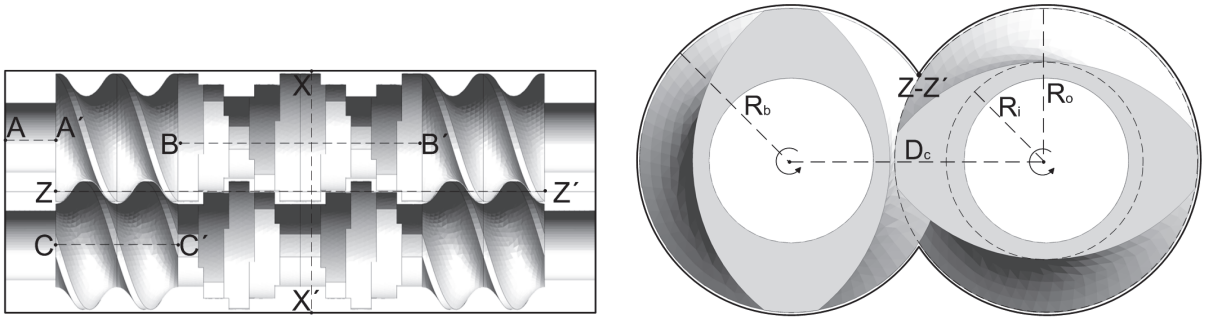

(a) (b)

Figure 5.3: Geometrical characteristics of the screws and the barrel. (a): Top view, (b): Front view.

velocity field in a time dependent simulation to obtain a physically relevant initial step. Due to symmetrical geometry, only half a turn of the screw was simulated. To obtain accurate evolution of flow pattern in time, 40 time steps were simulated for half a turn of screws. Finally, to analyze the dispersive and distributive mixing, particle tracking was performed by launching virtual particles into the flow fields obtained from time dependent simulation. The marker particles are assumed to be massless, volumeless, and noninteracting with each other. Under these assumptions, the particles can be located by integrating the velocity vectors with respect to time. Initially, these particles are randomly distributed in a small box at the inlet section of the flow domain (point Z in Figure 5.3). Along the trajectory, mixing characteristics experienced by each particle were computed. 1500 particles were tracked to obtain statistically representative results.

The numerical simulations were computed on a high performance parallel computer HP XC3000 (The Steinbuch Centre for Computing, KIT, Karlsruhe). For the computations, two Quad–core Intel Xeon processors E5540 (2.53 GHz, 4×256 KB level 2 cache and 8 MB level 3 cache) and 48 GB of main memory were used. The according computational costs for steady–state simulation, time–dependent simulation and particle tracking were

approximately 3.5 h, 33 h and 15 h, respectively.

5.4 Results and Discussion

5.4.1 Viscosity model

Viscosity model defines the rheological characteristics of the fluid inside the extruder and directly affects the flow behavior. Selection of the viscosity model and the according fit parameters play, therefore, a crucial role on the accuracy of the simulation results. Plasticized starch is a non–Newtonian fluid and its rheological behavior is very complex, depending on different parameters such as screw speed, temperature and moisture content (Lai and Kokini, 1991; Della Valle et al., 1998). Measurement of its rheological characteristics is also very challenging due to the intrinsic nature of the plasticized starch demanding measurement conditions at elevated temperature and pressure.

Online rheometry is accepted as most accurate method to measure the viscosity of plasticized starch (Della Valle et al., 1996; Padmanabhan and Bhattacharya, 1991; Senouci and Smith, 1988). Therefore, in the present study, a slit die rheometer mounted on the end of the extruder was used to measure the viscosity as described in section 5.3.2 in detail. Obtained results are given in Figure 5.4 for screw speeds of 300 rpm and 500 rpm. The symbols represent the measured apparent viscosities of plasticized starch at varying shear rates. The results show a shear thinning behaviour of plasticized starch, as also reported in (Vergnes and Villemaire, 1987; Willett et al., 1995; Xie et al., 2009).Furthermore, it can be seen that increasing screw speed led to decrease in viscosity. This happens due to higher mechanical energy input at higher screw speeds leading to more intensive degradation of the starch which eventually results in lower matrix viscosity (Lai and Kokini, 1991; Brümmer et al., 2002; van den Einde et al., 2004).

The Power law equation can satisfactorily describe the viscosity of starch at the shear rate range measured (i.e. 10^0 s^{-1} to 10^3 s^{-1}). However, at low shear rates, it gives physically absurd values which are very high viscosities preventing the convergence of the numerical simulation. The Bird–Carreau equation used here is more thorough at describing the rheological behavior of shear thinning fluids like plasticized starch, since it also includes the zero shear viscosity emerging at very low shear rates (Dus and Kokini, 1990). With an online slit die rheometer, zero shear viscosity of the plasticized starch

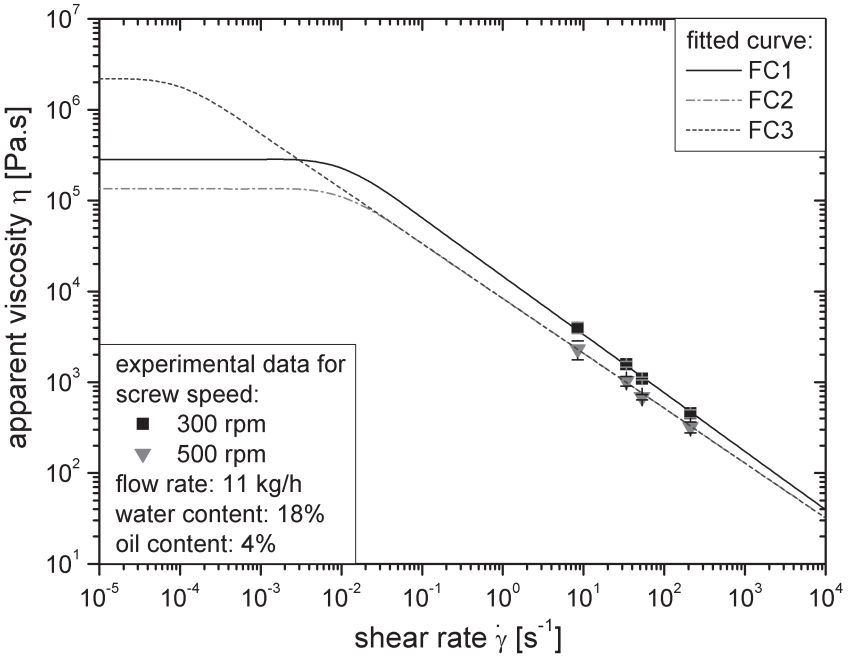

Figure 5.4: Viscosity curves of the plasticized starch fitted to Bird-Carreau viscosity model. Experimental data and fitted curves (FC) are depicted as symbols and lines, respectively. Experiments were performed in triplicates.

cannot be determined, because low shear rates are not possible to achieve at the flow rate (i.e. 11 kg/h) investigated. Dus and Kokini (1990) reported for a starch based matrix that the Newtonian behavior emerges primarily below a shear rate of 10^{-2} s^{-1} (i.e. natural time λ of 100 s).

To analyze the sensitivity of the simulation to the fit parameters of Bird–Carreau viscosity model, three different curves were fitted to the experimental data. Fitted curves (FC1, FC2 and FC3) and the according fit parameters are given in Figure 5.4 and Table 5.2, respectively. To investigate the influence of the zero shear viscosity (η_0) and natural time (λ), fit parameters of curve 2 (FC2) and curve 3 (FC3) were used to perform steady state simulations. The sensitivity of the simulation to the viscosity change at the shear thinning region was analyzed by comparing the pressure profile at the simulations performed with the fit parameters of curve 1 (FC1) and curve 2 (FC2). All other parameters were kept constant at screw speed of 500 rpm, flow rate of 11 kg/h and screw configuration 2.

Figure 5.5 shows the pressure drop along the extruder (axis Z–Z′) obtained from the simulations. The results from the simulations conducted using the fit parameters of FC2 and FC3 clearly show that about 16 times increase in zero shear viscosity has no

Table 5.2: Fit parameters used to investigate the sensitivity of simulation to the viscosity model. Screw speed: 500 rpm, flow rate: 11 kg/h, screw configuration: 2 (with forward kneading blocks).

viscosity η [Pa·s] $= \eta_0(1 + (\lambda\dot{\gamma})^2)^{\frac{n-1}{2}}$			
curve	η_0	λ	n
FC1	284310	100	0.375
FC2	135685	100	0.395
FC3	2200553	10000	0.395

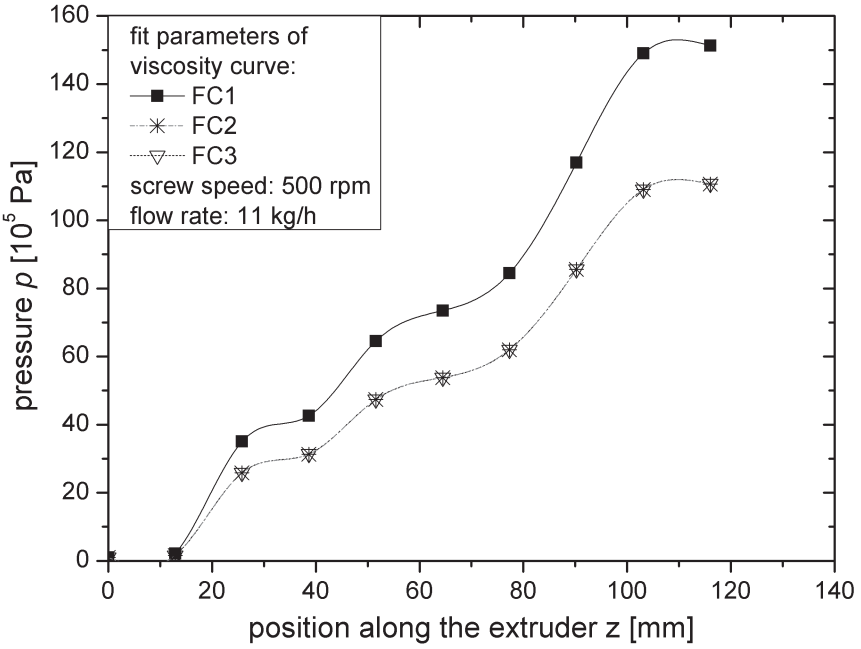

Figure 5.5: Pressure drops along the extruder (axis Z-Z′) obtained from simulations using various fit parameters for the Bird-Carreau viscosity model given in Table 5.2. Screw speed: 500 rpm, flow rate: 11 kg/h, screw configuration: 2.

influence on the flow in the mixing zone with respect to the pressure drop along this zone of the extruder. In contrast, simulations with FC1 and FC2 shows that a slight change in viscosity at the shear thinning region (e.g. 515 Pa·s to 762 Pa·s at $\dot{\gamma}$ = 100 s^{-1}) leads to significant increase in pressure drop (i.e. 11000 kPa to 15100 kPa).

The influence of the viscosity on simulated data was further investigated by comparing the viscosity distribution within the extruder channel as depicted in Figure 5.6. These cross–sections show that the change in natural time had no influence on the actual distribution

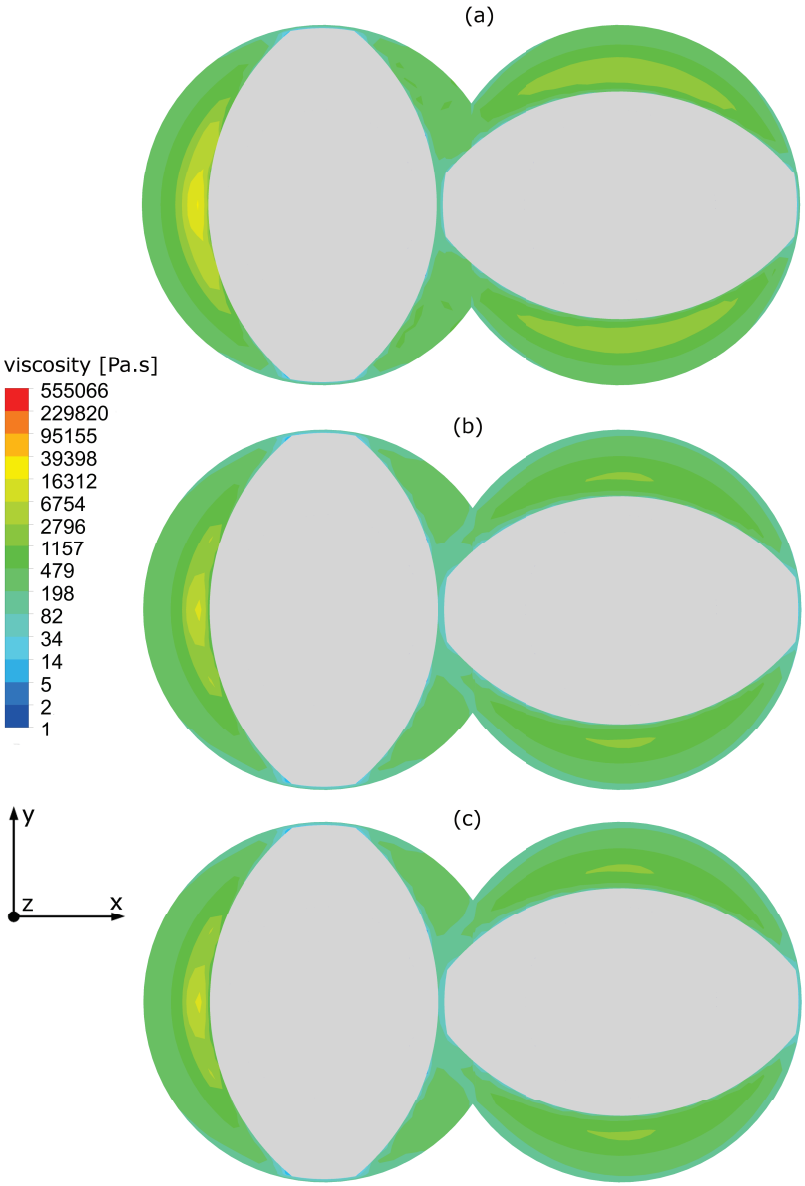

Figure 5.6: XY plane distribution of viscosity obtained from simulations using various fit parameters for the Bird–Carreau viscosity model given in Table 5.2: (a) FC1, (b) FC2, (c) FC3 ; screw speed: 500 rpm, flow rate: 11 kg/h, screw configuration: 2.

of the viscosity of the fluid in the extruder channel (Figure 5.6b and 5.6c), whereas the change in viscosity at higher shear rates (i.e. at shear thinning region) was reflected to the viscosity distribution within the extruder (see Figure 5.6a and 5.6b). These are expected results as the shear rates within the extruder are relatively high to reveal the influence of the zero shear viscosity. This will be discussed in section 5.4.3 in more detail. These results suggest that the viscosity data measured by the online slit die rheometer

is adequate for describing the viscosity of plasticized starch within the extruder at the process conditions studied.

5.4.2 Experimental validation

The physical relevance of the computational simulation of the flow within an extruder can be done by measuring the pressure difference along the simulated zone (Ishikawa et al., 2000). In the present study, pressure sensors were mounted on the inlet and outlet region of the mixing zone in the extruder as described in section 5.3.2. The online slit die rheometer was mounted on the extruder during the validation experiments to monitor simultaneously the rheological behaviour of plasticized starch matrix. Obtained rheological data and applied process parameters (e.g. screw speed, flow rate and screw geometry) were used to perform the computational simulations of the flow in extruder parallel to the experiments. Pressure differences between the inlet and outlet of the flow domain of the simulation were compared to the experimental values measured by inline mounted pressure sensors. The results obtained at different process conditions are given in Table 5.3 showing good agreement between experimental and computational values. The average values are given with the according deviations. The deviations in the experimental values resulted from pressure fluctuations during the pressure measurements, whereas the deviations in computational values show the differences at varying time steps of simulations.

Table 5.3: Comparison of experimental and computational pressure drop along the extruder for various process conditions. Screw configuration 2 with an outer diameter R_o of 12 mm were used during the experiments and simulations.

screw speed [rpm]	flow rate [kg/h]	water content [%]	viscosity η [Pa·s] $= \frac{\eta_0}{(1+(\lambda\dot{\gamma})^2)^{\frac{n-1}{2}}}$			$\triangle p$ experimental [10^5 Pa]	$\triangle p$ computational [10^5 Pa]
			η_0	λ	n		
200	13	30	1080910	100	0.15	14.5 ± 0.2	14.3 ± 1.5
200	11	18	2500910	100	0.11	30 ± 0.3	30.5 ± 3.2
400	26	30	1080910	100	0.15	16.2 ± 0.2	16 ± 1.7

5.4.3 Flow type and profile

In this section, the flow type and profile in the extruder are discussed by using the influence of screw speed and configuration as exemplary process parameters. For the viscosity model, the data measured by the online multiple step slit die rheometer were fitted to the Bird–Carreau equation as discussed in section 5.4.1. In the experiments performed at constant process parameters but with different screw configurations, very similar viscosities were measured. However, for the sake of better comparison, exact same viscosity data (i.e. FC1) is used to investigate the influence of screw geometry. The details of the input parameters for the simulations are given in Table 5.4.

Elongational flow is known to be more effective than simple shear flow for droplet breakup, and thus for dispersive mixing (Bentley and Leal, 1986; Grace, 1982). This is due to the presence of vorticity in shear flow, which causes the portion of droplets to align towards the flow direction and not breakup (Stone, 1994). This effect of shear flow is more pronounced at high viscosity ratios (Bentley and Leal, 1986; Grace, 1982). Mixing index introduced by Cheng and Manas–Zloczower, (1990) can be used for the mapping of flow type in the flow field of an extruder to have an insight into the mechanism of mixing at a given point in time.

Figure 5.7 and Figure 5.8 show the distributions of the mixing index on XY plane and XZ plane for varying process conditions with values from 0 for pure rotation to 0.5 for simple shear and 1 for irrotational flow (i.e. elongational flow). As representative of the flow field on the XY plane, images at two different screw positions were depicted in Figure 5.7 for each process condition. Regardless of minor differences, all the images show similar distribution of the mixing index: rotational flow ($\lambda_{MZ} < 0.4$) dominates the region close to the screw channel; maximum values of mixing index ($0.8 > \lambda_{MZ} > 0.7$) were found in

Table 5.4: Simulated process conditions with the according viscosity curves.

screw speed [rpm]	screw configuration	flow rate [kg/h]	water content [%]	viscosity curve
300	2	11	18	FC1
500	2	11	18	FC2
300	1	11	18	FC1

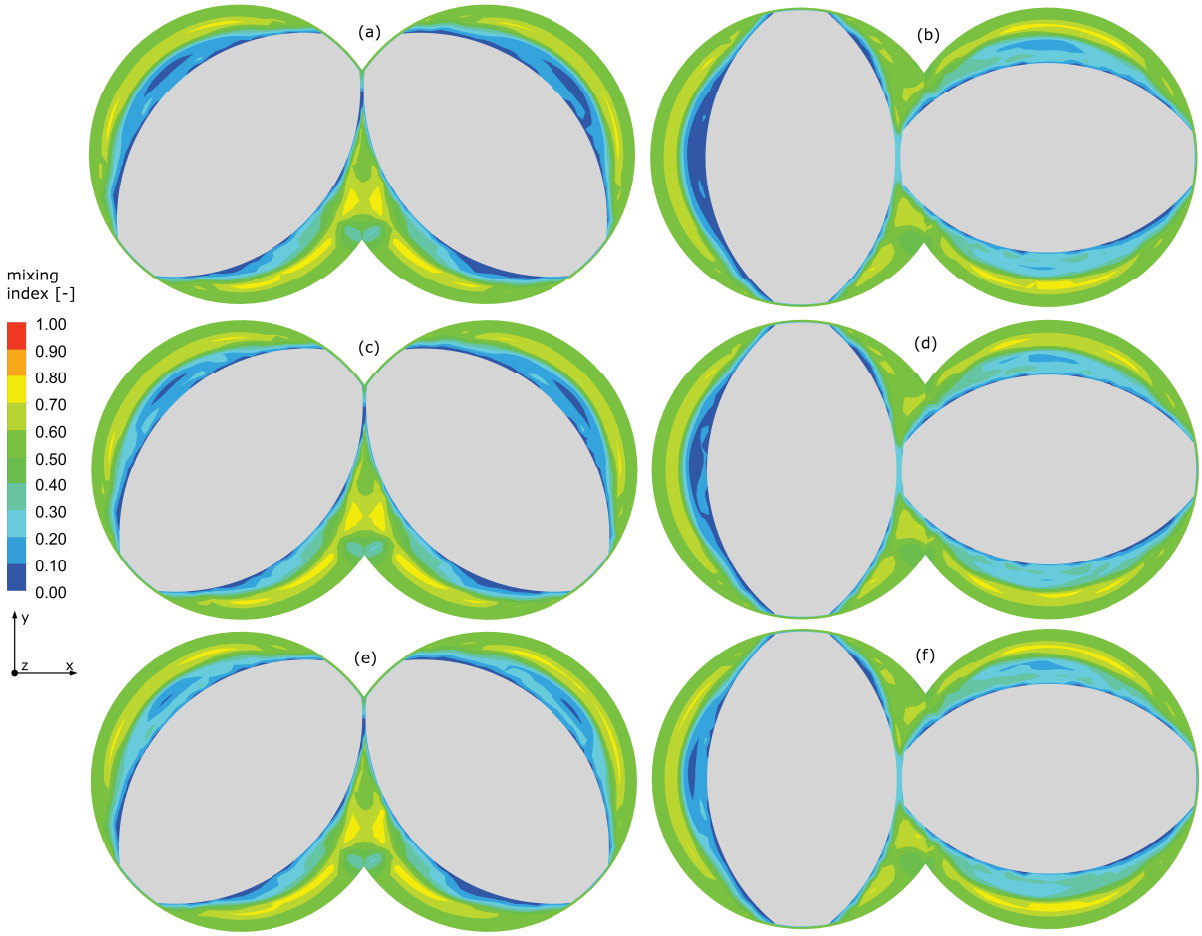

Figure 5.7: XY plane distribution of the mixing index for 3 different process conditions: (a, b) Viscosity curve: FC1, screw speed: 300 rpm, screw configuration: 2; (c, d) viscosity curve: FC2, screw speed: 500 rpm, screw configuration: 2; (e, f) viscosity curve: FC1, screw speed: 300 rpm, screw configuration: 1. Grey zones represent the location of screws. Images were taken at time step 30 (left) and time step 40 (right).

the middle of the channel; the rest and the most of the flow field is dominated by shear flow ($0.6 > \lambda_{MZ} > 0.4$). No region with zero vorticity ($\lambda_{MZ} = 1.0$) was found. The flow at the tip of the screws is mainly dominated by simple shear flow ($\lambda_{MZ} = 0.5$). Similar results were reported by Connelly and Kokini (2004) who conducted a 2–D simulation of a shear thinning fluid in an extruder channel.

The interpretation of mixing index in relation to dispersive mixing is possible, if it is combined with the magnitude of the shear rate (Cheng and Manas–Zloczower, 1997). Figure 5.9 and Figure 5.10 show the distributions of the local shear rate on XY plane and XZ plane for varying process conditions. The images were taken at the same positions as for the mixing index (i.e. Figure 5.7 and 8). Although the distributions of the local

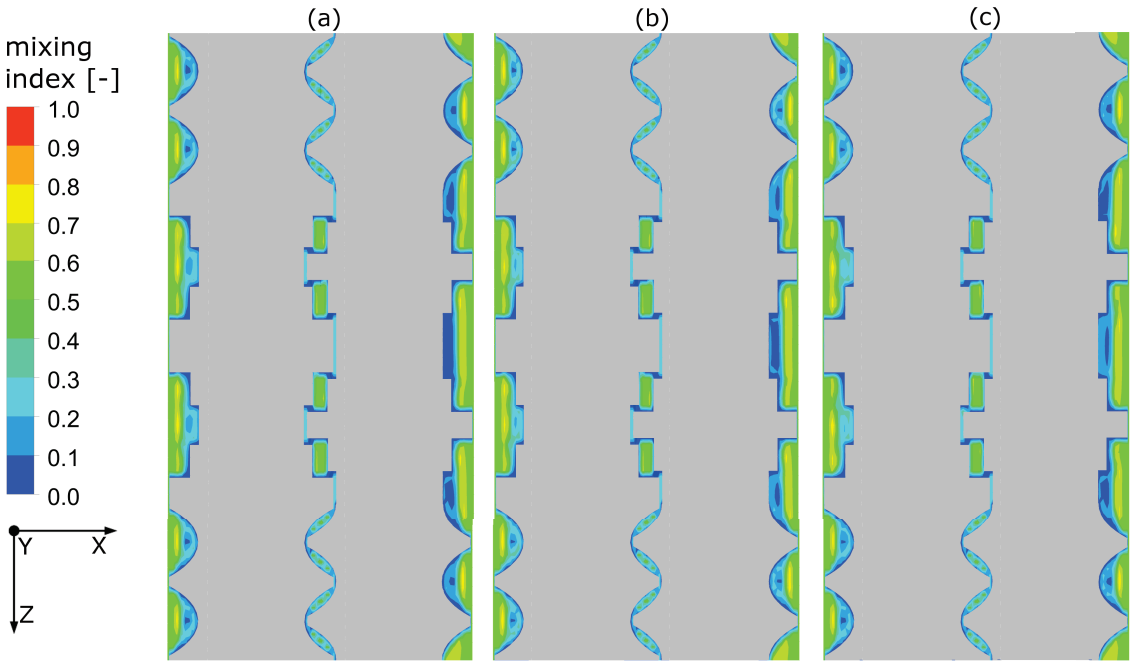

Figure 5.8: XZ plane distribution of the mixing index for 3 different process conditions: (a) viscosity curve: FC1, screw speed: 300 rpm, screw configuration: 2; (b) viscosity curve: FC2, screw speed: 500 rpm, screw configuration: 2; (c) viscosity curve: FC1, screw speed: 300 rpm, screw configuration: 1. Grey zones represent the location of screws. Images were taken at time step 40.

shear rate are similar for all the process conditions studied, increasing screw speed led to higher shear rates as expected (Figure 5.9c, Figure 5.9d and Figure 5.10b). Maximum shear rates are generated at the tip of the screws. Furthermore, it can be clearly seen that shear rates lower than 0.1 s^{-1} are not found, which also explains why the viscosity of the matrix at lower shear rates (i.e. zero shear viscosity) doesn't influence the flow as discussed in section 5.4.1. When the mixing index and shear rate distributions are compared, it can be seen that at the positions where the mixing index is maximum, shear rates are relatively low (< 574 s^{-1}). In contrast, at the positions where the shear rate is very high (> 2430 s^{-1}), the flow is mainly dominated by simple shear flow.

5.4.4 Distributive mixing efficiency

Although the main focus of the present study is to analyze the dispersive mixing efficiency, it is important to evaluate the quality of distributive mixing due to its successive

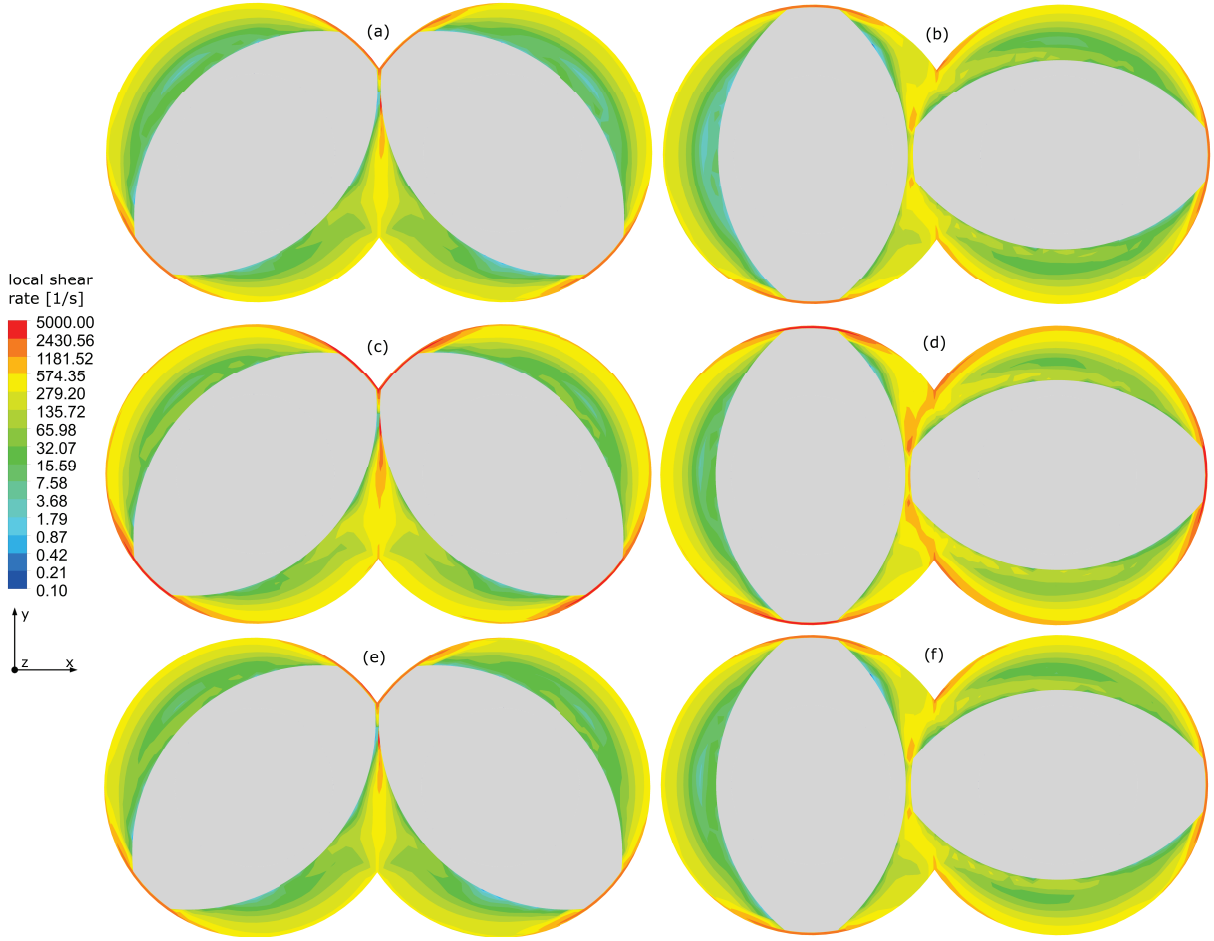

Figure 5.9: XY plane distribution of the local shear rate for 3 different process conditions: (a, b) viscosity curve: FC1, screw speed: 300 rpm, screw configuration: 2; (c, d) viscosity curve: FC2, screw speed: 500 rpm, screw configuration: 2; (e, f) viscosity curve: FC1, screw speed: 300 rpm, screw configuration: 1. Grey zones represent the location of screws. Images were taken at time step 30 (left) and time step 40 (right).

relation with dispersive mixing. The images from particle tracking were used to analyze qualitatively the ability of the extruder to distribute oil droplets in plasticized starch matrices. MCT–oil droplets have low density and viscosity compared to plasticized starch, and therefore tracked massless, denseless particles are expected to behave similar to the flow of MCT–oil droplet in plasticized starch. Figure 5.11 shows the distribution of the particles at first 4 seconds of the simulation. Figure 5.11a shows a cluster of particles at their initial location (t = 0) selected according to the feeding point of the MCT–oil at the extrusion trials. The images clearly show that good distribution of the particles was achieved even after 4 seconds. Hence, these qualitative results suggest that the distributive

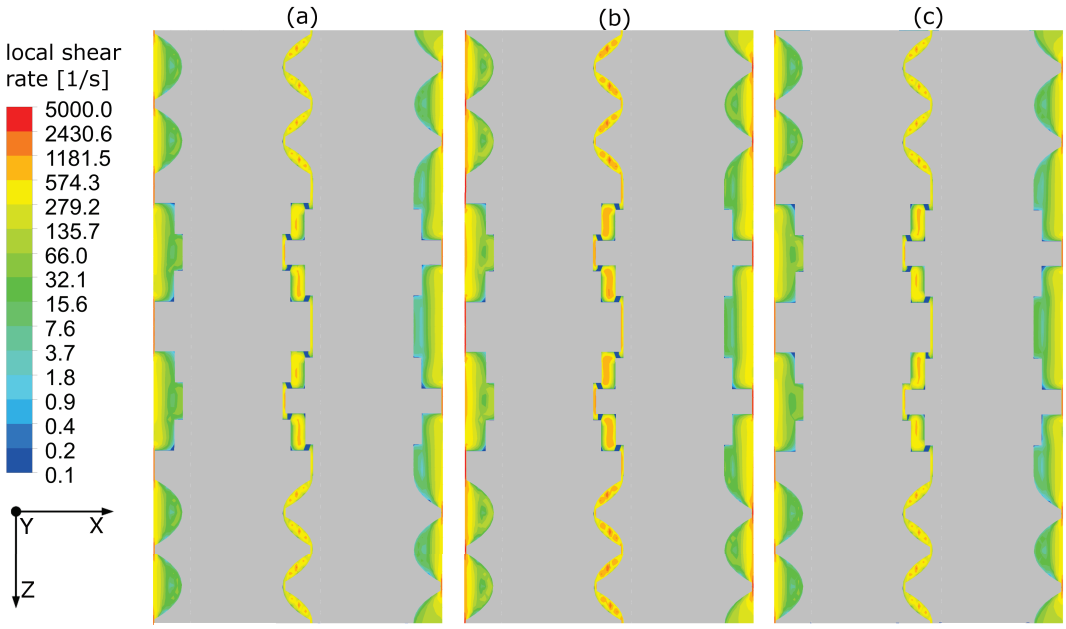

Figure 5.10: XZ plane distribution of the local shear rate for 3 different process conditions: (a) viscosity curve: FC1, screw speed: 300 rpm, screw configuration: 2; (b) viscosity curve: FC2, screw speed: 500 rpm, screw configuration: 2; (c) viscosity curve: FC1, screw speed: 300 rpm, screw configuration: 1. Grey zones represent the location of screws. Images were taken at time step 40.

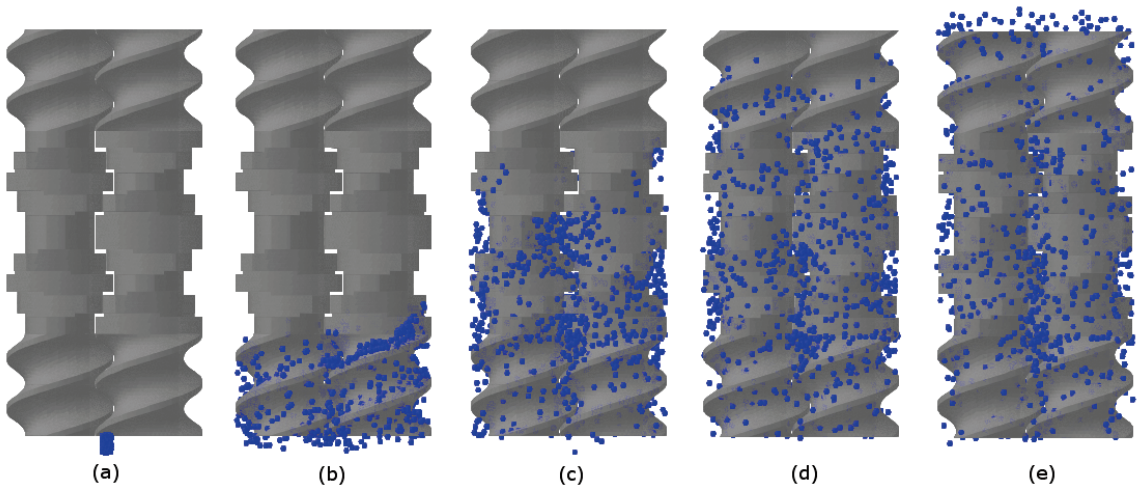

Figure 5.11: Distribution of the particles along the screws at a) t = 0 s; (b) t = 1 s; (c) t = 2 s; (d) t = 3 s and (e) t = 4 s, screw speed: 500 rpm, flow rate: 11 kg/h, screw configuration: 2.

mixing in the simulated flow domain is very good. For all the process parameters and screw configurations investigated, similar results were observed (results not shown).

5.4.5 Dispersive mixing efficiency

Capillary ratio (Ca/Ca_{crit}) is expected to be the main parameter defining droplet breakup as discussed in section 5.2.2. in detail. For MCT–oil droplets in plasticized starch matrix, the capillary ratio can be derived from Eq. 5.2, Eq. 5.3, and Eq. 5.4:

$$Ca/Ca_{crit} = \frac{\eta_b^{0.14} \cdot \eta_d^{0.86} \cdot \dot{\gamma} \cdot R \cdot 10^5}{6\sigma} \tag{5.16}$$

By keeping the initial droplet radius R constant, the capillary ratio can be considered to be a kinematic variable characterizing the efficiency of dispersive mixing. It must be however noted that this equation involves the critical capillary number which is only valid for simple shear flow. The droplet breakup in a complex geometry (i.e. intermeshing twin screws) is achieved by flow of the droplets through the high shear zones (Janssen, 1993; Sundararaj and Macosko, 1995; Cheng and Manas–Zloczower, 1997). The results from the numerical simulations (see Figure 5.7 and 5.9) suggest that these high shear zones are generated at the clearances between screws and barrel at which the flow is dominated by simple shear flow. Therefore, Eq. 5.16 can be used to determine the maximum capillary ratio experienced by the particles within the extruder. For this purpose, the capillary ratio experienced by each particle was monitored during particle tracking simulation.

To evaluate the dispersive mixing efficiency, cumulative number distributions of maximum capillary ratio along the 1500 particles were calculated. Since the dispersive mixing ability of the flow is aimed to be evaluated, the droplet radius R was kept arbitrarily constant at 5 μm. Interfacial tension σ was kept also constant at 10 mN/m, which was estimated in our previous study (i.e. Emin et al., 2012a) for the process conditions investigated.The results are depicted in Figure 5.12a for screw speeds of 300 rpm and 500 rpm. Similarly, maximum shear stress distribution is formed and depicted in Figure 5.12b for comparison. These distributions show that increasing screw speed leads to decrease in the maximum shear stress experienced by the particles. This happens due to degradation of starch molecules at higher screw speeds leading to decreased blend viscosity (van den Einde et al., 2004; Liu et al., 2010). In contrast, particles are exposed to higher capillary

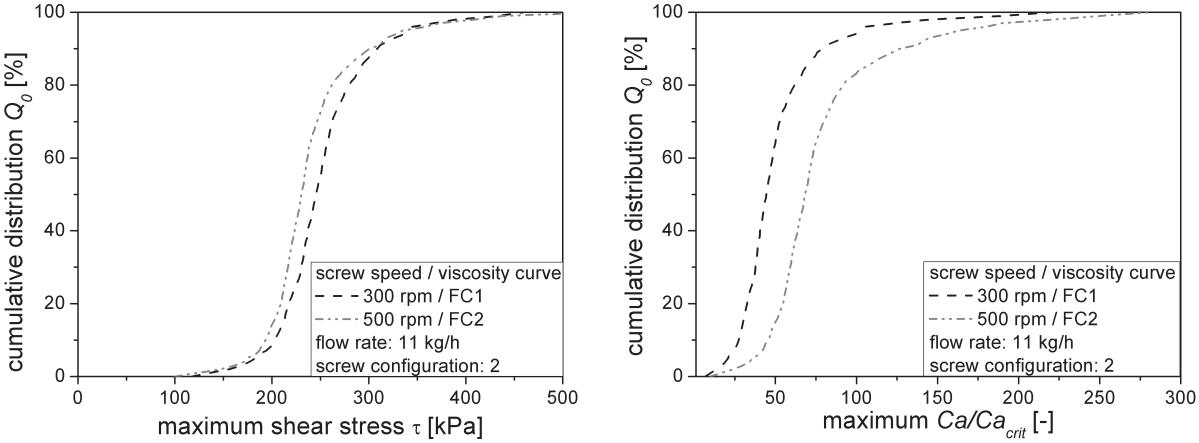

(a) (b)

Figure 5.12: Influence of screw speed on the cumulative number distribution of (a) maximum capillary ratio and (b) maximum shear stress along the 1500 tracked particles.

ratios at higher screw speeds indicating that dispersive mixing efficiency increased. These results suggest that the decrease in generated shear stresses does not necessarily lead to lower dispersive mixing efficiency, because simultaneous decrease in blend viscosity leads to higher viscosity ratio, and thus to higher capillary ratio (see Eq. 5.4). Such an effect of increasing screw speed was reported to be beneficial for the retention of lipophilic bioactives, which are susceptible to mechanical stresses but favourable to be dispersed finely (Emin et al., 2012c).

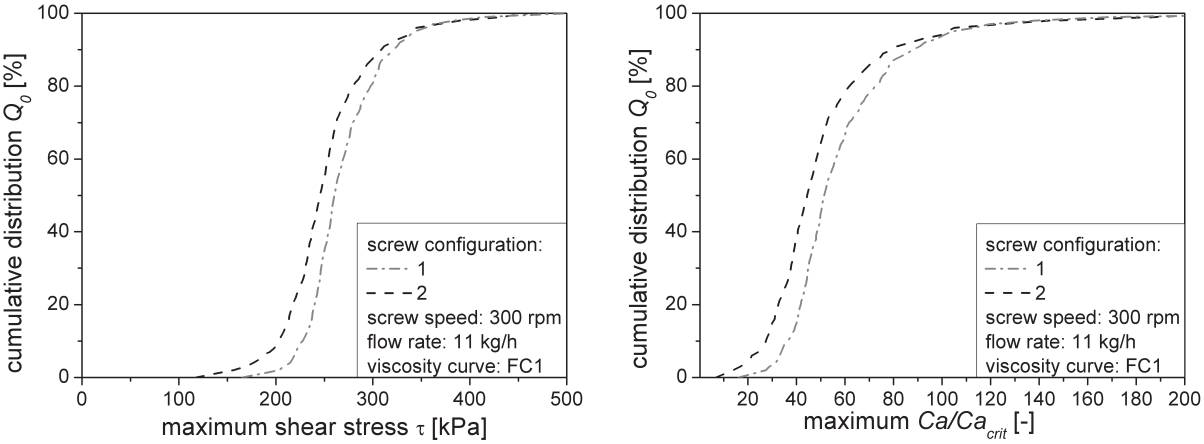

(a) (b)

Figure 5.13: Influence of screw configuration on the cumulative number distribution (a) maximum capillary ratio and (b) maximum shear stress along the 1500 tracked particles.

Another important aspect is the flow pattern which can be mainly altered by using different screw configurations. Figure 5.13a and Figure 5.13b shows the influence of two different screw configurations (shown in Figure 5.2) on maximum capillary ratio and maximum shear stress experienced by particles tracked. All other input parameters were kept constant. In this case, maximum shear stress and maximum capillary ratio distributions show similar trends. However, using screw configuration 1 increases the number of particles that are exposed to higher maxima. Such an effect results from reverse kneading blocks used in configuration 1 restricting the flow in the screw channel. This enforces the particles to flow through the tip of the screws and therefore leads to higher dispersive mixing efficiency.

5.5 Conclusions

Analysis of dispersive mixing of oil in rheologically complex plasticized starch matrices within an extruder is a very challenging task, since several parameters such as the complex rheological behaviour of the matrix, initial droplet size distribution, nature and strength of the flow with the time of exposure, are necessary to be known. An experimental access is practically impossible. Flow simulation, however, offers an access to local data on flow velocities and resulting shear stresses, capillary numbers and capillary ratio data, the latter being parameters of relevance for droplet break–up in laminar flow. Such an approach demands reliable characterization of the experimental conditions to be simulated. Therefore, experiments with a lab scale co–rotating twin screw extruder were performed and the rheological characteristics of the starch at the extrusion conditions were measured by an online multiple step slit die rheometer.

The flow of plasticized maize starch in a co–rotating twin screw extruder was simulated by using CFD. Sensitivity of the simulations to viscosity data was investigated by varying the fit parameters of Bird–Carreau viscosity model. The results suggest that about 16 times increase in zero shear viscosity has no influence on the flow, whereas a slight change in viscosity at the shear thinning region (e.g. 515 Pa·s to 762 Pa·s at $\dot{\gamma} = 100\ s^{-1}$) leads to significant increase in pressure drop along the mixing zone of extruder. To examine the physical relevance of the simulation, the pressure differences between inlet and outlet of flow domain of the simulation were compared to the experimental values measured by flush mounted pressure sensors. The results shows good agreement between experimental

and computational results obtained at different process conditions. Furthermore, the flow type and profile in the extruder were discussed by using the influence of screw speed and configuration as exemplary process parameters. The results suggest that high shear zones are generated at the clearances between screws and barrel or between two screws at which the flow is dominated by simple shear flow.

To evaluate the dispersive mixing efficiency, material specific critical capillary number were implemented into particle tracking simulations. Maximum capillary ratio distribution along 1500 particles was calculated to evaluate the dispersive mixing efficiency. The results show that increase in screw speed from 300 rpm to 500 rpm led to exposure of the particles to lower shear stresses, whereas the capillary ratio increases. These results suggest that the decrease in generated shear stresses does not necessarily lead to lower dispersive mixing efficiency. Furthermore, to investigate the influence of screw geometry, two different screw configurations were simulated. The results show that the dispersive mixing efficiency can be improved by using reverse kneading blocks that enforce the particles to flow through the tip of the screws. Therefore, more particles are exposed to these high shear zones. The developed procedure can be used for process parameter adaptation and optimization in terms of dispersive mixing efficiency for processes governed by complex flows as of plasticized starch matrices in an extruder.

Nomenclature

a	acceleration	ΔP	pressure drop
B	width of the slit	Q	volumetric flow rate
Ca	capillary number	Q_0	cumulative number distribution
Ca_{crit}	critical capillary number	R	droplet radius
d	rate of strain tensor	T	extra–stress tensor
g	gravity	v	velocity
h	slit height	v_p	velocity of the moving mesh
H	penalty force term	τ	shear stress
L	distance between pressure sensors	σ	interfacial tension
η_{app}	apparent viscosity	λ_{MZ}	mixing index
η_b	blend viscosity	λ	natural time
η_d	dispersed phase viscosity	$\dot{\gamma}$	shear rate
η_t	true viscosity	$\dot{\gamma}_{app}$	apparent shear rate
η_0	zero shear viscosity	$\dot{\gamma}_w$	wall shear rate
p	viscosity ratio	ω	vorticity tensor
ρ	density		

5.6 References

Alsteens, B., Legat, V., & Avalosse, T. (2004). Parametric study of the mixing efficiency in a kneading block section of a twin–screw extruder. *International Polymer Processing*, 3, 207–217.

Avalosse, T. (1996). Numerical simulation of distributive mixing in 3–D flows. *Macromolecular Symposium*, 112, 91–98.

Avalosse, T. & Rubin, Y., (2000). Analysis of mixing in co–rotating twin screw extruders through numerical simulation. *International Polymer Processing*, 15(2), pp.117–123.

Bentley, B., & Leal, L. (1986). An experimental investigation of drop deformation and breakup in steady, two–dimensional linear flows. *Journal of Fluid Mechanics*, 167(–1), 241–283.

Bertrand, F., Tanguy, P. a., & Thibault, F. (1997). A three–dimensional fictitious domain

method for incompressible fluid flow problems. *International Journal for Numerical Methods in Fluids*, 25(6), 719–736.

Bravo, V. L., Hrymak, A. N., & Wright, J. D. (2000). Numerical simulation of pressure and velocity profiles in kneading elements of a co–rotating twin screw extruder. *Polymer Engineering & Science*, 40(2), 525–541.

Brümmer, T., Meuser, F., van Lengerich, B., & Niemann, C. (2002). Effect of extrusion cooking on molecular parameters of corn starch. *Starch–Stärke*, 54, 1–8.

Cheng, H., & Manas–Zloczower, I. (1997). Study of mixing efficiency in kneading discs of co–rotating twin–screw extruders. *Polymer Engineering and Science*, 37(6), 1082–1090.

Cheng, J.J. & Manas–Zloczower, I., (1990). Flow field characterization in a banburry mixer. *International Polymer Processing*, 3, pp.178–183.

Connelly, R. (2004). The effect of shear thinning and differential viscoelasticity on mixing in a model 2D mixer as determined using FEM with particle tracking. *Journal of Non–Newtonian Fluid Mechanics*, 123(1), 1–17.

Debruijn, R. A. (1991). *Deformation and breakup of drops in simple shear flows*. Doctoral Thesis. Eindhoven University, The Netherlands.

Della Valle, G., Buleon, A., Carreau, P. J., Lavoie, P. A., & Vergnes, B. (1998). Relationship between structure and viscoelastic behavior of plasticized starch. *Journal of Rheology*, 42(3), 507.

Della Valle, G., Colonna, P., Patria, A. & Vergnes, B. (1996). Influence of amylose content on the viscous behavior of low hydrated molten starches. *Journal of Rheology*, 40(3), p.347.

Dus, S. J., & Kokini, J. L. (1990). Prediction of the nonlinear viscoelastic properties of a hard wheat flour dough using the Bird–Carreau constitutive model. *Rheology*, 34, 1069–1084.

Elmendorp, J. J. (1986). A study on polymer blending microrheology. *Polymer Engineering and Science*, 26(6), 418–426.

Emin, M. A., Hardt, N., van der Goot, A. J., & Schuchmann, H. P. (2012a). Formation of oil droplets in plasticized starch matrix in simple shear flow. *Journal of Food Engineering*, 112(3), 200–207.

Emin, M. A., Schmidt, U., van der Goot, A. J., & Schuchmann, H. P. (2012b). Coalescence of oil droplets in plasticized starch matrix in simple shear flow. *Journal of Food Engineering*, 113(3), 453–460.

Emin, M. A., Mayer–Miebach, E., & Schuchmann, H. P. (2012c). Retention of β–carotene as a model substance for lipophilic phytochemicals during extrusion cooking. *LWT – Food Science and Technology*, 48(2), 302–307.

Eswaran, R., Janeschitz–Kriegl, H., & Schijf, J. (1963). A slit viscometer for polymer melts. *Rheologica Acta*, 3 (2), 83 – 91.

French, D., Pulley, A. O., & Whelan, W. J. (1963). Starch fractionation by hydrophobic complex formation. *Starch–Stärke*, 15(10), 349–354.

Grace, H. P. (1982). Dispersion phenomena in high viscosity immiscible fluid systems and application of static mixers as dispersion devices in such systems. *Chemical Engineering Communications*, 14(3–6), 225–277.

Horn, D. (1989). Preparation and characterization of microdisperse bioavailable carotenoid hydrosols. *Die Angewandte Makromolekulare Chemie*, 166(1), 139–153.

Horn, D., & Rieger, J. (2001). Organic nanoparticles in the aqueous phase–theory, experiment, and use. *Angewandte Chemie International Edition*, 40(23), 4330–4361.

Ishikawa, T., & Analysis, N.–isothermal H. F. (2001). Mixing performance evaluation of kneading blocks in a co–rotating twin srew extruder. *Polymer Engineering and Science*, 41(5), 840–849.

Ishikawa, T., Kihara, S.–I., & Funatsu, K. (2000). 3–D numerical simulations of non-isothermal flow in co–rotating twin screw extruders. *Polymer Engineering & Science*, 40(2), 357–364.

Janssen, J. (1993). *Dynamics of liquid–liquid mixing*. Doctoral Thesis. Eindhoven University of Technology, The Netherlands.

Lai, L., & Kokini, J.L. (1991). Physicochemical changes and rheological properties of starch during extrusion (a review). *Biotechnology Progress*, 7(3), 251–266.

Lakkis, J. (2007). *Encapsulation and Controlled Release Technologies in Food Systems*. Ames, Iowa, USA: Blackwell Publishing.

Liu, W.–C., Halley, P. J., & Gilbert, R. G. (2010). Mechanism of degradation of starch, a highly branched polymer, during Extrusion. *Macromolecules*, 43(6), 2855–2864.

Mighri, F., Carreau, P. J., & Ajji, A. (1998). Influence of elastic properties on drop deformation and breakup in shear flow. *Journal of Rheology*, 42(6), 1477.

Padmanabhan, M. & Bhattacharya, M., (1991). Flow behavior and exit pressures of corn meal under high–shear–high–temperature extrusion conditions using a slit die. *Journal of Rheology*, 35(3), p.315.

Ribeiro, H. S., Guerrero, J. M. M., Briviba, K., Rechkemmer, G., Schuchmann, H. P., & Schubert, H. (2006). Cellular uptake of carotenoid–loaded oil–in–water emulsions in colon carcinoma cells in vitro. *Journal of Agricultural and Food Chemistry*, 54(25), 9366–9.

Schweizer, T. F., Reimann, S., Solms, J., Eliasson, A. C., & Asp, N. G. (1986). Influence of drum–drying and twin–screw extrusion cooking on wheat carbohydrates, II, effect of lipids on physical properties, degradation and complex formation of starch in wheat flour. *Journal of Cereal Science*, 4(3), 249–260.

Senouci, A. & Smith, A.C., (1988). An experimental study of food melt rheology. I. Shear viscosity using a slit die viscometer and a capillary rheometer. *Rheologica Acta*, 554(27), pp.546–554.

Sibillo, V., Simeone, M., & Guido, S. (2004). Break–up of a Newtonian drop in a viscoelastic matrix under simple shear flow. *Rheologica Acta*, 43(5), 449–456.

Stone, H. A. (1994). Dynamics of drop deformation and breakup in viscous fluids. *Annual Review of Fluid Mechanics*, 26(1), 65–102.

Strutt, D., Tzoganakis, C., & Duever, T. A. (2000). Mixing analysis of reactive polymer flow in conveying elements of a co–rotating twin screw extruder. *Advances in Polymer Technology*, 19(1), 22–33.

Sundararaj, U., & Macosko, C. W. (1995). Drop breakup and coalescence in polymer blends: the effects of concentration and compatibilization. *Macromolecules*, 28(8), 2647–2657.

Taylor, G. I. (1932). The viscosity of a fluid containing small drops of another fluid. *Proceedings of the Royal Society of London.* Series A, 138(834), 41–48.

Taylor, G. I. (1934). The formation of emulsions in definable fields of flow. *Proceedings of the Royal Society of London.* Series A, 146(858), 501–523. van den Einde, R. M., Akkermans, C., van der Goot, A. J., &

Boom, R. M. (2004). Molecular breakdown of corn starch by thermal and mechanical effects. *Carbohydrate Polymers*, 56(4), 415–422.

Vergnes, B., & Villemaire, J. P. (1987). Rheological behaviour of low moisture molten maize starch. *Rheologica Acta*, 576, 570–576.

Verhulst, K, Cardinaels, R., Moldenaers, P., Afkhami, S., & Renardy, Y. (2009). Influence of viscoelasticity on drop deformation and orientation in shear flow. Part 2: Dynamics. *Journal of Non–Newtonian Fluid Mechanics*, 156(1–2), 44–57.

Verhulst, K., Moldenaers, P., & Minale, M. (2007). Drop shape dynamics of a Newtonian drop in a non–Newtonian matrix during transient and steady shear flow. *Journal of Rheology*, 51(2), 261.

Willett, J. L., Jasberg, B. K., & Swanson, C. L. (1995). Rheology of thermoplastic starch: Effects of temperature, moisture content, and additives on melt viscosity. *Polymer Engineering and Science*, 35(2), 202–210.

Xie, F., Yu, L., Su, B., Liu, P., Wang, J., Liu, H., & Cheng, L. (2009). Rheological properties of starches with different amylose/amylopectin ratios. *Journal of Cereal Science*, 49(3), 371–377.

Yang, H.–H., & Manas–Zloczower, I. (1992). Flow field analysis of the kneading disc region in a co–rotating twin screw extruder. *Polymer Engineering and Science*, 32(19), 1411–1417.

Yue, P., Feng, J. J., Liu, C., & Shen, J. (2005). Viscoelastic effects on drop deformation in steady shear. *Journal of Fluid Mechanics*, 540(1), 427–437.

6 Droplet breakup and coalescence in a twin-screw extrusion processing of starch based matrix

This chapter is published as: Emin, M. A., & Schuchmann, H. P. (2013). Droplet breakup and coalescence in a twin-screw extrusion processing of starch based matrix. *Journal of Food Engineering*, 116(1),118–129.

Abstract

Formation of oil droplets during twin screw extrusion processing of maize starch was investigated by analyzing the droplet breakup and coalescence mechanisms separately. For this purpose, the flow was characterized by computational fluid dynamics (CFD) using material data derived from online rheological measurements. The simulated results on local flow conditions were coupled to experimental data on the dispersed phase morphology, which was analyzed by confocal laser scanning microscopy (CLSM). This was used to elucidate the influence of process characteristics relevant for droplet breakup and coalescence. The results showed that increasing screw speed does not necessarily result in smaller droplet sizes. This could be related to the contradictory effects: increasing screw speed improves the droplet breakup but also increases the coalescence. Smaller droplet sizes were obtained at higher blend viscosities, which could be achieved either by increasing the feed rate or by using screw configuration that applies less mechanical stress. The results suggest that an increase in blend viscosity reduced the coalescence. Moreover, increasing oil content led to an increased coalescence, and therefore to remarkably bigger droplets. Selection of process parameters (e.g. screw configuration, feed rate, screw speed) based on the findings of this study allowed enhancing the dispersive mixing efficiency of triglyceride droplets during extrusion processing of maize starch.

6.1 Introduction

Starch biopolymers are one of the most common raw materials used in food industry. The starch and its derivatives have several attributes which make them favourable for encapsulation applications. They are cost effective, vary in molecular size, and have desirable physicochemical properties such as solubility, melting and phase change (Forssell, 2004; Lakkis, 2007). In particular, extrusion technology is extensively used in the production of starch based delivery systems, since it possesses several advantages, such as its energy efficiency; the lack of process effluents; its mixing capability; and its versatility with respect to ingredient selection and the shapes and textures of products that can be produced (Lakkis, 2007). Incorporation of functional hydrophobic components (e.g. lipophilic bioactives, flavours, antimicrobials, antioxidants or drugs) into extruded starch based products has gained wide popularity by food industry as well as by chemical, pharmaceutical, and medical industries (Shogren et al., 1993; Yilmaz et al., 2001; Mano et al., 2003). In most cases, it is favourable to dissolve the functional components in lipid based delivery systems and disperse these solutions into small droplets to improve their stability, bioavailability and palatability (Horn, 1989; Horn and Rieger, 2001; Ribeiro et al., 2006). It is crucial to control the microstructure obtained during processing (i.e. size and shape of the dispersed phase), since the functional properties of hydrophobic components strongly depend on these structural characteristics.

Incorporation of health promoting lipophilic bioactives like carotenoids, fatty acids or phytosterols into an amorphous extruded starch matrix for food applications mainly involves the plasticization of starch and dispersive mixing of triglycerides in this blend. Starch plasticization requires shear and/or heat generated by the rotation of screws and heated barrels to transform the crystalline structure of starch into an amorphous phase. The lipid–based delivery system comprising bioactives is most favourably incorporated and dispersed into the plasticized starch at the end of the extruder to reduce a possible degradation of the bioactives during extrusion processing (Emin et al., 2012a[1]). This is followed by shaping/expanding and cooling to solidify the structure and form glass, thus, restricting loss due to molecular diffusion (Yilmaz et al., 2001; Lakkis, 2007).

To the best of our knowledge, there is only one study (i.e. Yilmaz et al., 2001) concerning droplet formation in a plasticized starch matrix in extrusion processing. Yilmaz et

[1] presented in this thesis as Chapter 2

al. (2001) studied the influence of processing parameters such as screw speed, screw geometry and emulsifier content on the morphology of the dispersed phase. Their study presents a good overview on the relation between the process parameters and the final droplet morphology, however, does not investigate underlying mechanisms in detail. The formation of oil droplets includes both droplet breakup and coalescence, which may occur simultaneously or stepwise. Therefore, to improve the fundamental understanding of the droplet formation in extrusion processing, clear distinction between droplet breakup and coalescence mechanisms, and identification of the important process characteristics influencing these mechanisms are crucial. The complex nature of both the process and the raw material presents several challenges due to the complex geometry of a twin screw extruder and non–Newtonian rheological behaviour of the plasticized starch, respectively.

The aim of this study is to understand the dynamics of morphology development during extrusion processing by analysing droplet breakup and coalescence separately. Recently introduced computational methodology (Emin and Schuchmann, 2013 [2]) was used to characterize local flow conditions influencing droplet breakup, whereas a new experimental method was introduced to analyze coalescence during extrusion processing. The findings were used to get insight into the formation of oil droplets in plasticized starch during twin screw extrusion processing, which involves both mechanisms.

6.2 Fundamentals

An initial step in dispersive mixing is the deformation of a droplet in a flow field, resulting in an increase in the interfacial area between the two phases followed by a decrease in local radii perpendicular to the flow direction (Taylor, 1934). In case of plasticized starch as continuous phase, the viscosity is high which leads to small Reynolds number ($Re \sim 10^{-3}$ at the tip of the screws). Therefore, inertia can be neglected with respect to viscous shear stresses generated by the rotation of the screws. Moreover, with respect to the interfacial effects, the buoyancy effects are negligible. Thus, the deformation of a droplet in a plasticized starch matrix is mainly governed by the ratio of deforming shear stress τ and the shape conserving interfacial stress σ/R (with σ the interfacial tension and R the local radius). This ratio is characterized by the capillary number Ca (Taylor, 1932; 1934):

[2] presented in this thesis as Chapter 5

$$Ca = \tau \cdot R/\sigma = (\eta_b \cdot \dot{\gamma} \cdot R)/\sigma \tag{6.1}$$

where η_b is the blend viscosity, and $\dot{\gamma}$ is the shear rate defined as:

$$\dot{\gamma} = \sqrt{(2d : d)} \tag{6.2}$$

with the rate of deformation tensor d. The capillary number indicates that the larger the local shear stress ($= \eta_b\dot{\gamma}$) relative to the interfacial stress ($= \sigma/R$) is, the more the droplet will deform until it breaks up. The specific value, above which the droplet breaks up in an external flow field of given shear stress, is called critical capillary number (Ca_{crit}). Taylor (1934) showed that the critical capillary number depends on the viscosity ratio p :

$$p = \eta_d/\eta_c \tag{6.3}$$

where η_d and η_c are the dispersed phase and continuous phase viscosity, respectively. The dependency of the critical capillary number on the viscosity ratio was established and validated for Newtonian systems (Grace, 1982; Bentley and Leal, 1986; Debruijn, 1991). The authors found that droplet breakup in a simple shear flow occurs most favorably at an intermediate range of $0.1 < p < 1$. At lower p values – as found for the systems investigated here –, Cacrit steadily increases with decreasing p values. No breakup is possible at $p > 4$. In contrast, no limit for droplet breakup was found in elongational flow which was reported to be more effective than simple shear flow (Grace, 1982).

The breakup time, a number and size distribution of the droplet fragments after breakup depend on system parameters and differ qualitatively for various breakup mechanisms. Thus, characterization of the decisive breakup mechanism is crucial for the reliable prediction of dispersed phase morphology. In the complex geometry of an extruder, the droplet breakup is expected to be driven by high shear regions that are generated at the tip of the screw (Janssen, 1993; Sundararaj and Macosko, 1995; Cheng and Manas–Zloczower, 1997; Emin and Schuchmann, 2013). For low viscosity ratios ($p < 1$), the flow of the droplet through these high shear regions (at which $Ca/Ca_{crit} >> 1$) results in affine deformation, followed by disintegration into very small droplets (Grace, 1982; Janssen, 1993). The number of the fragments increases with capillary ratio for $Ca/Ca_{crit} > 1$,

which results in smaller droplet sizes (Grace, 1982; Stone, 1994). Similarly, the total breakup time is a function of capillary ratio (Ca/Ca_{crit}), and decreases with increasing Ca/Ca_{crit} (Grace, 1982; Janssen, 1993). Therefore, the capillary ratio (Ca/Ca_{crit}) can be considered to be a kinematic variable characterizing the efficiency of dispersive mixing (Emin and Schuchmann, 2013).

Recent studies (i.e. Sibillo et al., 2004; Yue et al., 2005; Verhulst et al., 2009) further showed that the elasticity of the matrix fluid has a significant contribution on the deformation of dispersed droplets, most especially if the applied flow field is transient as in extruders. Plasticized starch is a non–Newtonian fluid. To determine the critical capillary number for the triglyceride droplets suspended in plasticized starch matrix, recently we performed experiments in simple shear flow (Emin et al., 2012b[3] , 2012c[4]). The results showed that critical capillary number is significantly lower compared to Newtonian fluids at the range of viscosity ratio (i.e. 10^{-7} to 10^{-5}) investigated:

$$Ca_{crit} = 6 \cdot 10^{-5} \cdot (p)^{-0.86} \tag{6.4}$$

From Eq. 6.1 and Eq. 6.4, capillary ratio for the triglyceride droplets in plasticized starch in simple shear flow can be calculated by (Emin and Schuchmann, 2013):

$$Ca/Ca_{crit} = \eta_c^{0.14} \cdot \eta_d^{0.86} \cdot \dot{\gamma} \cdot R \cdot 10^5/6\sigma \tag{6.5}$$

Flow induced coalescence is the second fundamental phenomenon that should be understood and properly described to evaluate the final dispersed phase morphology. Although several researchers performed both theoretical (e.g. Chesters, 1991; Janssen, 1993; Loewenberg and Hinch, 1997; Rother and Davis, 2001) and experimental (e.g. Sundararaj and Macosko, 1995; Minale et al., 1998; Vinckier et al., 1998,; Lyu et al., 2000; Ramic et al., 2000) work to characterize coalescence, the modelling of the complete picture remains still very challenging due to complex multivariate nature of the coalescence phenomena (Leal, 2004). Coalescence only occurs if at least two droplets collide and the film between those two droplets drains during their contact time. Therefore, the probability of coalescence P_{coal} is a function of probability of collision P_{coll} and

[3] presented in this thesis as Chapter 3
[4] presented in this thesis as Chapter 4

probability of drainage P_{drain} (Chesters, 1991; Janssen, 1993):

$$P_{coal} = P_{coll} \cdot P_{drain} \tag{6.6}$$

The flow field, volume fraction of the dispersed phase, viscosity, shear rate and shear stress are some of the important parameters regarding flow induced coalescence (Chesters, 1991; Leal, 2004).

6.3 Materials and methods

6.3.1 Materials

Native maize starch C*Gel 03401 at 10% water content (wet basis) was obtained from Cargill, Germany. Medium chain triglyceride (purchased from Schumann & Sohn, Germany) was used as lipid phase, because it does not form lipid–amylose complexes when mixed with starch (French et al., 1963; Schweizer et al., 1986). Native maize starch and medium chain triglyceride oil will be referred to as "starch" and "MCT–oil" throughout the paper, respectively. Nile Red (lipophilic fluorescent dye) and Tween20 (emulsifier), both of analytical grades, were obtained from Sigma–Aldrich, Germany.

6.3.2 Preparation of emulsion

An emulsion (dispersed phase content 70% w/w) was prepared by using water as continuous phase and MCT–oil as dispersed phase. To prevent coalescence and stabilize the emulsion, the hydrophilic emulsifier Tween20 was added. First, the emulsifier was mixed into water at 1% w/w (of water phase) by a propeller stirrer (IKA Labortechnik Eurostar Power B) at 400 rpm for 15 minutes. In parallel, the lipophilic fluorescent dye (i.e. Nile Red) was dissolved into the oil at 1% w/w by magnetic mixer to make the oil droplets visible under confocal laser scanning microscopy. A weight of oil equivalent to 70% of the emulsion was added drop wise to the continuous phase in order to prevent phase inversion, while the mixture was stirred with the propeller stirrer at 700 rpm. To obtain a fine and uniform distribution of droplets, this emulsion premix was passed three times through a rotor–stator type homogenizer (IKA magic lab) at 16000 rpm.

6.3.3 Extrusion trials

Experiments were performed using a co–rotating high speed twin–screw extruder ZSK 26 Mc (Coperion, Stuttgart, Germany) consisting of 7 barrels with length to diameter ratio of 29, screw and die diameter of 25.5 and 3 mm, respectively. The extrusion experiments were conducted varying screw speed, screw configuration, feed rate and oil content. The temperature of the plasticized starch was regulated by changing the barrel temperature. An illustration of the experimental set–up, screw configurations and feeding points can be seen in Figure 6.1. At the first part of the extruder, starch (10 kg/h to 30 kg/h) was mixed with water (1 kg/h to 3 kg/h) which was then plasticized under thermal and mechanical stresses generated by rotation of the screws. Oil or emulsion (previously stained with Nile Red at 1% w/w) was incorporated into the plasticized starch at the second part (i.e. mixing zone: where the mixing of lipophilic carrier takes place, see Fig. 6.1) of the extruder at the rate of 0.15 kg/h to 1.13 kg/h. Screw configuration 1 and 2 (named config. 1 and config. 2) differs from each other only at the second part, where they consist forward 45°kneading blocks and reverse 45°kneading blocks, respectively. Config. 3 is composed of forward transport elements, except its second part where it also consists of reverse 45°kneading blocks identical to the second part of Config. 2. The extruded samples were collected and stored in evacuated plastic packages at the refrigerator (4 °C). Subsequent analysis was performed not later than 48 h after the experiments.

6.3.4 Droplet size measurements

The droplet size distributions of oil in the extruded starch samples were analyzed by confocal laser scanning microscopy and evaluated by an image processing software. For the analysis, four specimens were taken from different locations of each sample using a tweezer and a blade. Each specimen was then placed on a separate glass slide that was wetted with distilled water and closed with a cover slide. The oil had already been stained with Nile Red before extrusion processing. The CLSM used was a Zeiss LSM 510–META 18 (Zeiss, Oberkochen, Germany) with a 63× Plan–Apochromat/1.4 oil immersion lens. Nile Red was excited with an Argon–laser at the wavelength of 514 nm and the emitted light was filtered by a LP 560 filter. From each specimen, minimum 10 images with a dimension of 202 × 202 μm were taken from different locations. The images were taken at the depth of 20 to 100 μm within the specimens by changing the

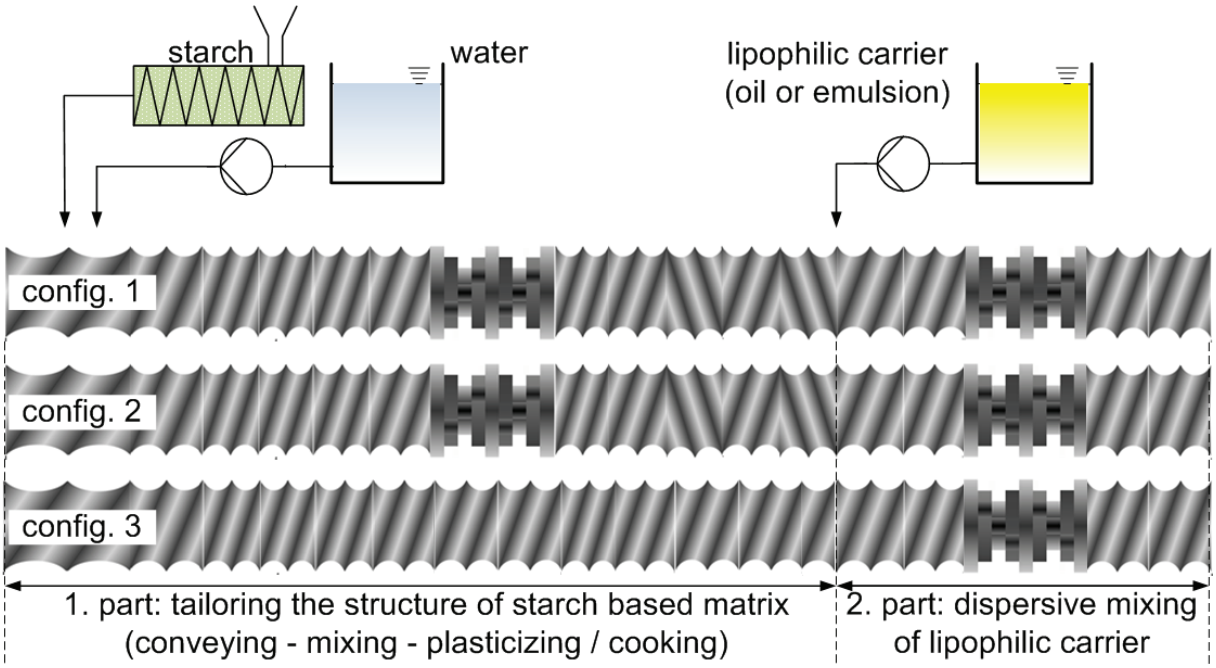

Figure 6.1: The schematic illustration of experimental set-up and screw configurations used.

focal point of the lens. Minimum 40 images from each sample were taken. The images obtained were further analyzed using digital image processing software (ImageJ software, National Institutes of Health, USA) at which droplet area and diameter were analyzed. CLSM images are produced from the light emitted from certain slice thickness (e.g. 1 μm). Since droplets are not always "cut" in the middle (at the biggest diameter of the sphere), the apparent size distribution of the droplets observed at the CLSM is not identical with the real size distribution. This problem is known as the "tomato salad problem". Several authors proposed algorithms to solve this problem (Fleischer, 1994; Gegner et al., 2004). Recently, Schuster et al., (2012) showed that the difference on mean droplet diameter is less than 7 % with and without consideration of this problem. Similarly, Scott (1990) as well as Sundararaj et al. (1995) found errors of less than 10 %. Therefore, the correction algorithm was not used in this study. Depending on the process parameters, 8000 to 20000 droplets per sample were counted. The results are plotted as an area–weighted cumulative size distribution (Q_2). The droplet sizes of $D_{90,2}$ and $D_{50,2}$ were determined from the cumulative area–weighted size distribution (Q_2). $D_{90,2}$ and $D_{50,2}$ refer the droplet size bigger than all droplets forming 90 % and 50 % of total droplet area, respectively.

6.3.5 Rheological measurements

Rheological characteristics of the plasticized starch were determined by a multiple step slit die rheometer mounted to the extruder. The schematic illustration of the rheometer is given in Figure 6.2. The thermo–mechanical stresses within the extruder leads to plasticization of the starch. The rheological properties of this plasticized matrix can be calculated from the pressure drop of the flow in the slit die which was measured using flush–mounted transducers. A slit die decreasing cross sections (i.e. triple steps) allowed varying shear rates without changing the process conditions (e.g. feed rate), which were necessary to determine a viscosity curve. Van den Einde et al. (2004) and Liu et al. (2010) showed that the transformation of starch molecules under mechanical stresses only depends on the maximum mechanical stress applied. At the screw configuration used in this study, it is expected that the matrix is exposed to maximum mechanical stresses at the inverse screw elements located in the first part of the extruder, at which they are forced to flow through the tip of the screws. Hence, it is assumed that the molecular transformation, and thus, the change in viscosity of the plasticized starch were already completed at the second part of extruder (i.e. mixing zone), which could be measured by the online slit die rheometer. The temperature of the rheometer was adjusted to the temperature of the

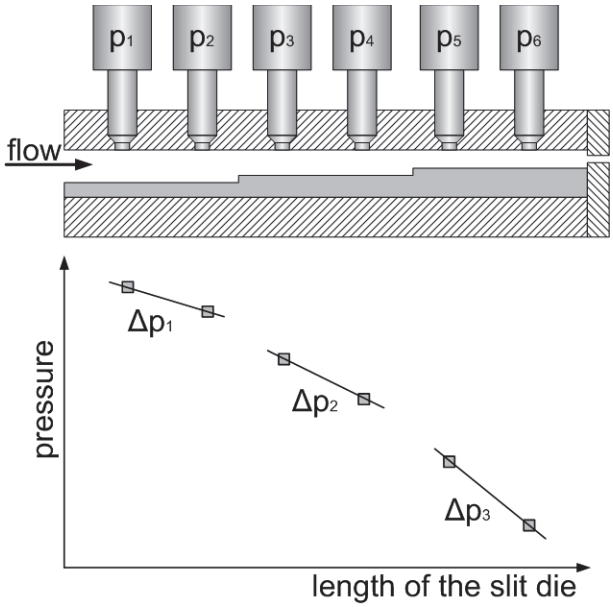

Figure 6.2: The schematic illustration of the slit die and the pressure loss along the die length.

starch at the die of the extruder using a heating jacket. The shear stress τ (Pa) can be calculated by Eq. 6.7:

$$\tau = (\triangle P/L) \times (h/2) \tag{6.7}$$

where $\triangle P$ is the pressure drop (Pa), L is the distance between two pressure sensors (mm) and h is the slit height (mm). The apparent shear rate $\dot{\gamma}_{app}$ (s^{-1}) was calculated at three different steps of the multiple step slit die rheometer by Eq. 6.8:

$$\dot{\gamma}_{app} = 6Q/(B \cdot h^2) \tag{6.8}$$

where Q is the volumetric mass flow (mm^3/s), B is the width of the slit (mm) and h is the slit height (mm). The apparent viscosity η_{app} (Pa·s) was calculated using Eq. 6.9:

$$\eta_{app} = \tau/\dot{\gamma}_{app} \tag{6.9}$$

The apparent viscosity of the oil was measured with a conventional Anton Paar Physica MCR301 rheometer with a cone and plate geometry (CP50–1/TG–SN15821). Measurements were conducted at varying temperature (60 to 140 °C) and shear rate (1 to 120 s^{-1}) similar to the conditions at extrusion processing.

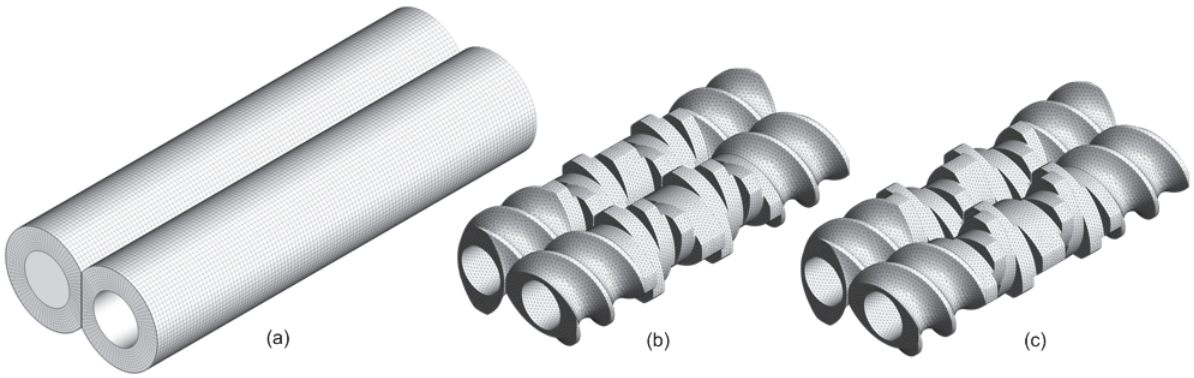

Figure 6.3: Computational domain: (a) barrel and (b) screw elements at the mixing zone of config. 1 and (c) screw elements at the mixing zone of config. 2 and 3.

6.3.6 CFD simulations

Flow of the plasticized starch at the mixing zone (i.e. second part) of the extruder was simulated by using CFD. For this purpose, only the flow through the screw elements located in the second part of the extruder (see Fig. 6.3) was simulated. Recently, we reported the details of computational methodology to perform such a simulation (Emin and Schuchmann, 2013). The flow was assumed to be isothermal in accordance with negligible temperature change of the material at this region. The rheological data of plasticized starch measured with the online slit die rheometer was fitted to the Bird–Carreau viscosity model:

$$\eta_{app} = \eta_0\{1 + (\lambda \cdot \dot{\gamma}_{app})^2\}^{\frac{n-1}{2}} \tag{6.10}$$

where η_0 is the zero shear viscosity, λ is the natural time and n is the power law index (Bird and Carreau, 1968). Since the feed rate of the starch is relatively low (i.e. 11 kg/h), creeping flow is assumed and gravity effects are neglected.

The governing equations regarding a time–dependent, isothermal and incompressible flow of a generalized Newtonian fluid is:

$$\rho\frac{Dv}{Dt} = -\nabla p + \nabla \cdot T + \rho g \tag{6.11}$$

$$\nabla \cdot v = 0 \tag{6.12}$$

where D/Dt is the material derivative, v is the velocity, p is the pressure, ρ is the density, g is the gravity and T is the extra stress tensor defined by:

$$T = 2\eta(\dot{\gamma})d \tag{6.13}$$

with the strain rate tensor d and the kinematic viscosity η. The shear rate $\dot{\gamma}$ is defined as the square root of the second invariant of the strain rate tensor:

$$\dot{\gamma} = \sqrt{2d : d} \tag{6.14}$$

CFD code ANSYS POLYFLOW 14.0, a finite element code dedicated to highly viscous flows, was used to calculate the governing equations. Due to two rotating intermeshing

Table 6.1: Dimensions of the screws and the barrel depicted in Figure 4.

Dimensions (mm)					
A-A′	10	B-B′	48	C-C′	24
X-X′	47.6	Z-Z′	96	D_c	21.1
R_b	13	R_i	8	R_o	12.75

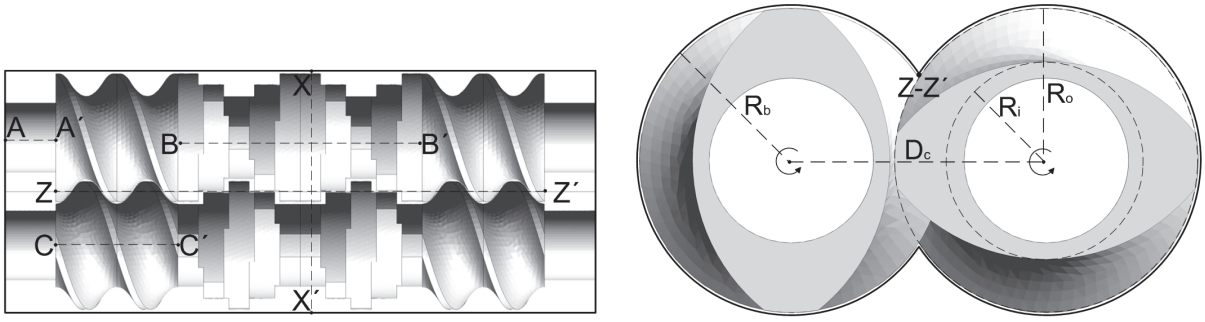

(a) (b)

Figure 6.4: Geometrical characteristics of the screws and the barrel. (a): Top view, (b): Front view.

screws, the flow in a co–rotating twin–screw extruder is three–dimensional (3–D) and unsteady. To simplify the set up of such a simulation and to avoid the use of a remeshing algorithm, the mesh superimposition technique (Avalosse, 1996) was used. After performing sensitivity analysis on mesh design and interpolation method, 503000 bricks (i.e. volume elements) for mesh size and enriched mini–element velocity and linear pressure for mixed interpolations were chosen. In order to capture the shear rate profile in between the tip of screws and barrel wall, this region was meshed by three bricks. Sufficiently long inlet and outlet channels (i.e. 10 mm) were added to the computational domain to be able to set boundary conditions. A developed velocity profile was assigned at the inlet section and vanishing normal velocity and tangential force are assigned at the exit section. Figure 6.4 and Table 6.1 present the geometrical characteristics and the dimensions of the computational domain, respectively.

To start the time dependent simulations with a physically relevant initial step, firstly a steady state simulation was performed and its result was used as an initial velocity field. Due to symmetrical geometry, only half a turn of the screw was simulated. To develop accurate evolution of the flow pattern in time, 40 time steps were simulated for half a

turn of the screws. Then, particle tracking was performed by launching virtual particles into the flow fields obtained from time dependent simulation. Initially, these particles are randomly distributed in a small box at the inlet section of the flow domain. The marker particles are assumed to be massless, volumeless, and noninteracting with each other. Under these assumptions, the particles can be located by integrating the velocity vectors with respect to time. Along the trajectory, mixing characteristics experienced by each particle were computed. 1500 particles were tracked to obtain statistically representative results. Consequently, the results of the numerical simulations had been post–processed to evaluate dispersive mixing efficiency in mixing zone at varying extrusion conditions.

By keeping the initial droplet radius R constant (i.e. 5 μm), the capillary ratio (see Eq. 6.5) can be considered to be a kinematic variable characterizing the efficiency of dispersive mixing (Emin and Schuchmann, 2013). This equation can only be used to determine the capillary ratio in simple shear flow. The high shear regions in a twin screw extruder are generated at the clearances between screws and barrel at which the droplet breakup takes place (Emin and Schuchmann, 2013; Cheng and Manas–Zloczower, 1997; Sundararaj and Macosko, 1995). Since the flow at these regions is dominated by simple shear flow (Emin and Schuchmann, 2013), the Eq. 6.5 can be used to calculate the maximum capillary ratio within the extruder. For this, the capillary ratio experienced by each droplet was monitored by particle tracking simulation. To evaluate the dispersive mixing efficiency, cumulative number distributions of maximum capillary ratio along the 1500 particles were calculated. The results are plotted as a number–weighted cumulative size distribution (Q_1).

6.4 Results and discussion

6.4.1 Rheology

An analysis of flow induced coalescence and breakup of droplets requires the knowledge of the rheological properties of the dispersed and the continuous phase. For concentrated systems, the formation of a droplet is determined by the average blend viscosity η_b rather than the continuous phase η_c viscosity (Armbruster, 1990; Jansen et al., 2001). The apparent viscosity of the blend was derived from online slit die measurements performed as described in section 6.3.5. Figure 6.5 shows the influence of screw speed and feed rate

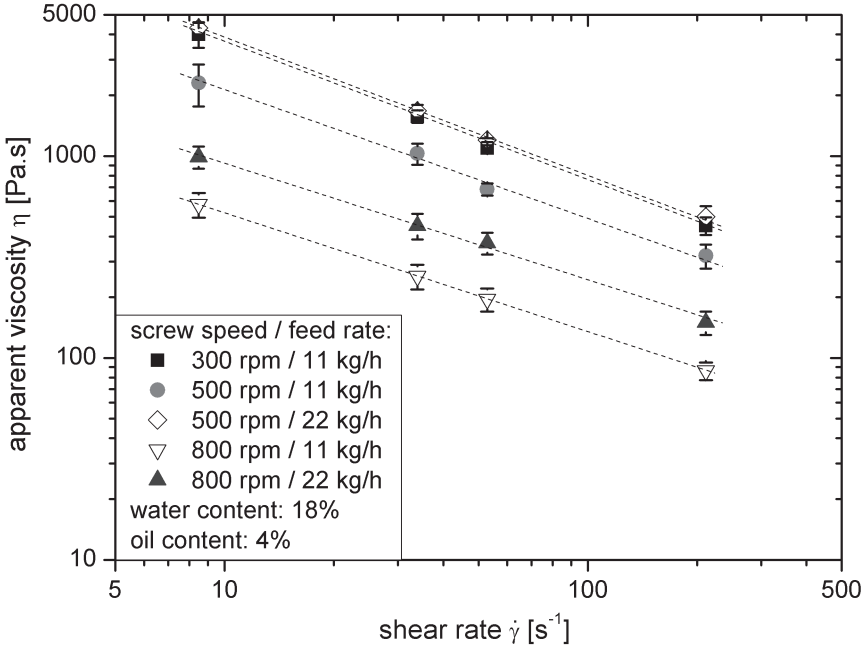

Figure 6.5: Flow curves of the blends extruded at varying screw speed and feed rate. Temperature: 140 °C, water content: 18%, oil content: 4%. The experiments were performed in triplicates.

on the apparent blend viscosity.

The results show a shear thinning behavior of the blend in the investigated shear rate range. This rheological behavior is typical for polymer melts (Dealy and Larson, 2006) and expected, as starch is a mixture of two (bio–) polymers with amylose and amylopectin, respectively. The results further show that increasing screw speed led to decrease in apparent viscosity. This happens due to higher mechanical stresses at higher screw speeds leading to more intensive degradation of the starch, which results in lower blend viscosity (Lai and Kokini, 1991; Brümmer et al., 2002; van den Einde et al., 2004; Liu et al., 2010). In contrast, increasing feed rate leads to higher blend viscosity due to decrease in mechanical energy input (van Lengerich, 1990). These results are in agreement with the previous studies (Vergnes and Villemaire, 1987; Vergnes et al., 1993; Willett et al., 1995).

6.4.2 Droplet coalescence

Most often, droplet breakup and coalescence occurs simultaneously making it challenging to study only one mechanism. Nevertheless, droplet breakup can be ceased, if the droplet

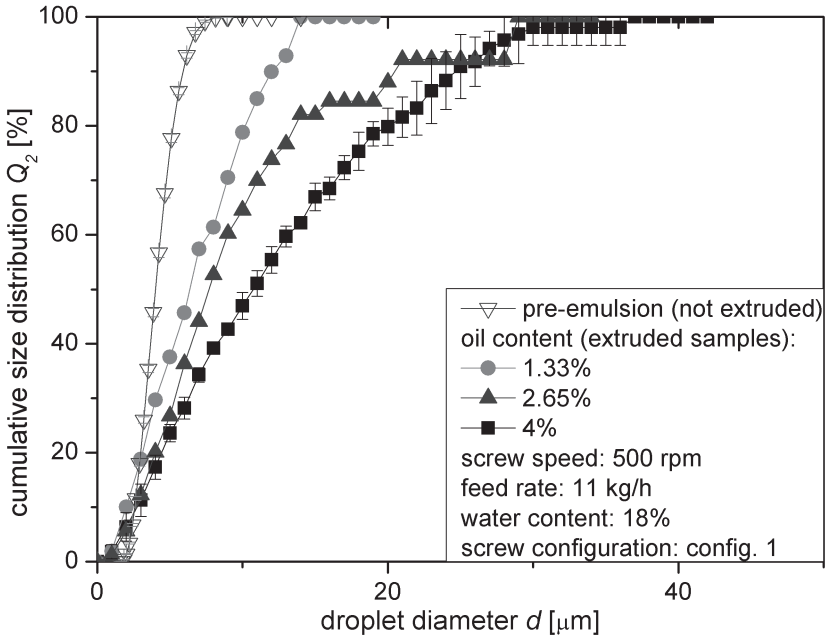

Figure 6.6: Influence of oil content on coalescence of pre-emulsified (70% O/W) droplets during extrusion processing. Temperature: 140 °C, screw speed: 500 rpm, feed rate: 11 kg/h and water content: 18%.

size is reduced below the critical value, at which $Ca < Ca_{crit}$. Therefore, to prevent the droplet breakup during extrusion processing and focus only on coalescence, oil was first emulsified in water by a dedicated emulsification device as described in section 6.3.2 to produce a sufficiently fine O/W emulsion. Then, this emulsion was fed into the extruder and the resulting droplet size distribution after the extrusion processing was analyzed by CLSM and image processing software as described in section 6.3.3 and 6.3.4 in detail. Figure 6.6 shows the influence of oil content on the droplet size distribution of pre–emulsified droplets during extrusion processing. All process parameters, besides oil content, were kept constant at screw speed of 500 rpm, temperature of 140 °C, feed rate of 11 kg/h and water content of 18%. Oil content of the blend was varied in the range of 1.33% to 4% (dry basis). The results clearly show that the sizes of droplets in extruded samples (filled symbols) is significantly bigger than the droplets of not–extruded emulsion (empty symbols) suggesting that coalescence of MCT–oil takes place during extrusion processing. Furthermore, the results show that increasing oil content led to bigger droplet size, which can be also seen qualitatively in CLSM images of these samples given in Figure 6.7. This is an expected result as the number of droplets

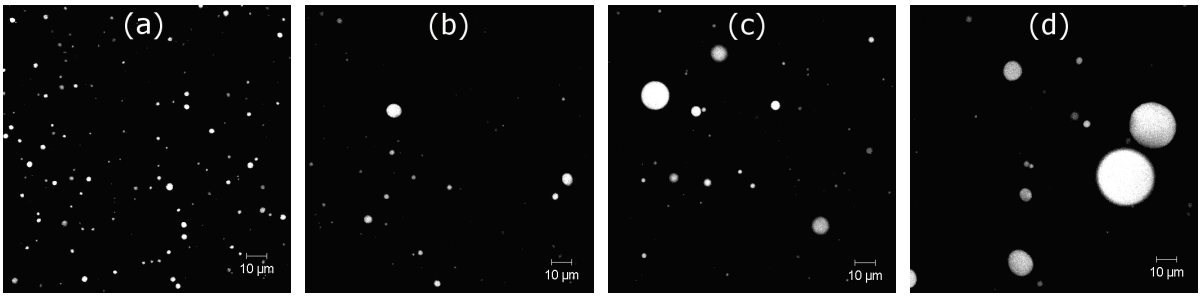

Figure 6.7: CLSM images showing the influence of oil content on coalescence of pre-emulsified (70% O/W) droplets during extrusion processing. (a) emulsion (not extruded), (b) 1.33% oil (extruded sample),(c) 2.65% oil (extruded sample), (d) 4% oil (extruded sample); temperature: 140 °C; screw speed: 500 rpm; feed rate: 11 kg/h and water content: 18%.

in the blend and therefore the frequency of their collision increases with increasing oil content (Chesters, 1991; Sundararaj and Macosko, 1995). This eventually leads to higher probability of coalescence (Elmendorp and Van Der Vegt, 1986; Chesters, 1991; Janssen, 1993; Sundararaj and Macosko, 1995). We found similar results for MCT–oil in plasticized starch in defined flow conditions (i.e. simple shear flow) in our previous study (Emin et al., 2012c), in which we further showed that coalescence takes place even at an oil content of 0.05%.

To investigate the influence of screw speed on coalescence of pre–emulsified droplets during extrusion processing, the experiments were carried out at 3 different screw speeds: 300 rpm, 500 rpm and 800 rpm. Oil content, water content and temperature were kept constant at 4%, 18% and 140 °C, respectively. Figure 6.8 shows that increasing screw speed from 300 rpm to 500 rpm leads to bigger droplets ($D_{90,2}$ increases from 16 μm to 25 μm). At higher screw speeds (i.e. higher shear rates), the droplets have higher approach velocities and higher collision frequencies, which might lead to an increased coalescence probability (Roland and Böuhm, 1984). Furthermore, the plasticized starch is a shear–thinning material and susceptible to mechanical stress, so that when screw speed is increased, the matrix viscosity decreases sharply, as shown in Figure 6.5. The decreased matrix viscosity might lead to lower drainage time necessary for the coalescence of colliding droplets, and therefore to higher probability of coalescence (Chesters, 1991; Janssen, 1993). Similar results were reported by Sundararaj and Macosko, (1995) and Emin et al. (2012c). However, a further increase of the screw speed from 500 rpm to 800 rpm showed no further increase in droplet sizes. In the sample extruded at 800

rpm, 80% of the droplets (i.e. $Q_{80,2}$) have smaller diameters compared to the droplet size distribution of the sample extruded at 500 rpm. This might be due to an excessive coalescence of the droplets (so that $Ca > Ca_{crit}$) which then broke up again at this screw speed.

Figure 6.9 depicts the influence of feed rate on coalescence of pre–emulsified droplets at screw speed of 500 rpm, oil content of 4 % and water content of 18%. The results clearly shows that increasing feed rate from 11 kg/h to 22 kg/h resulted in significantly smaller droplet sizes ($D_{90,2}$ decreased from 25 μm to 15 μm) suggesting that the coalescence probability was reduced at higher feed rate. Increasing feed rate has two important effects on the process variables: Higher blend viscosity (see Figure 6.5) and lower residence time of the blend in the extruder (Yeh et al., 1992; Unlu and Faller, 2002). These consequences are expected to increase the drainage time and to decrease the collision frequency, respectively, both leading to reduced coalescence probability (Janssen, 1993). The results depicted in Figure 6.9 are in good agreement with this theoretical interpretation.

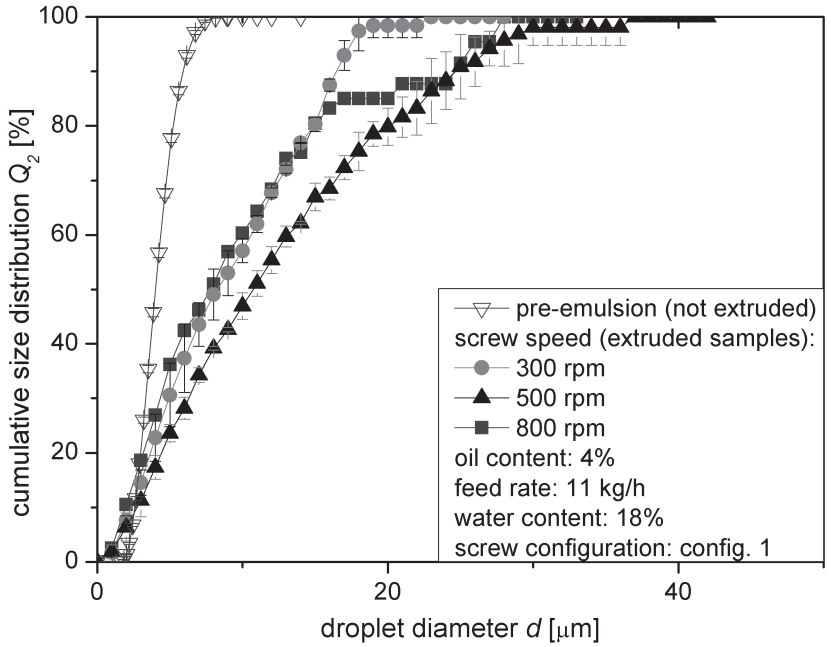

Figure 6.8: Influence of screw speed on coalescence of pre-emulsified (70% O/W) droplets during extrusion processing. Temperature: 140 °C, feed rate: 11 kg/h, water content: 18% and oil content: 4%.

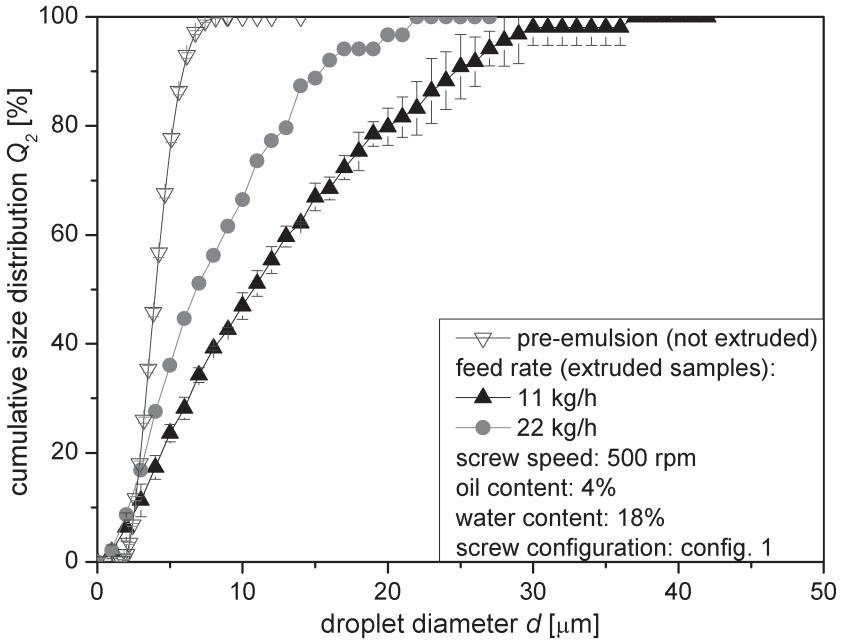

Figure 6.9: Influence of feed rate on coalescence of pre-emulsified (70% O/W) droplets during extrusion processing. Temperature: 140 °C, screw speed: 500 rpm, water content: 18% and oil content: 4%.

6.4.3 Droplet breakup

To investigate droplet breakup during extrusion processing, coalescence must be eliminated. This can be theoretically done by using a single droplet or an oil content below which droplets will not collide at all. Unfortunately, this is not applicable in practice since the droplets would be very difficult or even impossible to detect manually by CLSM. Therefore, recently we developed a numerical approach using CFD to identify the important process characteristics enhancing droplet breakup during extrusion processing by implementing the fundamental parameters such as capillary number and viscosity ratio into the numerical simulation (Emin and Schuchmann, 2013).

To obtain physically relevant results from the simulation, it is crucial to use a reliable model describing the rheological behaviour of the blend during its flow in the mixing zone of the extruder. Although the Power law equation can satisfactorily describe the viscosity of the starch–oil blend at the shear rate range measured (i.e. 100 s^{-1} to 103 s^{-1}), the Bird–Carreau viscosity model is more thorough at describing the rheological behavior of shear thinning fluids like plasticized starch, since it also includes the zero

Table 6.2: Simulated process conditions with the associated viscosity data.

process conditions no.	screw speed [rpm]	feed rate [kg/h]	water content [%]	screw config.	viscosity η [Pa·s] = $\eta_0(1+(\lambda\dot{\gamma})^2)^{\frac{n-1}{2}}$			viscosity η at $\dot{\gamma}$ = 100 s^{-1} [Pa·s]
					η_0	λ	n	
1	300	11	18	config. 1	284310	100	0.375	762
2	500	11	18	config. 1	135685	100	0.395	516
3	500	22	18	config. 1	406400	100	0.325	811
4	300	11	18	config. 2	284310	100	0.375	762

shear viscosity emerging at very low shear rates (Dus and Kokini, 1990). With the online slit die rheometer used in this study, zero shear viscosity of the plasticized starch cannot be determined, because low shear rates are not possible to achieve at the feed rates (i.e. 11 and 22 kg/h) investigated.

In our previous study (i.e. Emin and Schuchmann, 2013), we showed that the zero shear viscosity has no significant influence on the simulation results. Nevertheless, it is necessary to stabilize the numerical simulation and to achieve the convergence. Therefore, the zero shear viscosity and natural time were estimated according to the finding of Dus and Kokini (1990), who reported for a starch based matrix that the Newtonian behavior emerges primarily below a shear rate of 10^{-2} s^{-1} (i.e. natural time λ of 100 s). The simulated process conditions and the fit parameters of viscosity model are given in Table 6.2. To determine the fit parameters of the Bird–Carreau model, viscosity data measured by the online slit die rheometer was used.

Figure 6.10 shows the influence of screw speed on the distribution of maximum capillary ratio experienced by 1500 particles during their flow in the mixing zone of the extruder. These results were obtained from particle tracking simulations of the process conditions 1 and 2 given in Table 6.2. All process parameters, besides screw speed and resulting viscosity model, were kept constant. The results clearly show that increasing screw speed from 300 rpm to 500 rpm leads to higher capillary ratios Ca/Ca_{crit} experienced by the particles. Hence, we expect a more intense droplet breakup (i.e. smaller droplet fragments), and therefore a better dispersive mixing at 500 rpm than at 300 rpm in a coalescence–free system.

Increasing screw speed leads to both increased shear rate and decreased blend viscosity

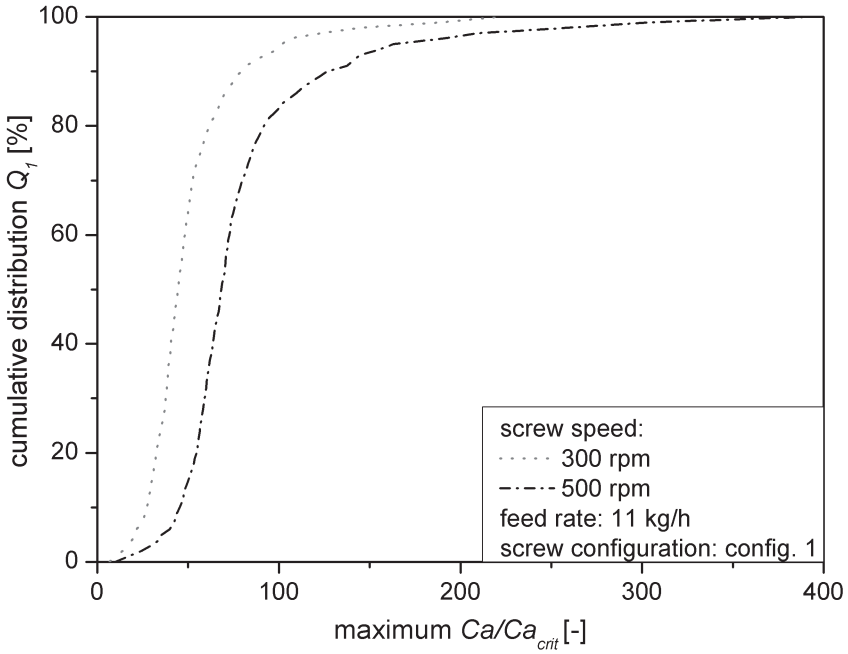

Figure 6.10: Influence of screw speed on the distribution of maximum Ca/Ca_{crit} calculated by numerical simulation. Feed rate: 11 kg/h, screw configuration: config. 1 and water content: 18%.

(see Figure 6.4) that have contrary effects on droplet breakup. To find out the reason of better dispersive mixing at higher screw speed, we performed simulations with constant screw speed of 500 rpm but different viscosities measured at 300 rpm and 500 rpm. The results depicted in Figure 6.11 show that a change in the viscosity has no significant influence on the distribution of capillary ratio along the particles tracked. On the one hand, a decrease in the viscosity reduces the shear stress generated by the screws (see Eq. 6.1). On the other hand, critical capillary number decreases simultaneously (see Eq. 6.4). These two contrary consequences of decreasing viscosity lead to no significant change in capillary ratio. Therefore, it can be concluded that the better dispersive mixing at 500 rpm is driven by the change in velocity field rather than the change in viscosity.

Figure 6.12 shows the influence of feed rate (i.e. 11 kg/h and 22 kg/h) on maximum capillary ratio distribution along the particles tracked by computational simulation. Details of the simulated process conditions and viscosity data are given in Table 6.2 as process condition 1 and 3. At the investigated range, doubling the feed rate showed no significant influence on capillary ratio distribution. Hence, increasing feed rate from 11 kg/h to 22 kg/h is expected to have no influence on the resulting droplet size distribution in a

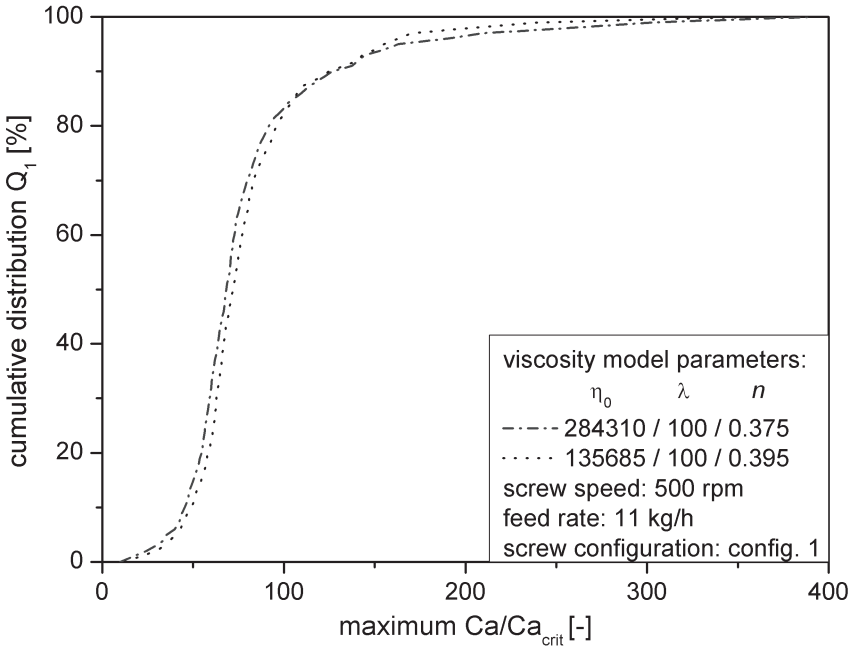

Figure 6.11: Influence of viscosity on the distribution of maximum Ca/Ca_{crit} calculated by numerical simulation. Screw speed: 500 rpm, feed rate: 11 kg/h, screw configuration: config. 1 and water content: 18%.

coalescence–free system.

Another important aspect is the flow pattern which can be mainly altered by using different screw configurations. Figure 6.13 shows the influence of two different screw configurations (config. 1 and config.2) on maximum capillary ratio experienced by the particles tracked. All other input parameters were kept constant. The results show that using

maxima. Such an effect results from reverse kneading blocks used in configuration 2 restricting the flow in the screw channel. This enforces the particles to flow through the tip of the screws and therefore leads to higher dispersive mixing efficiency.

6.4.4 Droplet formation

In the previous sections, the important process characteristics influencing droplet breakup and coalescence mechanisms have been discussed. In most of extrusion applications, however, both of these mechanisms takes place simultaneously. Therefore, in this section, we discuss the influence of extrusion conditions on droplet formation, which involves

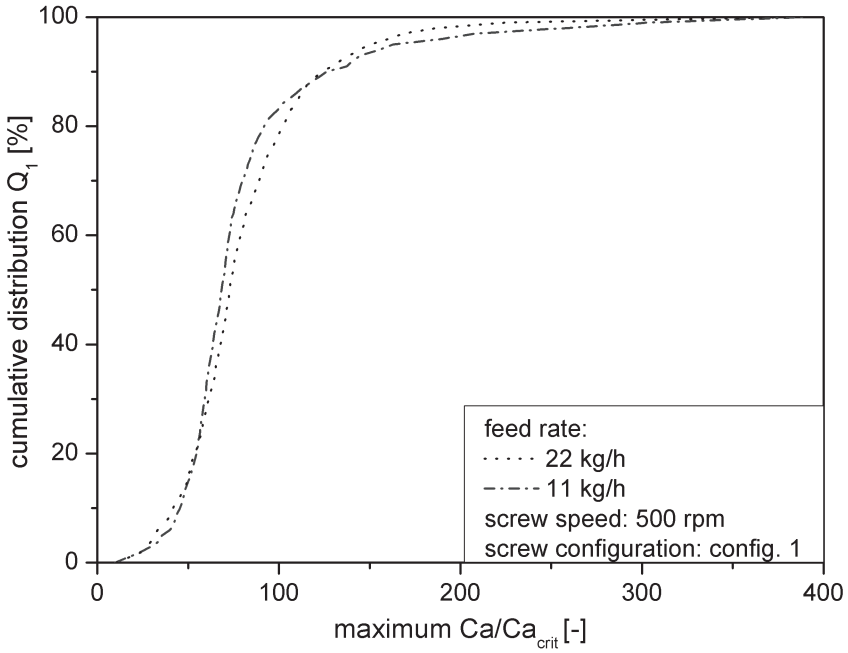

Figure 6.12: Influence of feed rate on the distribution of maximum Ca/Ca_{crit} calculated by numerical simulation. Feed rate: 11 kg/h, screw configuration: config. 1.

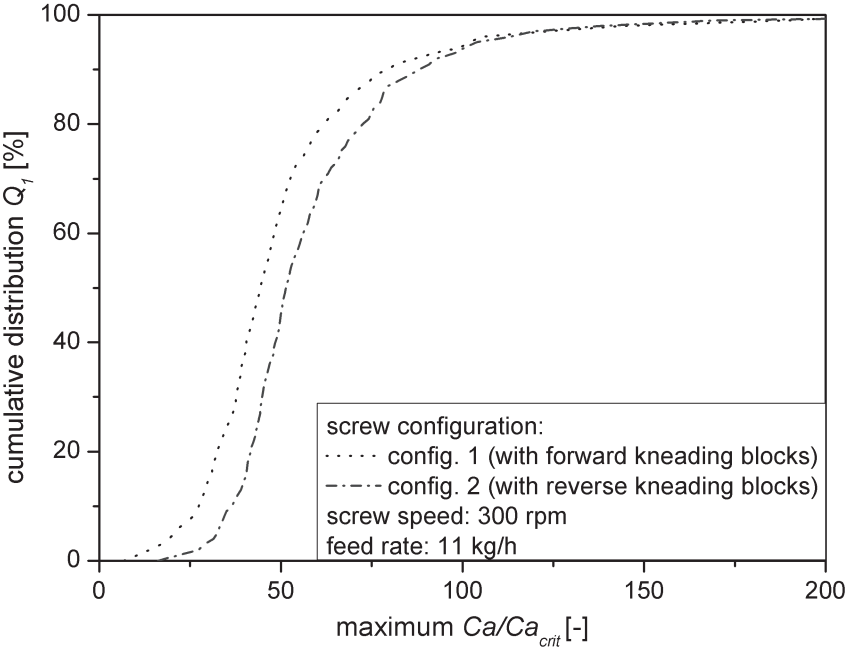

Figure 6.13: Influence of screw configuration on the distribution of maximum Ca/Ca_{crit} calculated by numerical simulation. Feed rate: 11 kg/h, screw speed: 300 rpm.

both droplet breakup and coalescence at the same time. For this purpose, MCT–oil was given into the extruder at various process conditions as described in section 6.3.3 and the resulting droplet size distribution was analyzed. The information obtained from isolated coalescence experiments (section 6.4.2) and breakup simulations (section 6.4.3) were used to understand the droplet formation during extrusion processing of plasticized starch.

Figure 6.14 shows the influence of screw configuration (square symbols and circle symbols) and screw speed (empty symbols and filled symbols) on droplet formation. Feed rate, water content and oil content were kept constant at 11 kg/h, 18% and 4%, respectively. The results show that the droplet sizes of the sample extruded with screw configuration 2 are smaller than of the sample extruded with screw configuration 1. These results are in agreement with the simulations (see Figure 6.12) which suggest that more droplets are exposed to higher maxima with screw configuration 2 (containing reverse kneading blocks). However, increasing screw speed showed no significant influence on droplet size distribution regardless of the screw configurations used. Although the results of computational simulation suggest a better dispersive mixing at higher screw speeds (Fig. 6.10), the results from coalescence experiments (Fig. 6.8) show that increasing screw speed also leads to higher coalescence probability. These two contradictory mechanisms might be the reason of similar droplet size distributions found in samples extruded at different screw speeds of 300 rpm and 500 rpm.

Figure 6.15 shows the influence of the feed rate (i.e. 11 kg/h and 22 kg/h) on the resulting droplet size distribution of the samples extruded by using two different screw configurations (i.e. config. 1 and 2). The screw speed, water content and oil content were kept constant at 800 rpm, 18% and 4%, respectively. Increasing feed rate led to smaller droplet size distribution both with screw configuration 1 and screw configuration 2. The results from coalescence experiments (Fig. 6.9) and breakup simulations (Fig. 6.12) show that increasing feed rate reduces the probability of coalescence, but has no significant influence on breakup of the droplets. Therefore, the smaller droplet sizes obtained at higher feed rate (i.e. 22 kg/h) is expected to be a result of reduced probability of coalescence.

The reduced coalescence at higher feed rate is supposed to be a result of an increase in blend viscosity. To test this hypothesis, we used a “mild” screw configuration (i.e. config. 3) which does not contain any reverse screw elements at the first part in contrast to the

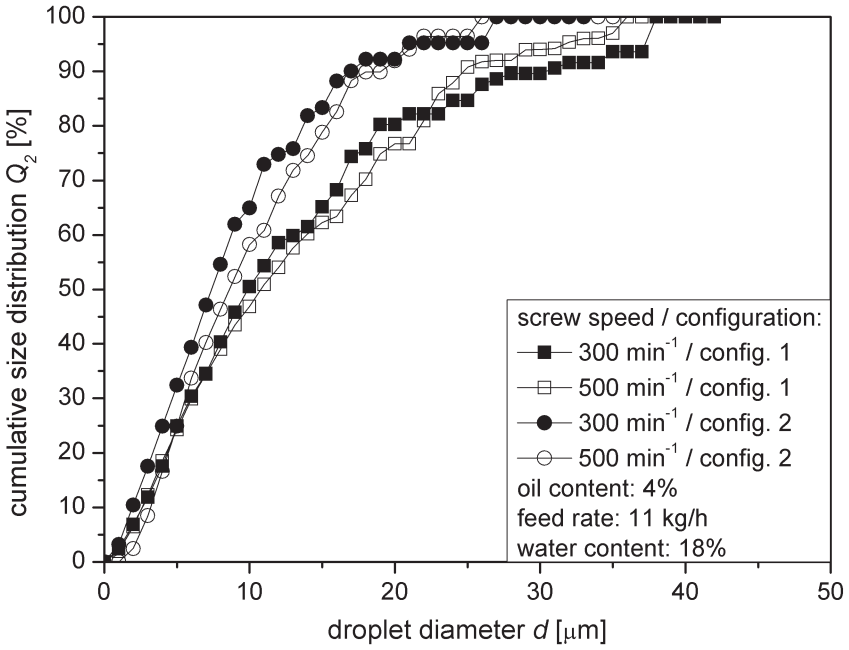

Figure 6.14: Influence of screw configuration and screw speed on droplet formation. Temperature: 140 °C, feed rate: 11 kg/h, screw speed: 300 rpm, oil content: 4%, water content: 18%.

other screw configurations (config. 1 and config. 2) used. This way, lower mechanical energy input at the first part of the extruder, and therefore a higher blend viscosity was aimed. Moreover, to achieve an effective droplet breakup, reverse kneading elements were located in the mixing zone as of screw configuration 2. Both the screw speed and feed rate were varied in the range of 300 rpm to 1100 rpm and 11kg/h to 22 kg/h, respectively. For the comparison, same experiments were performed with all three screw configurations. Water and oil content were kept constant at 18% and 4%, respectively. Obtained droplet sizes ($D_{50,2}$) were plotted in Figure 6.16 as a function of screw speed.

The results show that smallest droplet sizes were obtained with the screw configuration 3 regardless of the screw speed and the feed rate applied. Previous results (Fig. 6.11) show that increase in the blend viscosity has no influence on the droplet breakup, since both the capillary number and critical capillary number increase accordingly. Hence, the reduced coalescence is considered to be the reason for smaller droplet size obtained with screw configuration 3. In our previous study (i.e. Emin et al., 2012c), we also found similar results showing that an increase in viscosity of plasticized starch leads to lower coalescence during a simple shear flow of starch–oil blends. Furthermore, with the screw

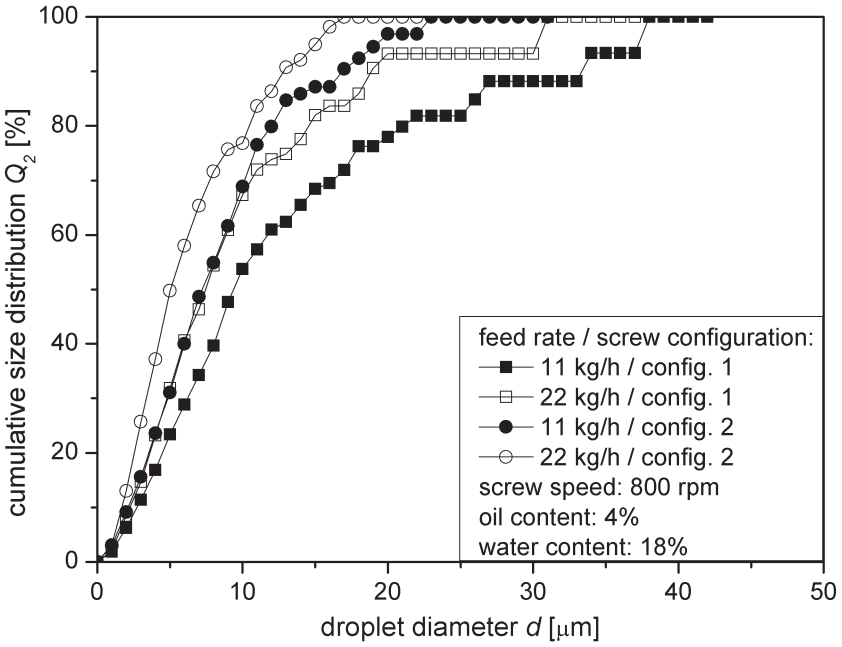

Figure 6.15: Influence of feed rate at two different screw configurations on droplet formation. Temperature: 140 °C, screw speed: 800 rpm, oil content: 4%, water content: 18%.

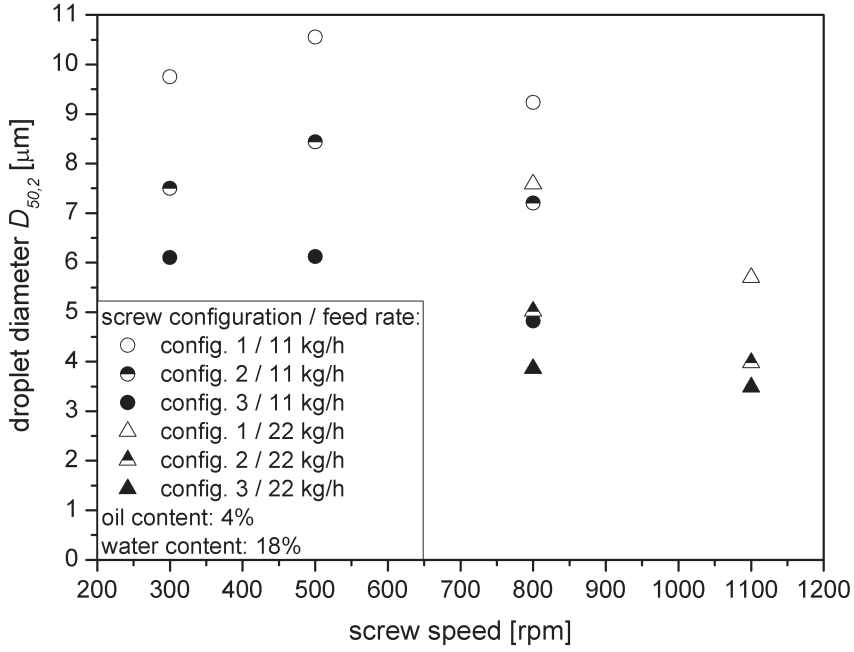

Figure 6.16: Influence of screw configuration, screw speed and feed rate on droplet formation. Temperature: 140 -170 °C, oil content: 4%, water content: 18%.

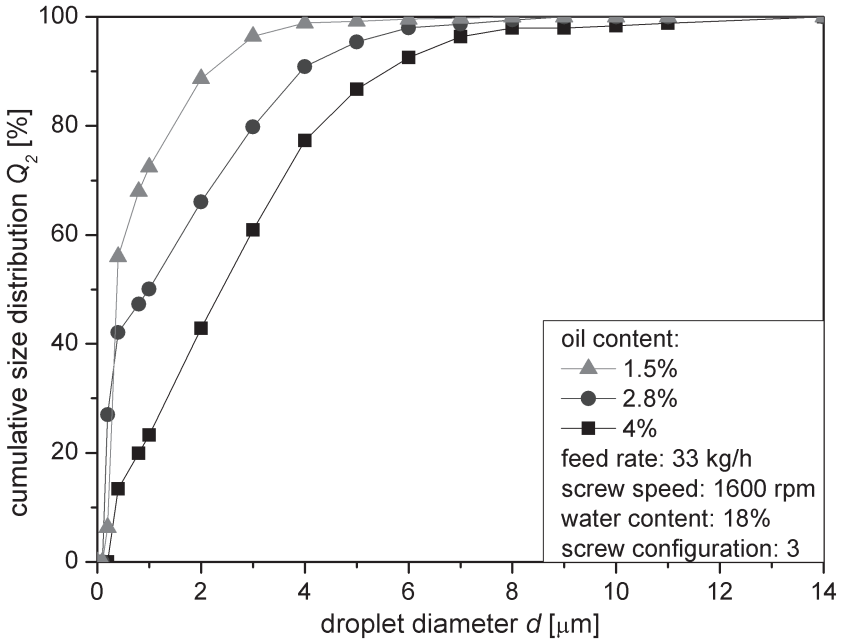

Figure 6.17: Influence of oil content on droplet formation. Temperature: 170 °C, screw configuration: 3, feed rate: 33 kg/h, screw speed: 1600 rpm.

configuration 1, the smallest droplet diameters ($D_{50,2}$ = 5.7 μm) were obtained at screw speed of 1100 rpm and feed rate of 22 kg/h. On the other hand, with screw configuration 3, similar droplet diameter was found at significantly lower screw speed and feed rate of 300 rpm and 11 kg/h, respectively. These results clearly show the importance of the screw configuration, which can be altered in a way to improve the droplet breakup and to decrease the coalescence by changing the flow field and increasing the matrix viscosity, respectively.

Based on our findings, we performed experiments to determine the influence of oil content and the smallest droplet size that can be achieved with the system used. For this purpose, we used the screw configuration 3 and varied the oil content in the range of 1.5% to 4%. Furthermore, we increased the screw speed and feed rate up to 1600 rpm and 33 kg/h, respectively. Obtained results are depicted in Figure 6.17. At the range investigated, droplet diameters ($D_{50,2}$) of 2.4 μm, 1 μm and 0.3 μm were obtained for the oil contents of 4%, 2.8% and 1.5%. It can be clearly seen that increasing oil content led to remarkably bigger droplets. At the range investigated, addition of oil had no influence on the blend viscosity (results not shown). Therefore, the results suggest that the oil content has a

strong influence on coalescence of oil droplets in plasticized starch during extrusion processing.

6.5 Conclusions

The use of experimental and computational methods allowed investigating both coalescence and breakup of triglyceride droplets during extrusion processing separately. The incorporation of pre–emulsified triglyceride droplets ($D_{50,2}$ = 4μm) resulted in formation of significantly bigger droplets ($D_{50,2}$ up to 11 μm) in the extruded samples showing that coalescence takes place in a twin–screw extrusion processing of maize starch. An increase in screw speed and oil content led to increased coalescence whereas an higher feed rate decreased it. The influence of screw speed and feed rate can be related to the change in matrix viscosity which is expected to play an important role on drainage probability of colliding droplets. Furthermore, increased screw speed and oil content are expected to increase the collision probability, and therefore the probability of coalescence.

The flow of plasticized starch in the mixing zone of the extruder was simulated by using CFD to identify the process conditions leading to improved droplet breakup. To obtain physically relevant results, the apparent viscosity of the blend in the mixing zone the extruder was measured by an online slit die rheometer. After simulating the flow field, the maximum capillary ratio (i.e. Ca/Ca_{crit}) experienced by 1500 particles was computed by a particle tracking simulation, which allowed evaluating the efficiency of dispersive mixing at varying process conditions. The results show that increasing screw speed from 300 rpm to 500 rpm leads to better dispersive mixing in a coalescence–free system, whereas doubling the feed rate from 11 kg/h to 22 kg/h had no significant influence. Another important aspect is the flow pattern which can be mainly altered by using different screw configurations. The results show that using a screw configuration containing reverse kneading blocks, increases the number of particles that are exposed to higher maxima of capillary ratio.

The information obtained from isolated coalescence experiments and breakup simulations were used to understand droplet formation during extrusion processing of plasticized starch. For this, extrusion experiments were conducted by incorporating oil into the extruder and analyzing the final droplet size distribution. The droplet sizes of the sample

extruded with screw configuration 2 (containing reverse kneading blocks in the mixing zone) were smaller than of the sample extruded with screw configuration 1 (containing forward kneading blocks in the mixing zone). These results are in agreement with the CFD simulations. The results further showed that increasing screw speed does not necessarily result in smaller droplet sizes. This could be related to the contradictory effects of increasing screw speed, which improves the droplet breakup but also leads to increased coalescence. Moreover the results showed that an increase in the feed rate led to formation of smaller droplets. This is expected to be the result of increased matrix viscosity leading to reduced coalescence probability. Therefore, the influence of increased blend viscosity at a constant feed rate was investigated by using a modified screw configuration (config. 3), with which the smallest droplet sizes were obtained. These results support the preceding hypothesis that a higher blend viscosity reduces the probability of coalescence. Moreover, increasing oil content led to increased coalescence, and therefore to remarkably bigger droplets. Nevertheless, selection of process parameters (e.g. screw configuration, feed rate, screw speed) based on the findings of this study allowed achieving droplet diameters ($D_{50,2}$) down to 2.4 μm, 1 μm and 0.32 μm at the oil contents of 4%, 2.8% and 1.5%, respectively.

Nomenclature

a	acceleration	∇P	pressure drop
B	width of the slit	Q	volumetric flow rate
Ca	capillary number	Q_0	cumulative number distribution
Ca_{crit}	critical capillary number	R	droplet radius
d	rate of strain tensor	T	extra–stress tensor
g	gravity	v	velocity
h	slit height	v_p	velocity of the moving mesh
H	penalty force term	τ	shear stress
L	distance between pressure sensors	σ	interfacial tension
η_{app}	apparent viscosity	λ_{MZ}	mixing index
η_b	blend viscosity	λ	natural time
η_d	dispersed phase viscosity	$\dot{\gamma}$	shear rate
η_t	true viscosity	$\dot{\gamma}_{app}$	apparent shear rate
η_0	zero shear viscosity	$\dot{\gamma}_w$	wall shear rate
p	viscosity ratio	ω	vorticity tensor
ρ	density	P_{coll}	probability of collision
P_{drain}	probability of drainage	P_{coal}	probability of coalescence

6.6 References

Armbruster, H. (1990). *Untersuchungen zum kontinuierlichen Emulgierprozess in Kolloidmühlen*. Doctoral Dissertation. Karlsruhe University, Germany.

Avalosse, T. (1996). Numerical simulation of distributive mixing in 3–D flows. *Macromolecular Symposium*, 112, 91–98.

Bentley, B., & Leal, L. (1986). An experimental investigation of drop deformation and breakup in steady, two–dimensional linear flows. *Journal of Fluid Mechanics*, 167(–1), 241–283.

Bird, R. B., & Carreau, P. J. (1968). A nonlinear viscoelastic model for polymer solutions and melts–I. *Chemical Engineering Science*, 23(5), 427–434.

Brümmer, T., Meuser, F., van Lengerich, B., & Niemann, C. (2002). Effect of extrusion

cooking on molecular parameters of corn starch. *Starch–Stärke*, 54, 1–8.

Cheng, H., & Manas–Zloczower, I. (1997). Study of mixing efficiency in kneading discs of co–rotating twin–screw extruders. *Polymer Engineering and Science*, 37(6), 1082–1090.

Chesters, A. K. (1991). The modelling of coalescence processes in fluid–liquid dispersions: a review of current understanding. *Chemical Engineering Research & Design*, 69(A4), 259–270.

Dealy, J. M., & Larson, R. G. (2006). *Structure and rheology of molten polymers: from structure to flow behavior and back again* (p. 516). Hanser Verlag.

Debruijn, R. A. (1991). *Deformation and breakup of drops in simple shear flows*. Doctoral Dissertation. Eindhoven University, The Netherlands.

Dus, S. J., & Kokini, J. L. (1990). Prediction of the nonlinear viscoelastic properties of a hard wheat flour dough using the Bird–Carreau constitutive model. *Rheology*, 34, 1069–1084.

Elmendorp, J. J., & Van Der Vegt, A. K. (1986). A study on polymer blending microrheology: Part IV. The influence of coalescence on blend morphology origination. *Polymer Engineering and Science*, 26(19), 1332–1338.

Emin, M. A., Mayer–Miebach, E., & Schuchmann, H. P. (2012a). Retention of β–carotene as a model substance for lipophilic phytochemicals during extrusion cooking. *LWT – Food Science and Technology*, 48(2), 302–307.

Emin, M. A., Hardt, N., van der Goot, A. J., & Schuchmann, H. P. (2012b). Formation of oil droplets in plasticized starch matrix in simple shear flow. *Journal of Food Engineering*, 112(3), 200–207.

Emin, M. A., Schmidt, U., van der Goot, A. J., & Schuchmann, H. P. (2012c). Coalescence of oil droplets in plasticized starch matrix in simple shear flow. *Journal of Food Engineering*, 113(3), 453-460.

Emin, M. A., & Schuchmann, H. P. (2013). Analysis of the dispersive mixing efficiency in a twin–screw extrusion processing of starch based matrix. *Journal of Food Engineering*, 115(1),132–143.

Fleischer, K. (1994). The Tomato Salad Problem Reconsidered. *Biometrical Journal*, 36(2), 193–203.

Forssell, P. (2004). Starch–based microencapsulation. In A. Eliasson (Ed.), *Starch in food: Structure, function and applications* (p. 461). Taylor & Francis.

French, D., Pulley, A. O., & Whelan, W. J. (1963). Starch fractionation by hydrophobic complex formation. *Starch–Stärke*, 15(10), 349–354.

Gegner, J., Henninger, C., & Öchsner, A. (2004). Stereologische Analyse und Modelierung von Objektverteilungen aus Schnittbildern. *Materialwissenschaft und Werkstofftechnik*, 35(1), 36–44.

Grace, H. P. (1982). Dispersion phenomena in high viscosity immiscible fluid systems and application of static mixers as dispersion devices in such systems. *Chemical Engineering Communications*, 14(3–6), 225–277.

Horn, D. (1989). Preparation and characterization of microdisperse bioavailable carotenoid hydrosols. *Die Angewandte Makromolekulare Chemie*, 166(1), 139–153.

Horn, D., & Rieger, J. (2001). Organic nanoparticles in the aqueous phase–theory, experiment, and use. *Angewandte Chemie International Edition*, 40(23), 4330–4361.

Jansen, K. M. B., Agterof, W. G. M., & Mellema, J. (2001). Droplet breakup in concentrated emulsions. *Journal of Rheology*, 45, 227.

Janssen, J. (1993). *Dynamics of liquid–liquid mixing*. Doctoral Dissertation. Eindhoven University of Technology, The Netherlands.

Lai, L., & Kokini, J. (1991). Physicochemical changes and rheological properties of starch during extrusion (a review). *Biotechnology Progress*, 7(3), 251–266.

Lakkis, J. (2007). *Encapsulation and Controlled Release Technologies in Food Systems* . Ames, Iowa, USA: Blackwell Publishing.

Leal, L. G. (2004). Flow induced coalescence of drops in a viscous fluid. *Physics of Fluids*, 16(6), 1833.

Liu, W.–C., Halley, P. J., & Gilbert, R. G. (2010). Mechanism of Degradation of Starch, a Highly Branched Polymer, during Extrusion. *Macromolecules*, 43(6), 2855–2864.

Loewenberg, M., & Hinch, E. J. (1997). Collision of two deformable drops in shear flow. *Journal of Fluid Mechanics*, 338, 299–315.

Lyu, S.–P., Bates, F. S., & Macosko, C. W. (2000). Coalescence in polymer blends during shearing. *AIChE Journal*, 46(2), 229–238.

Mano, J. F., Koniarova, D., & Reis, R. L. (2003). Thermal properties of thermoplastic starch/synthetic polymer blends with potential biomedical applicability. *Journal of Materials Science. Materials in Medicine*, 14(2), 127–35.

Minale, M., Mewis, J., & Moldenaers, P. (1998). Study of the morphological hysteresis in immiscible polymer blends. *AIChE Journal*, 44(4), 943–950.

Ramic, A., Hudson, S., Jamieson, A., & Manas–Zloczower, I. (2000). Temporary droplet–size hysteresis in immiscible polymer blends. *Polymer*, 41(16), 6263–6270.

Ribeiro, H. S., Guerrero, J. M. M., Briviba, K., Rechkemmer, G., Schuchmann, H. P., & Schubert, H. (2006). Cellular uptake of carotenoid–loaded oil–in–water emulsions in colon carcinoma cells in vitro. *Journal of Agricultural and Food Chemistry*, 54(25), 9366–9.

Roland, C. M., & Böuhm, G. G. A. (1984). Shear–induced coalescence in two–phase polymeric systems. I. Determination from small–angle neutron scattering measurements. *Journal of Polymer Science: Polymer Physics Edition*, 22(1), 79–93.

Rother, M. A., & Davis, R. H. (2001). The effect of slight deformation on droplet coalescence in linear flows. *Physics of Fluids*, 13(5), 1178.

Schuster, S., Bernewitz, R., Guthausen, G., Zapp, J., Greiner, A. M., Köhler, K., & Schuchmann, H. P. (2012). analysis of w1/o/w2 double emulsions with CLSM: Statistical image processing for droplet size distribution. *Chemical Engineering Research and Design*, 81, 84–90.

Schweizer, T. F., Reimann, S., Solms, J., Eliasson, A. C., & Asp, N. G. (1986). Influence of drum–drying and twin–screw extrusion cooking on wheat carbohydrates, II, effect of lipids on physical properties, degradation and complex formation of starch in wheat flour. *Journal of Cereal Science*, 4(3), 249–260.

Scott, C. I. (1990). *Characterization of the Reactive Polymer Blending Process*. Doctoral Dissertation. University of Minnesota, USA.

Shogren, R. L., Fanta, G. F., & Doane, W. M. (1993). Development of Starch Based Plastics – A Reexamination of Selected Polymer Systems in Historical Perspective. *Starch – Stärke*, 45(8), 276–280.

Sibillo, V., Simeone, M., & Guido, S. (2004). Break–up of a Newtonian drop in a viscoelastic matrix under simple shear flow. *Rheologica Acta*, 43(5), 449–456.

Stone, H. A. (1994). Dynamics of drop deformation and breakup in viscous fluids. *Annual Review of Fluid Mechanics*, 26(1), 65–102.

Sundararaj, U., Dori, Y., & Macosko, C. W. (1995). Sheet formation in immiscible polymer blends: model experiments on initial blend morphology. *Polymer*, 36(10), 1957–1968.

Sundararaj, U., & Macosko, C. W. (1995). Drop Breakup and Coalescence in Polymer Blends: The Effects of Concentration and Compatibilization. *Macromolecules*, 28(8), 2647–2657.

Taylor, G. I. (1932). The Viscosity of a Fluid Containing Small Drops of Another Fluid. *Proceedings of the Royal Society of London. Series A*, 138(834), 41–48.

Taylor, G. I. (1934). The formation of emulsions in definable fields of flow. *Proceedings of the Royal Society of London. Series A*, 146(858), 501–523. Unlu, E., & Faller, J. (2002). RTD in twin–screw food extrusion. *Journal of Food Engineering*, 53(2), 115–131.

Vergnes, B., Della Valle, G., & Tayeb, J. (1993). A specific slit die rheometer for extruded starchy products. Design, validation and application to maize starch. *Rheologica Acta*, 32(5), 465–476.

Vergnes, B., & Villemaire, J. P. (1987). Rheological behaviour of low moisture molten maize starch. *Rheologica Acta*, 576, 570–576.

Verhulst, K., Cardinaels, R., Moldenaers, P., Afkhami, S., & Renardy, Y. (2009). Influence of viscoelasticity on drop deformation and orientation in shear flow. Part 2: Dynamics. *Journal of Non–Newtonian Fluid Mechanics*, 156(1–2), 44–57.

Vinckier, I., Moldenaers, P., Terracciano, A., & N. (1998). Droplet size evolution during coalescence in semiconcentrated model blends. *AIChE*, 44(4).

Willett, J. L., Jasberg, B. K., & Swanson, C. L. (1995). Rheology of thermoplastic starch: Effects of temperature, moisture content, and additives on melt viscosity. *Polymer Engineering and Science*, 35(2), 202–210.

Yeh, A., Hwang, S., & Guo, J. (1992). Effects of screw speed and feed rate on residence time distribution and axial mixing of wheat flour in a twin–screw extruder. *Journal of Food Engineering*, 17, 1 – 13.

Yilmaz, G., Jongboom, R. O. J., Feil, H., & Hennink, W. E. (2001). Encapsulation of sunflower oil in starch matrices via extrusion: effect of the interfacial properties and

processing conditions on the formation of dispersed phase morphologies. *Carbohydrate polymers*, 45(4), 403–410.

Yue, P., Feng, J. J., Liu, C., & Shen, J. (2005). Viscoelastic effects on drop deformation in steady shear. *Journal of Fluid Mechanics*, 540(–1), 427.

van Lengerich, B. (1990). Influence of extrusion processing on in–line rheological behavior, structure, and function of wheat starch. In H. Faridi & J. M. Faubion (Eds.), *Dough Rheology and Baked Product Structure* (pp. 421–472). New York: Van Nostrand Reinhold.

van den Einde, R. M., Akkermans, C., van der Goot, A. J., & Boom, R. M. (2004). Molecular breakdown of corn starch by thermal and mechanical effects. *Carbohydrate Polymers*, 56(4), 415–422.

7 Comprehensive summary and general discussion

7.1 Introduction

The overall goal of this research project is to understand the dynamics of dispersive mixing in extrusion processing to design starch based functional foods containing lipophilic bioactives. Such a need of knowledge on dispersive mixing arises from the findings of previous studies, which has shown that dissolving lipophilic bioactives in a lipid based carrier and dispersing this solution into small droplets leads to dramatic increase in bioavailability, as well as to improved stability (Horn, 1989; Grolier et al., 1995; Horn and Rieger, 2001; Borel, 2003; Ribeiro et al., 2006; Parker et al., 2007; Gonnet et al., 2010).

Extrusion is a flexible process, yet it possesses many challenges with respect to the complex nature of the screw geometry, multivariate system parameters and material properties, such as rheological properties. Hence, a research approach based only on experimental design of extrusion trials generally fails to provide fundamental understanding and is not efficient in finding a rational compromise between the large numbers of system parameters influencing the microstructure of the lipophilic carrier and the food matrix.

In this thesis, the research approach utilized is based on first fractionation of the overall goal into logical interrelated sections, which can be investigated more thoroughly and conveniently using various scientific fields, including biochemistry, colloid science, fluid dynamics and rheology. The gained scientific understanding can then be used to develop a range of potential solution strategies with respect to the requirements of selected bioactives and the food product. The major advantage of this approach is that the methodologies developed and the knowledge obtained from each section can be easily and separately modified or updated according to the changes in the target application, e.g. different bioactives or matrix material.

Therefore, in this chapter, the goal and the research approach of each section (i.e. chapter) are briefly summarized to emphasize the interrelation between the preceding chapters. In particular, the main findings and their scientific and practical implications are discussed. Moreover, the limitations of each section and the recommendations for further research are presented. Finally, the main conclusions and general outlook of this thesis are provided.

7.2 Retention of β–carotene during extrusion cooking – *Chapter 2*

Goal: This section was designed to verify the principal applicability of extrusion processing to formulate sensitive lipophilic bioactives dissolved in a lipophilic carrier and to define the mixing zone at which the bioactives preserve their stability at the highest level. Furthermore, it aimed to determine the relation between the extrusion parameters and the resulting retention of bioactives.

Approach: β–carotene was chosen as model lipophilic bioactive, because it is easy to analyze and chemically well characterized. Medium chain triglyceride oil was chosen as lipophilic carrier, because it does not form amylose–lipid complexes (French et al., 1963; Schweizer et al., 1986). Native maize starch was used as a model substance for starch based matrices, since the amount of protein and fat in native maize starch is relatively low ($<$0.4%) which minimize the possible interactions at molecular level and prevents the potential complications during the analysis. To vary the mixing zone, the β–carotene–in–oil solution was given into the extruder at two different dosing points: before and after plastification of the starch. Moreover, the extrusion trials were designed in a way that β–carotene was exposed to various high temperature ($>$100 °C) and shear conditions corresponding to the processing of directly expanded ready–to–eat products. To calculate the maximum shear stresses applied, the viscosity of the plasticized starch was measured by an online slit die rheometer. The β–carotene content of the samples was analyzed by a method based on high pressure liquid chromatography, since it is accepted as one of the most reliable methods for the analyses of β–carotene (Feltl et al., 2005).

Main findings and scientific implications: Up to 75% retention of β–carotene could be achieved, if the β–carotene was incorporated after the plastification of the starch (i.e. at the end of the extruder). This could be explained by a shorter exposure time to thermal and mechanical stresses and, by lower absolute values of the shear stress at the end of the extruder, compared to the incorporation before the plastification (i.e. at the first barrel of the extruder). In the range investigated (i.e. 135 °C to 170 °C), temperature showed no influence on the retention, whereas an increase in screw speed from 300 rpm to 500 rpm led to a significant increase in the β–carotene retention from 45% to 71%. The rheological analysis showed that increasing screw speed from 300 rpm to 500 rpm

actually decreases the shear stress applied at the end of the extruder. These results suggest that the applied shear stress plays an important role at the retention of the bioactives and has to be considered as an important design parameter. The mechanism behind the degradation due to applied shear stress remains, however, unknown, since the shear stress might lead to either mechanical or thermal degradation. The latter one is due to the viscous dissipation of mechanical energy to heat that might lead to hot spots at the tip of screws, however can not be detected by the temperature sensors used. Nevertheless, taken together, the results suggest that the extrusion processing can be principally applied for the delivery of lipophilic bioactives such as β–carotene, and it is favorable to incorporate the β–carotene–in–oil solution after plastification of the starch, i.e. at the end of the extruder.

Limitations and recommendations: The experiments were performed at high temperature and high pressure conditions to allow a direct expansion at the die exit of the extruder similar to the conventional production of extruded ready–to–eat cereals. Expansion is driven by the flash evaporation of superheated water due to sudden pressure drop at the die. This may also lead to the escape of the β–carotene–in–oil solution to a certain extent. Furthermore, the porous structure of the product increases the surface area, at which the oxidation is more favorable. These factors could explain the minimum loss of 25% in almost all of the samples prepared. However, further research is necessary to control this hypothesis.

7.3 Droplet formation in plasticized starch in defined flow – *Chapter 3*

Goal: This section was set out to develop a method to investigate the formation of oil droplets in plasticized starch matrix in simple shear flow and to verify the predictability of available models developed for droplet breakup in Newtonian systems.

Approach: To control the development of dispersed phase morphology in an extruder, it is crucial to understand the relation between the key system parameters (e.g. shear rate, viscosity) and the resulting deformation and breakup of the droplets suspended in plasticized starch. To develop a mechanistic insight into these relationships, it is necessary to perform experiments under well defined flow conditions, which are not available within

an extruder due to the complex geometry of intermeshing twin screws.

There is a large volume of published studies describing deformation and breakup of droplets for various well characterized model systems under well defined flow conditions. However, neither plasticized starch (i.e. highly viscous non–Newtonian matrix), nor the influence of high temperature–high shear conditions as in an extruder was considered in these studies. One of the main challenges concerning such a study is the necessity of elevated temperature and pressure to plasticize the starch, and to prevent the evaporation of water. Furthermore, high torque levels (> 200 Nm) have to be achieved due to the high viscosity of plasticized starch. Under these experimental circumstances, traditional rheometers are hardly applicable. That is why a dedicated shearing device developed in University of Wageningen to process high viscosity biopolymers in simple shear was used.

In this shear cell, samples were exposed to constant shear rates, and therefore to constant shear stresses which could be calculated from the torque measurements. This also allowed a simultaneous measurement of the viscosity, which is one of the crucial parameters necessary to study droplet formation. After shearing treatment, resulting dispersed phase morphology was analyzed by confocal laser scanning microscopy (CLSM), as it allows taking images from certain depths in the sample so that the adverse influence of the cutting procedure can be prevented. Furthermore, large number of images could be taken easily, which were then analyzed by an image processing software to obtain statistically reliable results.

During the experiments, samples were sheared at constant shear stress for a long extent to allow dispersed phase reaching a steady–state morphology. The droplet formation at different conditions was investigated by varying the matrix viscosity, oil content and shear rates applied. Obtained results were compared to the predictions of the models developed and validated for Newtonian systems in order to verify their applicability on the system used in this study.

Main findings and scientific implications: The most obvious finding to emerge from this section is that the droplets formed in simple shear flow of plasticized starch are significantly smaller (factor 10 to 100) than the predicted values for a Newtonian systems. On one hand, this is a promising result regarding the need of small droplet sizes in the target application (i.e. delivery of lipophilic bioactives). On the other hand, this means

that the available models validated for Newtonian systems cannot be used to characterize the droplet breakup in plasticized starch matrix. Furthermore, the results showed that an increase in oil content led to an increase in droplet diameter. This indicates that the steady–state dispersed phase morphology is not only driven by droplet breakup but also by coalescence. This further suggests that the results cannot be used to develop a model describing solely the influence of droplet breakup due to the additional coalescence. This problem is addressed in the following section (i.e. Chapter 4). This section has shown that the application of simple shear flow by the dedicated shearing device allowed a successful investigation of the droplet formation in plasticized starch matrices, while keeping the complexity of the system as close as possible to those found in the industrial food extrusion processing.

Limitations and recommendations: Many of the questions brought up in this section, such as the occurrence of coalescence or the dependency of droplet breakup and coalescence on process parameters, are addressed in the following section. However, there are still several questions that need further investigation. The current section was not specifically designed to evaluate the influence of specific factors related to the viscoelasticity and interfacial properties, since the available methods are not capable of measuring these properties of plasticized starch above the water boiling point of 100 °C. Although the possible consequences of these factors on droplet formation are discussed in detail in Chapter 3, development of thorough mechanistic insight into droplet formation demands a good characterization of these factors. Future research should therefore concentrate on the development or the modification of the measurement methods to characterize the viscoelastic and interfacial properties of plasticized starch.

7.4 Coalescence in plasticized starch in defined flow – *Chapter 4*

Goal: In this section, the aim was to verify the occurrence of coalescence in defined flow and to determine the influence of important process and material parameters such as shear stress, shear rate and viscosity on the rate of coalescence. Moreover, the aim was to minimize the coalescence with the understanding gained to investigate the droplet breakup in plasticized starch, which could be further used to evaluate the dispersive

mixing efficiency within an extruder.

Approach: The method developed with the shearing device in the previous section was used as basis for the investigations in the current section. Initial effort was given on verification of the occurrence of coalescence. For this, a method based on double staining was developed. To characterize the coalescence rate, the experimental approach was based on application of controlled shear stresses for a long extent to reach a steady–state morphology, which is the result of a dynamic equilibrium between breakup and coalescence of the droplets. The experimental conditions and resulting dispersed phase morphology were then analysed by dimensionless numbers, such as capillary number and viscosity ratio, to define the associated correlations.

Main findings and scientific implications: This study has shown that coalescence of oil droplets in plasticized starch takes place even at very low oil content (i.e. 0.05%) and very high blend viscosity (i.e. 1500 Pa·s). Dimensionless analysis of the results revealed that coalescence becomes more favourable at higher shear rates and oil contents, whereas an increase in blend viscosity decreases the rate of coalescence. In general, it seems that coalescence plays an important role in the development of final dispersed phase morphology in a plasticized starch in simple shear flow. It was also shown that the approach developed to characterize the rate of coalescence can be further used to decrease it and determine the critical capillary number as a function of dispersed phase viscosity to blend viscosity. This finding has a particular importance, as it allows evaluating the efficiency of dispersive mixing of oil in plasticized starch by extrusion processing. This is discussed in the Chapter 5 in detail.

Limitations and recommendations: The major limitation lies in the fact that this study has only examined limited number of trials. Although the tendencies can be clearly observed, number of trials clearly affects the degree of accuracy. Considerably more work needs to be done to improve the model defining the correlation between process variables and coalescence.

7.5 Analysis of dispersive mixing in extruder – *Chapter 5*

Goal: The purpose of this section was to develop a method to simulate the non–Newtonian

flow of plasticized starch in a mixing zone of an extruder and implement a kinematic variable into the simulation to characterize the efficiency of dispersive mixing by considering the flow field and mapping the underlying mixing mechanisms.

Approach: The success of simulation depends on the quality of the available data on the system being investigated. Therefore, special effort was given for reliable monitoring and implementation of the data necessary for the numerical simulation. For this, experiments were performed using a co–rotating high speed twin–screw extruder. Rheological characteristics of the plasticized starch were determined by a multiple step slit die rheometer mounted on the extruder during all the experiments. The measured data was fitted to the Bird–Carreau viscosity model describing the rheological behavior of shear thinning fluids like plasticized starch. The degree of fill at mixing zone of the extruder was verified by inline mounted pressure sensors. Furthermore, these two pressure sensors were used to monitor the pressure difference at this region to validate the simulation results.

The computational fluid dynamics simulation of the flow was performed by ANSYS POLYFLOW, which is one of the few available finite element codes dedicated to highly viscous non–Newtonian flows. The flow through the mixing zone was assumed to be isothermal in accordance with negligible temperature change of the material at this region. Firstly, a steady state simulation was performed. Then, the result of the steady state simulation was used as an initial velocity field in a time dependent simulation to obtain a physically relevant initial step. Due to symmetrical geometry, only half a turn of the screw was simulated. The flow type was analyzed by using mixing index in combination with shear rate to gain an insight into the mechanism of mixing at a given point in time. Finally, particle tracking was performed by launching virtual particles into the flow fields obtained from time dependent simulation. To evaluate the dispersive mixing efficiency, critical capillary number defined in the previous section was implemented into the particle tracking simulations. Influences of screw speed and configuration were used as exemplary process parameters.

Main findings and scientific implications: The developed method based on CFD simulation of flow offers an access to local data on flow velocities and resulting shear stresses, capillary numbers and capillary ratio, the latter being the parameters of relevance for droplet break–up in laminar flow. The results have shown good agreement between experimental and computational results obtained at various process conditions, which

was verified by pressure difference along the mixing zone. The results suggest that high shear zones are generated at the clearances between screws and barrel at which the flow is dominated by simple shear flow. Therefore, the ratio of capillary number to material specific critical number defined in the preceding section can be implemented as a kinematic variable evaluating the efficiency of dispersive mixing. In general, it seems that the developed method can be used for process parameter adaptation and optimization in terms of dispersive mixing efficiency for processes governed by complex flows as of plasticized starch matrices in an extruder.

Limitations and recommendations: The developed computational method is limited to certain processing conditions with respect to the assumptions made in this study. This means that the concerned extrusion region must be fully filled and the change in temperature and rheological behavior must be negligible. The CFD simulation of partially filled extrusion regions remains challenging due to the technical limitation of the available computational codes. In contrast, simulation of non–isothermal flow with a dynamic rheological model by the available computational methods is technically possible. However, in this case, the problem is the lack of reliable techniques to measure the necessary experimental data. Hence, if such conditions will be considered, techniques measuring inline thermophysical properties of starch must first be developed to achieve a reliable simulation of the flow at such conditions.

7.6 Droplet breakup and coalescence in extruder – *Chapter 6*

Goal: The aim of this final section is to gain a mechanistic insight into the dispersive mixing in extrusion processing of starch based matrix by utilizing the methods/techniques developed and understandings gained in this thesis. This section is further set out to demonstrate how better understanding at mechanistic level can be used in practice to improve the dispersive mixing in an extruder.

Approach: Initially, oil droplets were incorporated into plasticized starch in the mixing zone of the extruder, which was defined previously in Chapter 2. Important extrusion parameters such as feed rate, screw speed, screw geometry, oil content were varied and resulting droplet size distribution was analyzed by CLSM and image processing software.

Since the resulting droplet size distribution is a result of both droplet breakup and coalescence, special effort was given to differentiate the influence of these two mechanisms. For this purpose, pre–emulsified droplets with defined droplet size were incorporated into the extruder and the influence of various processing conditions on resulting droplet size distribution was analyzed. This allowed excluding the influence of coalescence on droplet formation and characterize it solely. Furthermore, computational procedure introduced in the preceding section was used to characterize local flow conditions influencing droplet breakup. Since the simulation did not involve the influence of coalescence, it could be used to analyze the influence of various extrusion conditions only on droplet breakup. The results from these isolated analyses were used to understand the droplet breakup and coalescence taking place simultaneously at the target application, i.e. dispersing oil droplets in plasticized starch by extrusion processing. Finally, to verify the suggestions of the analyses, the process was redesigned in a way to achieve improved dispersive mixing, and therefore smaller droplet sizes.

Main findings and implications: One of the most significant findings to emerge from this study is that an increase in screw speed led to both improved droplet breakup and increased coalescence. This is due to the increase in shear rate but decrease in matrix viscosity, which clearly together have contrary effects on the dispersed phase morphology as described in Chapter 6 in detail. On one hand, it seems that the screw speed cannot be used to control the dispersed phase morphology. On the other hand, this allows screw speed to be used as design parameter to change the structure of the matrix without altering the dispersed phase morphology. Therefore, this effect of the screw speed will allow a higher degree of flexibility at the target application.

The results have also shown that an increase in oil content leads to remarkably bigger droplet sizes due increased rate of coalescence. Since the previous studies showed that there is a correlation between the droplet size and the bioavailability, the amount of oil added should be kept at levels at which the resulting droplet sizes do not decrease the bioavailability. For incorporation of higher amounts, it is clearly crucial to control the rate of coalescence.

Another major finding is that an increase in feed rate decreases the rate of coalescence, whereas it has no significant influence on droplet breakup at the range investigated. The results have also shown that increasing viscosity is the main reason of the reduced rate

of coalescence with increasing feed rate. These results are in good agreement with the previous findings of the experiments performed in defined flow conditions (see Chapter 4). It was also shown that droplet breakup can be improved by using different screw elements, such as reverse kneading blocks, with which more droplets are exposed to high shear regions.

Taken together, the implications of these findings are that both matrix viscosity and screw geometry should be taken into account as important design parameters that control the dispersed phase morphology. The results of extrusion experiments redesigned accordingly showed a significant decrease in the droplet sizes, which therefore verify the implications of previous findings and demonstrate how better understanding at mechanistic level can be actually used to improve the dispersive mixing in an extruder.

Limitations and recommendations: The current study did not evaluate the effects of various flow profiles on the rate of coalescence. This is clearly an important aspect which might be used to control coalescence. It must therefore be considered for future research.

7.7 Main conclusions

- Extrusion processing can be principally applied to deliver β–carotene, a model lipophilic bioactive, through ready–to–eat starch based foods without any need of extra processing steps, such as emulsification or microencapsulation.
- A mechanistic insight into droplet breakup and coalescence in extrusion processing of starch based matrix is gained and described by using dimensionless numbers. This allows controlling and altering the dispersed phase morphology according to the needs of lipophilic bioactives to be delivered.
- The approach and methods developed offer an access to understand the dispersive mixing of various lipophilic components in extrusion processing, and assist at achieving the desired dispersed phase morphology in the final product.

7.8 Outlook

The current study focuses mainly on the characterization of an extrusion process to control the factors important for the delivery of lipophilic bioactives through starch based

food products, i.e. bioactive stability and droplet formation. The design requirements of health promoting food products give rise to several questions that can be answered only by extensive interdisciplinary studies. For instance, considerably more work will need to be done to determine if lipophilic bioactives can conserve their stability during the shelf life and ingestion of the food product. Another important aspect is the release characteristics of the starch based matrices in the gastrointestinal tract of a human body. It is known that the starch structure, such as crystallinity and molecular size distribution, has strong influence on its release characteristics (Ispas–Szabo et al., 2000; Tolstoguzov, 2003; Lakkis, 2007), which might eventually affect the bioavailability. Future research should also assess the effects of dispersed phase characteristics on the final sensory quality of the product. The essential need of these studies is a process with good control on the intrinsic characteristics of the food defining its functional properties. This thesis can therefore be considered as an initial step in this direction allowing an initiation of such a comprehensive interdisciplinary research.

7.9 References

Borel, P. (2003). Factors affecting intestinal absorption of highly lipophilic food microconstituents (fat–soluble vitamins, carotenoids and phytosterols). *Clinical Chemistry and Laboratory Medicine*, 41(8), 979–94.

Feltl, L., Pacakova, V., Stulik, K., & Volka, K. (2005). Reliability of Carotenoid Analyses: A Review. *Current Analytical Chemistry*, 1(1), 93–102.

French, D., Pulley, A. O., & Whelan, W. J. (1963). Starch fractionation by hydrophobic complex formation. *Starch–Stärke*, 15(10), 349–354.

Gonnet, M., Lethuaut, L., & Boury, F. (2010). New trends in encapsulation of liposoluble vitamins. *Journal of Controlled Release*, 146(3), 276–90.

Grolier, P., Agoudavi, S., & Azais–Braesco, V. (1995). Comparative bioavailability of diet–, oil– and emulsion–based preparations of vitamin A and β–carotene in rat. *Nutrition Research*, 15(10), 1507–1516.

Horn, D. (1989). Preparation and characterization of microdisperse bioavailable carotenoid hydrosols. *Die Angewandte Makromolekulare Chemie*, 166(1), 139–153.

Horn, D., & Rieger, J. (2001). Organic nanoparticles in the aqueous phase–theory,

experiment, and use. *Angewandte Chemie International Edition*, 40(23), 4330–4361.

Ispas—-Szabo, P., Ravenelle, F., Hassan, I., Preda, M., & Mateescu, M. a. (2000). Structure–properties relationship in cross–linked high–amylose starch for use in controlled drug release. *Carbohydrate Research*, 323(1–4), 163–75.

Lakkis, J. (2007). *Encapsulation and Controlled Release Technologies in Food Systems*. Ames, Iowa, USA: Blackwell Publishing.

Parker, R. S., Swanson, J. E., You, C.–S., Edwards, A. J., & Huang, T. (2007). Bioavailability of carotenoids in human subjects. *Proceedings of the Nutrition Society*, 58(01), 155–162.

Ribeiro, H. S., Guerrero, J. M. M., Briviba, K., Rechkemmer, G., Schuchmann, H. P., & Schubert, H. (2006). Cellular uptake of carotenoid–loaded oil–in–water emulsions in colon carcinoma cells in vitro. *Journal of Agricultural and Food Chemistry*, 54(25), 9366–9.

Schweizer, T. F., Reimann, S., Solms, J., Eliasson, A. C., & Asp, N. G. (1986). Influence of drum–drying and twin–screw extrusion cooking on wheat carbohydrates, II, effect of lipids on physical properties, degradation and complex formation of starch in wheat flour. *Journal of Cereal Science*, 4(3), 249–260.

Tolstoguzov, V. (2003). Thermodynamic considerations of starch functionality in foods. *Carbohydrate Polymers*, 51(1), 99–111.

Summary

Health and well–being are the major drivers for the increased interest in the creation of functional food products. For this purpose, functional food ingredients that provide health benefits beyond basic nutrition can be incorporated into food products. Especially, the lipophilic bioactives are of special interest due to their specific health benefits, such as preventing cancer and coronary heart disease. Key challenge is the delivery of the bioactives through the food product without sacrificing the appeal and convenience character of the food and in a manner that they will indeed promote health and well–being of the consumers.

Extrusion processing possesses several advantages due to its multifunctional nature combining several unit operations, which can be manipulated to provide desired product characteristics and functional properties, at the same time. Typically, starch-based foods such as ready–to–eat cereals, pastas, salty and sweet snacks are produced by extrusion processing and are highly appreciated by consumers.

For the delivery of lipophilic bioactives through foods, it is mostly favourable to dissolve the lipophilic bioactives in a lipophilic carrier (e.g. triglyceride oil), disperse this solution into small droplets and then microencapsulate these droplets into certain type of matrix to improve their stability, bioavailability and palatability. These can be integrated into the extrusion process by dispersing the bioactives–in–oil solution directly into plasticized starch during extrusion processing, which simplifies the design route by eliminating extra emulsification and microencapsulation steps.

However, such a process demands a high degree of understanding over the stability of bioactives and dispersive mixing of lipophilic components during extrusion processing. The objective of this thesis is therefore to develop a mechanistic insight into the dynamics of dispersive mixing in extrusion processing of plasticized starch with respect to the incorporation of lipophilic bioactives into directly expanded ready–to–eat foods.

Chapter 1 initially focuses on the challenges (e.g. stability, bioavailability) relating to the delivery of lipophilic bioactives through foods to provide specific health benefits to humans. Then, the traditional approach and techniques used for the manufacture of

functional foods are briefly reviewed. Finally, the potential of extrusion technologies are discussed and the associated challenges together with the aim and outline of this thesis are presented.

Chapter 2 describes the retention of β-carotene, a model lipophilic bioactive, during extrusion processing of directly expanded starch based products. It was favourable to incorporate bioactives such as β–carotene only after the plastification of the starch (i.e. at the end of the extruder). In that way, β–carotene retention could be increased by 10%. This could be explained by the shorter exposure time to thermal and mechanical stresses and, especially, by lower absolute values of the shear stress. β–carotene retention was independent of temperature in the range investigated (135 – 170 °C): in this range, the retention of total contents was always at about 70%. Increasing the screw speed from 300 to 500 rpm led to significant increase in the retention of β–carotene by about 25% ($P < 0.05$). This could be explained by decreased mechanical stress at higher screw speeds, which were calculated using online measurements of the matrix viscosity.

In **Chapter 3**, the influence of defined flow conditions, namely simple shear flow, on the formation of triglyceride droplets in plasticized starch was studied, using a specific shearing device and a confocal laser scanning microscopy (CLSM). Increasing shear rate had no influence on droplet diameter at the shear rate ranges (i.e. 5 s^{-1} to 120 s^{-1}) investigated. An increase in oil content led to an increase in droplet diameter. This indicates that the steady-state dispersed phase morphology is not only driven by droplet breakup but also by coalescence. The maximum stable droplet sizes in plasticized starch are significantly smaller (factor of 10 to 100) than the predicted values for a Newtonian matrix. This difference might be related to the non-Newtonian behavior of the system evaluated. Overall, it was concluded that the use of simple shear flow conditions by a dedicated shearing device allowed a successful investigation of the droplet formation in plasticized starch matrices, while keeping the complexity of the system as close as possible to those found in the industrial food extrusion processing.

In **Chapter 4**, simple flow conditions generated in the shearing device were used to investigate the coalescence phenomena of triglyceride droplets in plasticized starch. A double staining method in combination with CLSM was introduced and the occurrence of coalescence was demonstrated visually. Even at very low oil content (i.e. 0.05% dry basis) and very high blend viscosity (i.e. 1500 Pa·s), droplet coalescence was observed.

Droplet sizes resulting from breakup and coalescence were used to calculate the critical capillary number. As it included the influence of coalescence on the final droplet sizes, it was used to quantify the coalescence as a function of process and material parameters. An increase in shear rate and oil content led to an increased coalescence rate whereas an increase in blend viscosity decreased the rate of coalescence.

Chapter 5 introduces a procedure to simulate the flow of plasticized starch in a mixing zone of a co-rotating twin screw extruder by using the computational fluid dynamics (CFD). Sensitivity of the simulation to the selected viscosity model was analyzed. The results suggest that an increase in zero shear viscosity has no influence on the flow field, whereas a slight change in viscosity at the shear thinning region affects the flow significantly. Simulation results were validated quantitatively by experimental data. The results suggest that high shear zones are generated at the clearances between screws and barrel or between two screws at which the flow is dominated by simple shear flow. To evaluate the dispersive mixing efficiency, the material specific critical capillary number was implemented into particle tracking simulations. Increasing screw speed led to better dispersive mixing, although the generated shear stresses decreased. The dispersive mixing efficiency can be improved by using reverse kneading blocks at which more particles are exposed to high shear stresses.

In **Chapter 6**, formation of oil droplets in plasticized starch were investigated for the complex extrusion conditions by analyzing the droplet breakup and coalescence mechanisms separately. Increasing screw speed led to both improved droplet breakup and increased coalescence. This is due to the increase in shear rate but decrease in matrix viscosity, together which clearly have contrary effects on the formation of oil droplets. An increase in feed rate decreased the coalescence rate, whereas droplet breakup was not significantly affected. This study has also shown that increasing viscosity is the main reason of the reduced rate of coalescence with increasing feed rate. These results are in good agreement with the previous findings of the experiments performed in defined flow conditions. Based on the results of CFD simulations, droplet breakup could be improved by using different screw elements, such as reverse kneading blocks, with which more droplets are exposed to high shear regions. Taken together, the implications of these findings suggest that both matrix viscosity and screw geometry should be taken into account as important design parameters to control the dispersed phase morphology. The results of extrusion experiments redesigned accordingly showed a significant decrease

in the droplet sizes, which therefore verify the implications of previous findings and demonstrate how the better understanding at mechanistic level can be actually used to improve the dispersive mixing in an extruder.

In **Chapter 7**, the research approach of this thesis was provided. To highlight the links between the preceding chapters, the goals and approaches of each chapter were summarized. In most particular, the scientific and practical implications of the main findings as well as the limitations of the current study and recommendations for the future research were discussed. Finally, the main conclusions and outlook of the thesis were presented.

Zusammenfassung

Der Wunsch nach einer gesünderen Ernährung und dem Wohlbefinden der Konsumenten sind die Hauptgründe für das gesteigerte Interesse an der Entwicklung von funktionellen Lebensmitteln. Aus diesem Grund werden funktionelle Lebensmitteinhaltsstoffe, die über den Nährwert hinaus eine gesundheitsfördernde Wirkung haben, in Lebensmittel eingebracht. Insbesondere lipophile Bioaktivstoffe sind wegen ihrer speziellen gesundheitsfördernden Eigenschaften von Interesse. Sie können z.B. das Risiko senken, an Krebs zu erkranken oder einen Herzinfarkt zu erleiden. Die grösste Herausforderung ist es, ein für den Verbraucher ansprechendes Produkt zu gestalten, welches gleichzeitig die Bioverfügbarkeit der eingebrachten Moleküle durch gezielte Formulierung und Prozessführung gewährleistet.

Die Extrusion als Verfahren zur Herstellung von funktionellen Lebensmitteln bietet durch die Kombination mehrerer Grundoperationen in einer Anlage viele Vorteile: Da die einzelnen Grundoperationen unabhängig voneinander gesteuert werden können, ist es möglich, die gewünschten Produkt– und funktionellen Eigenschaften gezielt einzustellen. Viele auf Stärke basierende Lebensmittel wie Cerealien, Nudeln, süsse und salzige Snacks werden bereits mittels Extrusion hergestellt und werden vom Verbraucher gut angenommen.

Um lipophile Bioaktivstoffe in Lebensmitteln verfügbar zu machen, werden diese meist in einem lipophilen Trägerstoff, z.B. in einem Triglycerid, gelöst. Diese Lösung wird zu kleinen Tropfen dispergiert, mikroverkapselt und anschliessend in die gewünschte Lebensmittelmatrix eingebracht. Durch diese Art der Mikroverkapselung kann die Stabilität und Bioverfügbarkeit der lipophilen Substanzen erhöht und der Geschmack des Produktes verbessert werden. Die dafür notwendigen Prozessschritte können im Extrusionsprozess kombiniert werden, indem die in Öl gelösten Bioaktivstoffe während der Extrusion direkt in die plastifizierte Stärke hineindosiert werden. Hierdurch vereinfacht sich die Herstellung, da das Emulgieren und die Mikroverkapselung in einem einzigen Prozessschritt zusammengefasst werden. Dafür ist ein tiefgehendes Verständnis des Extrusionsverfahrens notwendig. Insbesondere Kenntnisse über die Stabilität von Bioaktivstoffen während des Extrusionsprozesses und das dispergierende Mischen mit

einem Extruder sind hierbei von Bedeutung. Daher ist das Ziel dieser Arbeit, einen mechanistischen Einblick in das dispersive Mischen im Extrusionsprozess von plastifizierter Stärke hinsichtlich des Einbringens von lipophilen Bioaktivstoffen in direktexpandierte, verzehrfertige Lebensmittel zu erarbeiten.

Kapitel 1 beschreibt zunächst die durch die Verarbeitung von lipophilen Bioaktivstoffen bedingten Herausforderungen: Stabilität und Bioverfügbarkeit der bioaktiven Substanzen müssen gewährleistet sein, wenn diese Stoffe vom Verbraucher mit einem Lebensmittel aufgenommen werden und eine gesundheitsfördernde Wirkung haben sollen. Anschliessend wird kurz das traditionelle Vorgehen zur Herstellung von funktionalen Lebensmitteln beschrieben. Am Ende wird auf die Möglichkeiten der Extrusion zur Herstelllung von funktionalen Lebensmittel und den damit zusammenhängenden Herausforderungen eingegangen. Weiter wird ein Überblick über die Arbeit gegeben und ihr Ziel beschrieben.

In **Kapitel 2** wird der Erhalt von β–Carotin, einem lipophilen bioaktiven Modelstoff, während der Herstellung von stärkebasierten direktexpandierten Produkten mittels Extrusion untersucht. Es wird gezeigt, dass bioaktive Stoffe wie β–Carotin bevorzugt nach der Plastifizierung der Stärke, das heisst am Ende des Extruders, zugegeben werden sollten. Hierdurch kann der Erhalt des β–Carotins um bis zu ca. 10% gesteigert werden. Das kann durch die kürzere thermische und mechanische Belastung des β–Carotins aufgrund einer kürzeren Verweilzeit im Prozessraum erklärt werden. Insbesondere die niedrigere Belastung durch Schubspannungen spielt hier eine Rolle. Der Erhalt von β–Carotin ist im untersuchten Temperaturbereich (135 °C – 170 °C) von der Temperatur unabhängig und liegt immer bei etwa 70%. Eine Erhöhung der Schneckendrehzahl von 300 auf 500 rpm führt zu einem ca. 25% höheren Erhalt des β–Carotins. Das kann durch die Abnahme der mechanischen Belastung mit steigenden Drehzahlen erklärt werden. Die mechanischen Belastungen wurden mit Hilfe von online gemessenen Matrixviskositäten berechnet.

In **Kapitel 3** wird der Einfluss definierter Fliessbedingungen, hier einer einfachen Scherströmung, auf die Bildung von Triglyceridtropfen in plastifizierter Stärke mit Hilfe einer Scherzelle und eines konfokalen Laser–Scanning–Mikroskops (CLSM) untersucht. Bei Scherraten zwischen 5 s^{-1} und 120 s^{-1} ist kein Unterschied in den resultierenden Tropfengrössen zu erkennen. Ein höherer Ölanteil führt zu grösseren Tropfen. Das weist darauf hin, dass bei stationären Bedingungen nicht nur der Tropfenaufbruch sondern auch die Koaleszenz ergebnisbestimmend ist. Die in der plastifizierten Stärke stabilsten Tropfen, waren signifikant kleiner (Faktor 10 bis 100) als es für eine newtonische Matrix

zu erwarten ist. Der Unterschied könnte auf das nicht–newtonsche Verhalten der plastifizierten Stärkematrix zurückzuführen sein. Insgesamt kann festgestellt werden, dass mit der Scherzelle erfolgreich der Einfluss einer einfachen Scherströmung auf das Verhalten der Tropfen in einer Matrix aus plastifizierter Stärke untersucht werden kann.

Nachdem in Kapitel 3 aufgezeigt wurde, dass der Koaleszenzvorgang einen entscheidenden Einfluss auf das Dispergierergebnis hat, wird deser in **Kapitel 4** näher be- schrieben. Dazu wird wiederum die Scherzelle genutzt, um eine einfache Scherströmung zu generieren und die Koaleszenzphänomene der Triglyceridtropfen in plastifizierter Stärke zu untersuchen. Eine doppelte Färbemethode wurde eingeführt und zusammen mit dem CLSM genutzt, um die Koaleszenz optisch darzustellen und nachzuweisen. Selbst bei einem sehr niedrigen Ölanteil (z.B. 0.05% bezogen auf die Trockenmasse) und sehr hohen Viskositäten der Mischungen (z.B. 1500 Pa·s) konnte Koaleszenz beobachtet werden. Die aus den Aufbruchs– und Koaleszenzversuchen resultierenden Tropfengrössen wurden genutzt, um die kritische Kapillarzahl zu berechnen. Diese dimensionslose Kennzahl beinhaltet auch den Einfluss der Koaleszenz auf die resultierenden Tropfengrössen, und ist daher geeignet, Koaleszenz als Funktion der Prozess– und Materialparameter quantitativ darzustellen. Eine höhere Scherrate und ein höherer Ölanteil führen zu höheren Koaleszenzraten, eine höhere Viskosität der Mischung hingegen reduziert die Koaleszenzrate.

In **Kapitel 5** wird eine Methode eingeführt, mit der die Strömung plastifizierter Stärke in der Mischzone eines gleichläufigen Doppelschneckenextruders mittels nummerischer Strömungsmechanik (CFD) simuliert werden kann. Der Einfluss des gewählten Viskositätsmodels auf die Simulation wird ermittelt. Die Ergebnisse deuten darauf hin, dass ein Anstieg der Nullviskosität keinen Einfluss auf das Strömungsfeld hat. Dagegen hat eine kleine Veränderung der Viskosität im strukturviskosen Bereich einen grossen Einfluss auf die Fliesseigenschaften. Die Ergebnisse der Simulation werden quantitativ mit im Extruder experimentell gewonnenen Daten belegt. Die Simulation zeigt, dass sich im Bereich zwischen den Schnecken und dem Extrudergehäuse sowie zwischen den beiden Schnecken Zonen mit hoher Scherbelastung ausbilden. In diesen Zonen wird der Materialfluss von einer einfachen Scherströmung dominiert. Um die effektive dispersive Mischeffizienz zu ermitteln, werden die materialspezifischen kritischen Kapillarzahlen in eine Partikel–Tracking–Simulation eingebunden. Diese zeigt, dass eine Erhöhung der Drehzahl das dispersive Mischen verbessert. Gleichzeitig werden die erzeugten

Schubspannungen verringert. Die dispersive Mischeffizienz kann durch den Einsatz von Knetelementen weiter verbessert werden. Hierdurch werden mehr Partikel hohen Schubspannungen ausgesetzt.

Kapitel 6 beschäftigt sich mit der Bildung von Öltropfen in plastifizierter Stärke unter komplexen Extrusionsbedingungen. Dabei werden Tropfenaufbruch und Koaleszenz getrennt betrachtet. Eine erhöhte Schneckendrehzahl führt sowohl zu einem verbesserten Tropfenaufbruch als auch zu einer Zunahme der Koaleszenz. Erklären lässt sich das durch die Zunahme der Schubspannung bei gleichzeitiger Abnahme der Matrixviskosität. Diese beiden Effekte haben einen gegenläufigen Einfluss auf die resultierende Öltropfengrösse. Wird der Massenstrom erhöht, sinkt die Koaleszenzrate, wobei der Tropfenaufbruch nicht signifikant beeinflusst wird. Es wird gezeigt, dass die erhöhte Viskosität der Hauptgrund für die Reduktion der Koaleszenzrate ist. Die Ergebnisse stimmen gut mit den gezeigten Resultaten aus den Versuchen unter definierten Fliessbedingungen (Kapitel 4) überein. Auf den Ergebnissen der CFD Simulationen aufbauend, kann der Tropfenaufbruch durch die Verwendung anderer Schneckenelemente verbessert werden. Insbesondere Rückwärtselemente, durch die mehr Tropfen hohen Schubspannungen ausgesetzt werden, verbessern den Tropfenaufbruch signifikant. Fasst man die Ergebnisse zusammen, lässt sich sagen, dass sowohl die Matrixviskosität als auch die Schneckengeometrie als wichtige Prozessdesignparameter angesehen werden müssen, um die Morphologie der dispersen Phase zu gezielt einstellen zu können. Die Ergebnisse der angepassten Extrusionsversuche zeigen eine signifikante Abnahme der Tropfengrösse. Dies bestätigt die Schlussfolgerungen aus den bisherigen Ergebnissen und demonstriert, wie ein besseres mechanistisches Verständnis genutzt werden kann, um das dispersive Mischen in einem Extruder zu verbessern.

Kapitel 7 ordnet die zuvor beschriebenen Ergebnisse in den grösseren Forschungskontext ein. Es wird dargestellt, wie die vorhergehenden Kapitel mit einander verbunden sind. Dazu werden jeweils die Ziele und das Vorgehen in den einzelnen Kapiteln zusammengefasst. Die wissenschaftlichen und praktischen Folgen der wichtigsten Ergebnisse werden erläutert und die Grenzen der Arbeit werden aufgezeigt. Abschliessend wird aufgezeigt, welche weiteren Forschungsarbeiten auf die hier beschriebenen Ergebnisse folgen sollten und die Kernaussage der Arbeit wird formuliert.

Acknowledgements

It would not have been possible to write this doctoral thesis without the help and support of numerous people around me, to only some of whom it is possible to give particular mention here.

First and foremost, I want to thank my promoter Prof. Dr.–Ing. Heike P. Schuchmann. She has allowed me to grow as a research scientist. She has oriented and supported me with patience and care, and has always been motivating and encouraging in times of new ideas and difficulties. I am very grateful for her contributions of discussions and ideas to make my Ph.D. experience productive and stimulating. I would also like to thank my second promoter, Prof. Dr. Ir. Remko Boom, for his valuable advice and feedback on all aspects of my doctoral research.

During my PhD, I had a chance to work with Dr. Atze Jan van der Goot from Wageningen University und Dr. Esther Mayer–Miebach from Max Rubner Institute in Karlsruhe. Their cooperation, positive attitude and understanding really deserve a great appreciation. It has been a great pleasure to work with them, which has also allowed improving the quality of this thesis substantially.

I am very thankful to all of my colleagues/friends in my institute for providing a comfortable and co-operative working environment. They have helped me in any way, whether by useful scientific discussions or by aiding me on my experiments or simply by providing welcome and interesting conversation when my mind required rest. They have made my time in the institute rewarding and fun.

Thanks to my students – Nicolas Hardt, Ulrike Schmidt, Mangesh Muttal Murhe, Sushil Kumar Singh, José Otávio Matias, Natalia Vallilengua and Priscila Takayama Matsumoto – who have contributed to this thesis by helping me a lot with my experiments and keeping me focused and motivated better on my work.

I am very grateful to my wife Gözde for her personal support, encouragement and great patience at all times. My mother Hamide, my father Sermed and my sister Esra have given me their unequivocal support throughout, as always, for which my mere expression of thanks likewise does not suffice.

Publications

Articles

Emin, M. A., & Schuchmann, H. P. (2013). Droplet breakup and coalescence in a twin-screw extrusion processing of starch based matrix. *Journal of Food Engineering*, 116(1),118–129.

Horvat, M., Emin, M. A., Hochstein, B. , Willenbacher, N. & Schuchmann, H. P. (2013). Influence of medium-chain triglycerides on expansion and rheological properties of extruded corn starch. *Carbohydrate Polymers*, 93(2), 492–498.

Horvat, M., Emin, M. A., Hochstein, B. , Willenbacher, N. & Schuchmann, H. P. (2013). A multiple-step slit die rheometer for rheological characterization of extruded starch melts. *Journal Food Engineering*, 116(2), 398-403.

Emin, M. A., & Schuchmann, H. P. (2013). Analysis of the dispersive mixing efficiency in a twin–screw extrusion processing of starch based matrix. *Journal of Food Engineering*, 115(1),132–143.

Emin, M. A., Hardt, N., van der Goot, A. J., & Schuchmann, H. P. (2012). Formation of oil droplets in plasticized starch matrix in simple shear flow. *Journal of Food Engineering*, 112(3), 200–207.

Emin, M. A., Schmidt, U., van der Goot, A. J., & Schuchmann, H. P. (2012). Coalescence of oil droplets in plasticized starch matrix in simple shear flow. *Journal of Food Engineering*, 113(3), 453-460.

Emin, M. A., Mayer–Miebach, E., & Schuchmann, H. P. (2012). Retention of β–carotene as a model substance for lipophilic phytochemicals during extrusion cooking. *LWT – Food Science and Technology*, 48(2), 302–307.

Sauter, C., Emin, M. A., Schuchmann, H. P., & Tavman, S. (2008). Influence of hydrostatic pressure and sound amplitude on the ultrasound induced dispersion and de–agglomeration of nanoparticles. *Ultrasonics Sonochemistry*, 15(4), 517-523.

Book chapters

Schuchmann, H. P., Köhler, K., Emin, M. A. & Schubert, H.. Food process engineering research and innovation in a fast changing world - Paradigms / Case studies. In: *Advances in Food Process Engineering Research and Applications*, edited by S. Yanniotis, P. Taoukis, N. G. Stoforos and V. T. Karathanos, Springer (In Press).

Emin, M. A., Schmidt, U., Hardt, N., & van der Goot, A. J. (2012). Formulierung in festen Matrices: Dispergieren von Öltropfen in plastifizierten Stärkematrices. In: *Emulgiertechnik*, 2. Auflage, Edited by H.P. Schuchmann and K. Köhler, Behr's Verlag, Hamburg.

Emin, M. A. , Köhler, K., Schlender, M. & Schuchmann, H. P. (2011). Characterization of mixing in food extrusion and emulsification processes by using CFD. In: *High Performance Computing in Science and Engineering "10*, edited by W. E. Nagel, D. B. Kröner, and M. M. Resch, Stuttgart, Springer.

Proceedings

Emin, M. A., Matias, J. O. , Horvat, M. & Schuchmann, H. P. (2009). Bewertung der Mischeffizienz eines Doppelschneckenextruders mithilfe von CFD. *Chemie Ingenieur Technik*, 82(9), 1395-1396.

Horvat, H., Hirth, M., Emin, M. A., Schuchmann, H. P., Hochstein, B. & Willenbacher, N. (2009). Online-Rheologie zur Produktentwicklung extrudierter, funktioneller Zerealien, *Chemie Ingenieur Technik* 81(8), 1173.

Horvat, M., Emin, M. A., Schuchmann, H. P., Hochstein, B. & Willenbacher, N. (2009). A multiple-step online-slit-die rheometer for investigations of the influence of extrusion process parameters on the rheological behaviour of starch–based food products, *Proceedings of the 5th International Symposium on Food Rheology and Structure*, ETH Zürich, 474–475, 2009.